NUREG/CR-4219
ORNL/TM-9593/V8&N1
Vol. 8, No. 1

Heavy-Section Steel Technology Program

Semiannual Progress Report for October 1990–March 1991

Prepared by
W. E. Pennell

Oak Ridge National Laboratory

Prepared for
U.S. Nuclear Regulatory Commission

AVAILABILITY NOTICE

Availability of Reference Materials Cited in NRC Publications

Most documents cited in NRC publications will be available from one of the following sources:

1. The NRC Public Document Room, 2120 L Street, NW., Lower Level, Washington, DC 20555

2. The Superintendent of Documents, U.S. Government Printing Office, P.O. Box 37082, Washington, DC 20013-7082

3. The National Technical Information Service, Springfield, VA 22161

Although the listing that follows represents the majority of documents cited in NRC publications, it is not intended to be exhaustive.

Referenced documents available for inspection and copying for a fee from the NRC Public Document Room include NRC correspondence and internal NRC memoranda; NRC bulletins, circulars, information notices, inspection and investigation notices; licensee event reports; vendor reports and correspondence; Commission papers; and applicant and licensee documents and correspondence.

The following documents in the NUREG series are available for purchase from the GPO Sales Program: formal NRC staff and contractor reports, NRC-sponsored conference proceedings, international agreement reports, grant publications, and NRC booklets and brochures. Also available are regulatory guides, NRC regulations in the *Code of Federal Regulations*, and *Nuclear Regulatory Commission Issuances*.

Documents available from the National Technical Information Service include NUREG-series reports and technical reports prepared by other Federal agencies and reports prepared by the Atomic Energy Commission, forerunner agency to the Nuclear Regulatory Commission.

Documents available from public and special technical libraries include all open literature items, such as books, journal articles, and transactions. *Federal Register* notices, Federal and State legislation, and congressional reports can usually be obtained from these libraries.

Documents such as theses, dissertations, foreign reports and translations, and non-NRC conference proceedings are available for purchase from the organization sponsoring the publication cited.

Single copies of NRC draft reports are available free, to the extent of supply, upon written request to the Office of Administration, Distribution and Mail Services Section, U.S. Nuclear Regulatory Commission, Washington, DC 20555.

Copies of industry codes and standards used in a substantive manner in the NRC regulatory process are maintained at the NRC Library, 7920 Norfolk Avenue, Bethesda, Maryland, for use by the public. Codes and standards are usually copyrighted and may be purchased from the originating organization or, if they are American National Standards, from the American National Standards Institute, 1430 Broadway, New York, NY 10018.

DISCLAIMER NOTICE

NUREG/CR-4219
ORNL/TM-9593/V8&N1
Vol. 8, No. 1
RF

Heavy-Section Steel Technology Program

Semiannual Progress Report for October 1990–March 1991

Manuscript Completed: January 1992
Date Published: February 1992

Prepared by
W. E. Pennell

Oak Ridge National Laboratory
Operated by Martin Marietta Energy Systems, Inc.

Oak Ridge National Laboratory
Oak Ridge, TN 37831-6285

Prepared for
Division of Engineering
Office of Nuclear Regulatory Research
U.S. Nuclear Regulatory Commission
Washington, DC 20555
NRC FIN B0119
Under Contract No. DE-AC05-84OR21400

Abstract

The Heavy-Section Steel Technology (HSST) Program is conducted for the Nuclear Regulatory Commission (NRC) by Oak Ridge National Laboratory (ORNL). The program focus is on the development and validation of technology for the assessment of fracture-prevention margins in commercial nuclear reactor pressure vessels. The HSST Program is organized in 10 tasks: (1) program management, (2) fracture methodology and analysis, (3) material characterization and properties, (4) special technical assistance, (5) fracture analysis computer programs, (6) cleavage-crack initiation, (7) cladding evaluations, (8) pressurized-thermal-shock technology, (9) analysis methods validation, and (10) fracture evaluation tests. The program tasks have been structured to place emphasis on the resolution fracture issues with near-term licensing significance. Resources to execute the research tasks are drawn from ORNL with subcontract support from universities and other research laboratories. Close contact is maintained with the sister Heavy-Section Steel Irradiation (HSSI) Program at ORNL and with related research programs both in the United States and abroad. This report provides an overview of principal developments in each of the ten program tasks from October 1, 1990, to March 31, 1991.

Contents

List of Figures

List of Tables

Preface

The Heavy-Section Steel Technology (HSST) Program, which is sponsored by the Nuclear Regulatory Commission, is an engineering research activity devoted to extending and developing the technology for assessing the margin of safety against fracture of the thick-walled steel pressure vessels used in light-water-cooled nuclear power reactors. The program is being carried out in close cooperation with the nuclear power industry. This report covers HSST work performed in October 1990–March 1991. The work performed by the Oak Ridge National Laboratory (ORNL) and by subcontractors is managed by the Engineering Technology Division (ETD) of ORNL. Major tasks at ORNL are carried out by the ETD and the Metals and Ceramics Division. Prior progress reports on this program are ORNL-4176, ORNL-4315, ORNL-4377, ORNL-4463, ORNL-4512, ORNL-4590, ORNL-4653, ORNL-4681, ORNL-4764, ORNL-4816, ORNL-4855, ORNL-4918, ORNL-4971, ORNL/TM-4655 (Vol. II), ORNL/TM-4729 (Vol. II), ORNL/TM-4805 (Vol. II), ORNL/TM-4914 (Vol. II), ORNL/TM-5021 (Vol. II), ORNL/TM-5170, ORNL/NUREG/TM-3, ORNL/NUREG/TM-28, ORNL/NUREG/TM-49, ORNL/NUREG/TM-64, ORNL/NUREG/TM-94, ORNL/NUREG/TM-120, ORNL/NUREG/TM-147, ORNL/NUREG/TM-166, ORNL/NUREG/TM-194, ORNL/NUREG/TM-209, ORNL/NUREG/TM-239, NUREG/CR-0476 (ORNL/NUREG/TM-275), NUREG/CR-0656 (ORNL/NUREG/TM-298), NUREG/CR-0818 (ORNL/NUREG/TM-324), NUREG/CR-0980 (ORNL/NUREG/TM-347), NUREG/CR-1197 (ORNL/NUREG/TM-370), NUREG/CR-1305 (ORNL/NUREG/TM-380), NUREG/CR-1477 (ORNL/NUREG/TM-393), NUREG/CR-1627 (ORNL/NUREG/TM-401), NUREG/CR-1806 (ORNL/NUREG/TM-419), NUREG/CR-1941 (ORNL/NUREG/TM-437), NUREG/CR- 2141, Vol. 1 (ORNL/TM-7822), NUREG/CR-2141, Vol. 2 (ORNL/TM-7955), NUREG/CR-2141, Vol. 3 (ORNL/TM-8145), NUREG/CR-2141, Vol. 4 (ORNL/TM-8252), NUREG/CR-2751, Vol. 1 (ORNL/TM-8369/V1), NUREG/CR-2751, Vol. 2 (ORNL/TM-8369/V2), NUREG/CR-2751, Vol. 3 (ORNL/TM-8369/V3), NUREG/CR-2751, Vol. 4 (ORNL/TM-8369/V4), NUREG/CR-3334, Vol. 1 (ORNL/TM-8787/V1), NUREG/CR-3334, Vol. 2 (ORNL/TM-8787/V2), NUREG/CR-3334, Vol. 3 (ORNL/TM-8787/V3), NUREG/CR-3744, Vol. 1 (ORNL/TM-9154/V1), NUREG/CR-3744, Vol. 2 (ORNL/TM-9154/V2), NUREG/CR-4219, Vol 1 (ORNL/TM-9593/V1), NUREG/CR-4219, Vol. 2 (ORNL/TM-9593/V2), NUREG/CR-4219, Vol. 3, No. 1 (ORNL/TM-9593/V3&N1), NUREG/CR-4219, Vol. 3, No. 2 (ORNL/TM-9593/V3&N2), NUREG/CR-4219, Vol. 4, No. 1 (ORNL/TM-9593/V4&N1), NUREG/CR-4219, Vol. 4, No. 2 (ORNL/TM-9593/V4&N2), NUREG/CR-4219, Vol. 5, No. 1 (ORNL/TM-9593/V5&N1), NUREG/CR-4219, Vol. 5, No. 2 (ORNL/TM-9593/V5&N2), NUREG/CR-4219, Vol. 6, No. 1 (ORNL/TM-9593/V6&N1), NUREG/CR-4219, Vol. 6, No. 2 (ORNL/TM-9593/V6&N2), NUREG/CR-4219, Vol. 7, No. 1 (ORNL/TM-9593/V7&N1), and NUREG/CR-4219, Vol. 7, No. 2 (ORNL/TM-9593/V7&N2).

Executive Summary

W. E. Pennell

The Heavy-Section Steel Technology (HSST) Program is conducted for the Nuclear Regulatory Commission (NRC) by Oak Ridge National Laboratory (ORNL). The program focus is the development and validation of technology for the assessment of fracture-prevention margins in commercial nuclear reactor pressure vessels (RPVs). Prior program achievements include the generation and validation of a fracture-mechanics-based, fracture-margin-assessment technology and the transfer of that technology to national consensus codes and standards. Subsequent data from materials-irradiation effects research, reactor vessel surveillance programs, and large-scale fracture-technology-validation experiments have revealed additional fracture technology issues with regulatory significance. Current HSST Program activities are structured to provide resolution of those issues and support near-term licensing actions.

1 Program Management

The HSST Program is organized in the following ten interrelated tasks: (1) program management, (2) fracture methodology and analysis, (3) materials characterization and properties, (4) special technical assistance, (5) fracture analysis computer programs, (6) cleavage-crack initiation, (7) cladding evaluations, (8) pressurized-thermal-shock (PTS) technology, (9) analysis methods validation, and (10) fracture evaluation tests. Research on these tasks is conducted by staff from the Engineering Technology, Metals and Ceramics, and Computing and Telecommunications Divisions at ORNL with extensive support from university and research laboratory subcontractors. A comprehensive cost/schedule control system is used to monitor progress against objectives.

During the current reporting period, HSST Program personnel produced 8 reports and presentations, gave 16 presentations, organized a fracture technology exchange with the VTT research center in Finland, and organized four sessions on Pressure Vessel Integrity for the American Society of Mechanical Engineers (ASME)-PVP annual meeting to be held in San Diego, California, in June 1991. Cost and schedule control measures implemented on the shallow-flaw program have been effective. The total HSST Program cost and schedule variances are +1.1% and –4%, respectively.

2 Fracture Methodology and Analysis

Work continued on the evaluation of the effects of positive out-of-plane strains on fracture toughness. Crack front contraction data were collected from the characterization specimens used for the wide-plate tests. The intent was to use these data to establish a relationship between transverse strain and fracture initiation in the plane stress-to-plane strain domain and then extrapolate this relationship into the beyond-plane-strain domain. Analysis of the test data, however, showed that the transverse strains associated with propagation of the crack contributed substantially to the overall crack front contraction, making it impossible to isolate the crack front contraction at crack initiation. An elastic-plastic, finite-element analysis has now been initiated in an attempt to isolate the crack front transverse contraction at crack initiation.

Studies of the effect of positive out-of-plane strains on fracture toughness continued, using a refined model of a 1T compact-test specimen. The refinement in the crack-tip finite-element mesh reduced the minimum crack-tip radius the model could simulate by approximately one order of magnitude. Effects of out-of-plane strain were measured in terms of the effect on the term A_{CR} in the dual parameter J-A_{CR} fracture correlation. A_{CR} is the area within a critical stress contour. In the current study the critical stress is selected to correspond with that required for fracture in ferrite grains. Results obtained were similar to those previously reported from the less-refined analysis model. A decrease in fracture toughness of only a few percent was predicted when prototypical RPV out-of- plane strains were applied.

Development continued on a modified boundary layer (MBL) model for the study of crack-tip constraint effects. The model uses boundary conditions derived from single parameter K or J fields. During the current reporting period benchmarking of a number of candidate finite-element computer programs was completed. Results from this work led to the selection of the ABAQUS program for use in the further development of the MBL model. The MBL model is intended for use in studies of the transferability of fracture-toughness data. It can also provide predictions of the effect on fracture toughness of beyond-

plane-strain out-of-plane boundary conditions such as those encountered in the analysis of circumferential flaws.

Studies of crack-tip constraint effects are in progress at the University of Maryland (UM) under an HSST Program subcontract. These studies utilize a two-dimensional finite-element model of a reactor vessel with boundary conditions and applied loading adjusted to simulate plane stress, plane strain, and multiaxial stress constraint conditions. The model provides a definition of the crack-tip elastic-plastic stress and strain fields for each of the constraint conditions analyzed. Results from this analysis are expressed in terms of the O'Dowd and Shih Q factor. A somewhat surprising result was obtained from the case in which pressure loading was used to simulate the stress field that would be comprised primarily of pressure and thermal stresses in a PTS transient. A consequence of the loading approximation was that high radial pressure loads were imposed on the model. These pressures dominated the Q field, resulting in lower values of Q for the biaxial case than for either the plane-stress or plane-strain cases. While this result is clearly nonprototypic, it does indicate that at prototypic pressure loads, some reduction of crack-tip constraint will occur for all cracks influenced by the radial compressive stress field in the reactor vessel wall.

Finite-element analysis of the shallow-flaw fracture-toughness specimens has shown that the Rice-Corten-Merkle single-specimen load vs load-line displacement formula cannot be used directly to interpret the shallow-flaw fracture-toughness test results.

A survey of the effect of constraint on crack-arrest toughness has been conducted by G. R. Irwin at UM. The survey considered crack-arrest data from small-scale specimens conforming with ASTM E1221 requirements, together with data from the large-scale HSST thermal-shock and wide-plate experiments. The crack propagation model used in the evaluation was based on the concept of a "cloud" of cleavage fracture facets, which ultimately join when the intervening material fails in a ductile manner to form an extension of the fracture surface. Under plane-strain constraint, the cloud is elongated in the direction of crack propagation. Additional stresses parallel to the crack front cause the cloud to thicken, and may cause crack branching, but do not influence the crack-arrest toughness.

HSST Program support of the multisponsor Japanese program investigating elastic-plastic fracture in inhomogeneous materials and structures continued. The program is under the direction of Professor G. Yagawa of the University of Tokyo.

In the current reporting period residual stress measurements in welds were made using diverse techniques. The destructive residual-stress determination technique gave residual stresses lower than those obtained from the nondestructive techniques. Additional fracture tests have been conducted to determine the effects of specimen thickness and crack orientation and location relative to the weld-fusion line on fracture toughness. Measurements of crack-tip strain fields have been made using both Moire grid and interferometry methods. Results showed the crack-tip fields to be divided into three zones, with characteristics clearly defined by the strain-field slopes. Crack-growth experiments have been run with surface cracks crossing a weld fusion line at right angles. They showed no significant difference in crack-growth behavior in the weld metal or parent material segments of the crack.

Round-robin, finite-element analyses of test specimens were conducted to evaluate the various J-integral formulations. Calculated and measured J values were found to agree to within 10%. A single fracture test was completed under nonisothermal conditions, with the objective being to detect any effect of crack-tip temperature gradients on fracture toughness. No effect was detected. Elastic-plastic, finite-element analysis of three-dimensional (3-D) cracks was performed to determine under what conditions HRR-type singular crack-tip fields exist. Results showed that the fields did not exist in many cases of practical importance, such as the case where stresses in the ligament are tensile across its entire width. Work continued on the development of estimation schemes for application of the program results.

3 Material Characterization and Properties

Characterization of material for the shallow-flaw fracture-toughness testing program is in progress. Test specimen types and locations within the test plate have been defined and plate cut-up drawings prepared.

Thermal aging testing of stainless steel cladding material is in progress. Aging for 1605 h at prototypical reactor vessel operating temperatures produced a 16% decrease in the Charpy upper-shelf energy.

Work continued on the development of a common test method that will permit requirements for K_{Ic}, J_{Ic}, J-R, and crack-tip-opening displacement (CTOD) testing to be combined in a single American Society for Testing and Materials (ASTM) standard. A draft of a proposed common test method was prepared and presented to the ASTM. A first draft of a proposed ASTM standard for fracture-toughness testing in the transition region was also completed.

Research continued to determine if a case exists for the K_{Ic} curve to be substituted in place of the K_{IR} curve in the fracture margin analysis required by Appendix G of Sect. III of the *American Society of Mechanical Engineers Boiler and Pressure Vessel [ASME (B&PV)] Code*. An important finding was that the fracture toughness was not reduced when the crack initiated from an arrested cleavage crack rather than from a fatigue-sharpened crack.

Exploratory testing was performed to determine if cyclic softening of the crack-tip material would increase the fracture toughness of irradiation-hardened material. Results obtained indicated no increase in fracture toughness beyond that attributable to warm prestressing.

4 Special Technical Assistance

At the request of the NRC, the HSST Program undertook a review of a report "Reactor Pressure Vessel Evaluation Report for the Yankee Nuclear Power Plant," YEAC No. 1735, July 1990. Review topics included a detailed comparison of the VISA II computer program used in the analysis with the OCA-P computer program, the PTS fracture-mechanics analysis input and results, treatment of the low-upper-shelf (LUS) fracture-toughness issue, estimates of the vessel material irradiation embrittlement, and specification of the number and magnitude of PTS transients.

The review revealed some significant differences between the treatment of crack arrest in the version of the VISA II program used in the analysis and OCA-P. The VISA II program permits the material composition and therefore the amount of irradiation embrittlement to differ for the crack initiation and crack-arrest calculations for a single vessel in the multiple vessel probabilistic failure analysis, whereas the OCA-P program requires consistent material composition within a single vessel.

The reviewers estimate the frequency of the dominant transients to be approximately one order of magnitude higher than that given in the report. They also concluded that the specification of the dominant transient was less severe than a best-estimate definition.

The reviewers concluded that the RT_{NDT} shift for the circumferential weld would be up to 22°C higher than that given in the report. This difference was due to the low irradiation temperature for this vessel. The RT_{NDT} shift for this vessel exceeds the screening criteria defined in 10 *CFR* 50.61. The LUS toughness of the vessel was considered by the reviewers to have little influence on the vessel failure probability estimates.

The review concluded that the vessel mean failure frequency was 40 times higher than the acceptance criteria failure frequency given in NRC Regulatory Guide 1.154.

Task 4 also provided assistance to the ASME Sect. XI Working Group on Flaw Evaluation in their ongoing effort to develop criteria to govern the operation of reactor vessels when the 50-ft-lb LUS Charpy energy requirements of 10 *CFR* 50, Appendix G, are exceeded. A major challenge in the development of these rules has been the unavailability of validated procedures for extrapolation of material J-R curves. This has been overcome in the proposed ASME Sect. XI criteria by basing the rules on a demonstration of crack stability rather than on the demonstration of fixed margins on load carrying capability. The pressure loading used in the proposed rules reflects the reactor system relief valve setpoint pressure and the relief valve pressure-volumetric discharge characteristics but will not exceed 110% of the vessel design pressure.

5 Fracture Analysis Computer Programs

Validation of the current version of the OCA-P computer program for the probabilistic fracture-mechanics analysis of

reactor vessels subject to PTS loading was completed. Comparisons with results from the VISA II, ADINA-T, and ADINA computer programs were used in the validation process. One result from this activity was the identification of an area in which it appeared that the VISA II computer program required modification; this modification has since been implemented.

Development of the OCA-P program to give it the capability to perform PTS sensitivity analyses was completed. The revised program can evaluate sensitivity of the PTS analysis result to subclad and embedded flaws and to spatial variations in irradiation fluence.

Plans were completed for the development of the next-generation PTS analysis computer program. The program will use the OCA-P program as a point of departure and incorporate the latest PTS analysis technology refinements. The program will conform with the requirements of NQA-1 and is designed to be "user friendly."

6 Cleavage-Crack Initiation

The development phase of the shallow-flaw testing program has been completed. Square test specimens (100 mm) have been selected for the production phase of the program since this will permit the use of prototypical crack depths. Results from the program can then be interpreted both in terms of the absolute crack depth "a" and the relative crack depth a/W.

Tests with beam thicknesses of 50, 100, and 150 mm gave very similar results. This suggests that the current ASTM E399 requirements for test specimen thickness may be overly conservative.

The shallow-flaw fracture-toughness tests were conducted at temperatures in the lower transition region. At $T - RT_{NDT}$ of –25°C, the shallow-flaw specimens showed a 70% increase in toughness relative to the deep-crack toughness. This translates to an RT_{NDT} shift of 30°C.

A modification of the Irwin factor is being studied as a possible means for application of the shallow-flaw fracture-toughness data to pressure-vessel fracture margin analysis.

Development of techniques for determining lower-bound fracture-toughness properties using small specimens continued at UM. The program uses Charpy and notched tensile specimens, with the notches sharpened by precompression of the specimen. Lower-bound fracture toughness was successfully predicted for temperatures up to $T - RT_{NDT} = 50°C$. A draft paper summarizing this work has been prepared.

7 Cladding Evaluations

At NRC request, an independent analysis was performed to evaluate a vendors proposal for an alternate procedure for demonstrating compliance with low temperature overpressurization protection (LTOP) requirements. A key element of the vendors proposal was the inclusion in the analysis of a crack-tip stress-intensity factor contribution due to clad-base material differential thermal expansion. The objective for the independent analysis was to check the validity of this element of the vendor's proposal.

The analysis was performed using both 3-D finite-element models and the model incorporated into the OCA-P computer program. Results obtained confirmed the overall adequacy of the vendors analysis procedure for treating the effects of cladding differential thermal expansion. Maximum differences between results from the proposed and check analysis methods did not exceed 15%.

8 Pressurized-Thermal-Shock Technology

Thermal streaming in the reactor vessel downcomer annulus has been reported in experiments performed in the German HDR reactor vessel. Thermal streaming results when cool safety system flow is injected into a stagnant inlet pipe. The resulting circumferential nonuniform temperature can generate increased axial thermal stresses in the circumferential welds. These stresses are not currently included in the PTS analysis computer programs.

During the current reporting period, finite-element analyses of a reactor vessel shell under thermal-streaming boundary conditions was initiated. Output from the analysis will provide the basis for a thermal-streaming model to be incorporated into the updated OCA-P computer program.

9 Analysis Methods Validation

During the current reporting period, the focus for this task has been on the evaluation of results from the CSNI/FAG project FALSIRE. Results from analysis of large-scale fracture experiments contributed by an international group of fracture technology research organizations were collected, compared, and evaluated by ORNL and GRS-Koln. Application of J_R methodology using small-specimen data was generally successful in distinguishing between stable crack growth and tearing instability. The technology was much less successful in predicting the amount of crack extension caused by ductile tearing. The analysis experience highlighted the problem of diagnosing the cause of a deviation between test observations and analysis predictions when the test involves multiple variables. The need for more extensive characterization of the test material was also determined. A draft report on Project FALSIRE is in preparation.

10 Fracture Evaluation Tests

Fracture-toughness testing to determine the elevation of fracture toughness for prototypical shallow flaws in A 533 grade B class 1 material continued. The shallow-flaw program is structured into development and production phases. Activity in the current reporting period was in both the development and production phase of the program. Fourteen development tests were completed.

Two alternate techniques for locating the beam center of rotation under conditions of nonlinear response were evaluated. A technique using strain gages located ahead of the crack was demonstrated to give predictable and consistent results and was selected for use in the production phase of the program. Clip-gage attachment techniques were also refined and finalized, and tests were conducted on beams with out-of-plane thicknesses of 51, 102, and 145 mm (2, 4, and 6 in.). Fracture toughness appeared to be insensitive to the thickness variation. A thickness of 102 mm (4 in.) was selected for the production-phase beams. The auxiliary test fixture was delivered, as was material from the surplus Midland reactor vessel. This material is planned for use in a later phase of the program to investigate structural weld and cladding weld effects on shallow-flaw fracture toughness.

HEAVY-SECTION STEEL TECHNOLOGY P .OGRAM SEMIANNUAL PROGRESS REPORT FOR OCTOBER 1990–MARCH 1991*

1 Program Management

W. E. Pennell

The Heavy-Section Steel Technology (HSST) Program is conducted for the Nuclear Regulatory Commission (NRC) by Oak Ridge National Laboratory (ORNL). The program focuses on the development and validation of technology for the assessment of fracture-prevention margins in commercial nuclear reactor pressure vessels (RPVs).

Prior HSST Program actions resulted in the generation and validation of a fracture-mechanics-based, fracture-margin-assessment technology and the transfer of that technology to national consensus codes and standards. Subsequent input from materials-irradiation effects research, reactor vessel surveillance programs, and large-scale fracture technology validation experiments have revealed additional fracture-technology issues with regulatory significance. Current HSST Program activities have been structured to provide resolution of those issues and support near-term licensing actions.

Licensing issues of current concern include pressurized-thermal-shock (PTS), low-temperature overpressure protection (LTOP) set-point criteria, low-upper-shelf (LUS) material, and plant aging. Research tasks are selected and planned to provide NRC with timely input for the resolution of these issues. Specific research tasks in progress address shallow-flaw fracture toughness, PTS analysis methodology, development and validation of PTS analysis computer programs, cladding effects, constraint effects, circumferential flaws and out-of-plane loading effects, local brittle zones (LBZs), cyclic straining effects, ductile tearing, reviews of industry reports, embrittlement issue investigations, and the development of codes and standards.

The program is implemented in a series of tasks, each with its own task leader. A level 1 work breakdown structure outlining the program is given in Fig. 1.1. Staffing for the program tasks is drawn from the Engineering Technology,

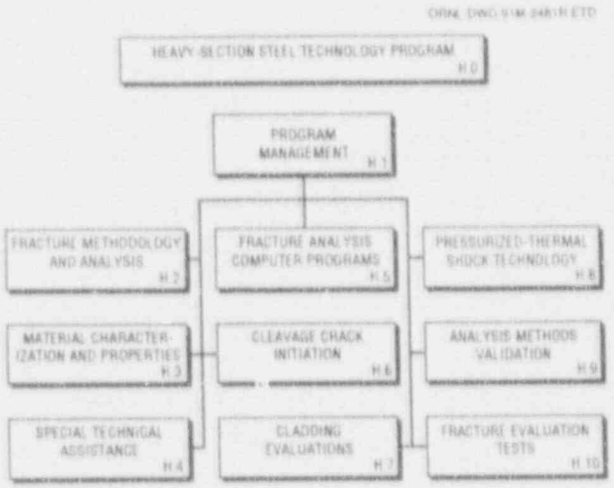

Figure 1.1 Level 1 work breakdown structure for HSST Program

Metals and Ceramics, and Computing and Telecommunications Divisions at ORNL. In addition, extensive use is made of university and other laboratory subcontractors and interaction with other research organizations to ensure efficient and timely achievement of the program's research objectives. In the current reporting period a contract was placed with Prof. S. T. Rolfe of the University of Kansas for consulting services on the shallow-flaw fracture-toughness testing program. Figure 1.2 provides a summary of the resources applied to the program tasks.

A comprehensive cost/schedule control system is used to monitor progress against objectives, identify and quantify variances, and guide corrective actions. At the end of the reporting period the program cost and schedule variances were +$17.8K and –$64.2K, respectively, on a total planned expenditure of $1570K. The principal contribution to the negative schedule variance was from the shallow-flaw, fracture-toughness testing program (Task 10). Corrective actions applied to that program corrected this negative schedule trend and produced a significant recovery in both the cost and schedule variances.

*This report is written in metric units. Conversions from SI to English units for all SI quantities are listed on a foldout page at the end of this report.

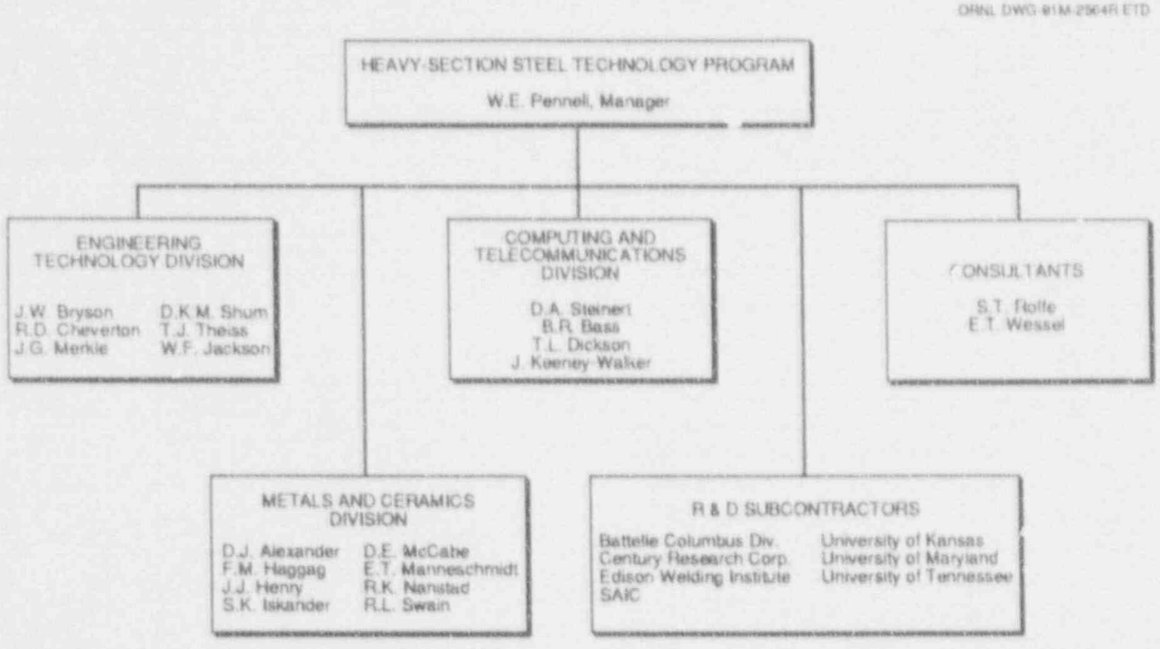

Figure 1.2 Resources applied to HSST Program R&D tasks

During the current report period, HSST Program personnel published one semiannual progress report,[1] two presentations[2,3] as NUREG/CP documents, three ORNL/NRC Letter Reports,[4–6] one paper[7] in an international proceedings, and one article[8] in a peer-reviewed journal. Two presentations[9,10] were made at the NRC 18th Water Reactor Safety Information Meeting, one administrative review[11] was made for NRC, and three presentations[12–14] were made to technical societies. ORNL organized and hosted a technology exchange with the VTT research center of Finland on Structural Safety Assessment of Nuclear Power Plant Components.* The program management joined with personnel from Framatome (France) in organizing four sessions on Pressure Vessel Integrity for the ASME-PVP meeting scheduled for June 1991 in San Diego, California.

References

1. W. E. Pennell, Martin Marietta Energy Systems, Inc., Oak Ridge Natl. Lab., "Heavy-Section Steel Technology Program Semiannual Prog. Rep. October 1989–March 1990," USNRC Report NUREG/CR-4219, Vol. 7, No. 1 (ORNL/TM-9593/V7&N1), March 1991.*

2. J. Keeney-Walker, B. R. Bass, and R. H. Bryan, "Ductile Fracture Analysis of Low-Upper-Shelf Tearing Experiment V-8A," pp. 3–81 in *Proceedings of the Seminar on Assessment of Fracture Prediction Technology: Piping and Pressure Vessels*, Nashville, Tenn., June 18, 1990, USNRC Report NUREG/CP-0037, February 1991.*

3. J. Keeney-Walker et al., "Fracture Analysis of a Thick-Walled Pressure Vessel Under Pressurized-Thermal-Shock Loading (PTSE-2)," pp. 3–131 in *Proceedings of the Seminar on Assessment of Fracture Prediction Technology: Piping and Pressure Vessels*, Nashville, Tenn., June 18, 1990, USNRC Report NUREG/CP-0037, February 1991.*

4. E. F. Rybicki and J. R. Shadley, The University of Tulsa for Martin Marietta Energy Systems, Inc., *Residual Stress Evaluation of a K-Bevel Weld*, ORNL/NRC/LTR-90/27, October 31, 1990.

*The HSST staff made ten presentations at the Joint VVT-ORNL Seminar on Structural Safety Assessment of Nuclear Power Plant Components, Oak Ridge, Tenn., December 10–11, 1990.

5. F. M. Haggag and R. K. Nanstad, Martin Marietta Energy Systems, Inc., Oak Ridge, Natl. Lab., *Effect of Thermal Aging on the Mechanical Properties of Stainless Steel Cladding*, ORNL/NRC/LTR-91/5, March 6, 1991.

6. J. Keeney-Walker and B. R. Bass, Martin Marietta Energy Systems, Inc., Oak Ridge Natl. Lab., *Analysis of Low-Temperature Overpressurization Transient in a Reactor Pressure Vessel*, ORNL/NRC/LTR-91/6, March 27, 1991.

7. J. G. Merkle, "An Application of the J Integral to an Incremental Analysis of Blunting Crack Behavior," pp. 319–332 in *Defect Assessment in Components—Fundamentals and Applications*, ESIS/EGF9, J. G. Blauel and K.H. Schwalbe, eds., Mechanical Engineering Publications, London, 1991. †

8. R. D. Cheverton et al., "Impact of an Apparent Radiation Embrittlement Rate on the Life Expectancy of PWR Vessel Supports," *Nucl. Safety* 32(1), 91–102 (January–March 1991).†

9. T. L. Dickson, "Potential Impact of Enhanced Fracture Toughness Data on Pressurized-Thermal-Shock (PTS) Analysis," presented at the *Eighteenth Water Reactor Safety Meeting, October 22–24, 1990*, Rockville, Md.

10. W. E. Pennell, "Heavy-Section Steel Technology Program Overview," presented at the *Eighteenth Water Reactor Safety Meeting, October 22–24, 1990*, Rockville, Md.

11. W. E. Pennell, ORNL, "Heavy-Section Steel Technology Program," presented to E. S. Beckjord et al. from NRC Headquarters as part of an review of NRC HSST Program at ORNL on November 28, 1990.

12. D. E. McCabe, *A Comparison of Weibull and β_{1c} Analysis of Transition Range Data*, presented at the ASTM E24 Committee Meetings in San Antonio, Texas, November 13, 1990.

13. T. L. Dickson, *Impact of Probabilistic Fracture Mechanics Methodology, Enhanced Fracture Toughness Data, and Thermal Streaming on PTS Analysis*, presented at the ASME Section XI Working Group on Flaw Evaluation, San Diego, Calif., February 5, 1991.

14. W. E. Pennell, *Heavy-Section Steel Technology Program*, presented at the ASME Section XI Working Group on Flaw Evaluation, San Diego, Calif., February 5, 1991.

---

*Available for purchase from National Technical Information Service, Springfield, VA 22161.

†Available in public technical libraries.

2 Fracture Methodology and Analysis

B. R. Bass*

2.1 Introduction

The following sections describe recent advances made in the coordinated effort being conducted under the HSST Program by ORNL and several subcontracting groups to develop the experimental data base and the analytical tools required to construct improved fracture models for RPV steels.

During this report period, work continued on (1) an investigation of the relationship between positive straining parallel to the crack front and crack-initiation toughness, (2) studies of analysis methods for shallow cracks in beams loaded in 3-point bending (3PB), (3) relationships between constraint and cleavage crack-arrest toughness, and (4) the joint Japanese/U.S. EPI Program for the development of an engineering estimation scheme applicable to inhomogeneous materials and structures.

2.2 Applicability of Plane-Strain Fracture Toughness Toward the Evaluation of Circumferential Surface Cracks

The objective of this subtask is the development of analysis methods for estimating the decrease in crack-initiation toughness, from a reference plane-strain value, due to positive straining along the crack front of a circumferential flaw in an RPV. This objective is accomplished by examining the influence of a given magnitude of the transverse strain on the near-crack-tip fields. The results from the above stress and strain analyses are viewed in the context of various fracture prediction models, thereby providing a methodology for estimating the influence of positive transverse strain on fracture toughness.

2.2.1 Compilation of Experimental Data Correlating Transverse Strain with Fracture-Toughness Data
(D. K. M. Shum)

A part of the transverse straining workscope in FY 1991 is the preparation of available experimental data in formats suitable for comparison with analytical model predictions. In this context, work has been undertaken to re-examine the ORNL wide-plate enhanced (WP-1) and nonenhanced (WP-2) cleavage crack-initiation fracture-toughness data. Two distinct approaches to the interpretation of wide-plate data have been taken. Emphasis of the first approach is in terms of T-stress effects, while the second approach is in terms of the thickness reduction correlation scheme (based on work by George Irwin at the University of Maryland, University of Maryland Technical Report No. 90-3, May 1990).

Analyses based on a modification of the Ritchie-Knott-Rice (RKR) cleavage crack-initiation model in which T-stress and transverse strain effects are included are being performed to determine if this approach would provide an explanation of the observed wide-plate cleavage initiation data for both series WP-1 and -2. The absence of valid small-specimen cleavage initiation data in the transition region appears to preclude a similar analysis of the cleavage reinitiation data. Work is also progressing on the application of the thickness reduction correlation scheme to series WP-1 and -2 data.

Metals and Ceramics Division at ORNL has obtained posttest residual transverse displacement measurements for a number of small specimens for which the fracture toughness values are available. Specifically, transverse displacement measurements were taken from the 1/2T to 4T compact-tension (CT) specimens previously tested to provide wide-plate series WP-1 characterization data. These measurements were taken at two locations: (1) approximately 10 times the crack-tip-opening displacements (CTODs) ahead of the original crack front, and (2) a distance ahead of the original crack front that appeared to yield a maximum value of the transverse displacement. Most of the small specimens examined have the common feature that the posttest transverse strains are much larger than those encountered during the wide-plate series WP-1 tests, even though much higher initiation toughnesses are associated with the wide-plate tests. The primary difficulty encountered in data interpretation is that the transverse strain contribution due to crack growth appears to dominate the posttest measurements. As a result, it is not possible to extract the magnitude of the transverse strain in the vicinity of the crack front at the onset of crack initiation in a straightforward manner. Transverse-strain values at the onset of crack initiation are

*Computing and Telecommunications Division, Martin Marietta Energy Systems, Inc., Oak Ridge, Tenn.

needed for the purpose of validating analytical model predictions against available negative transverse strain experimental data. Three-dimensional (3-D) finite-element analyses have been undertaken to determine an empirical scheme that would identify and eliminate the contribution to transverse strain due to crack growth from the posttest data.

2.2.2 Fracture Analysis of a CT Specimen Subjected to Generalized Plane-Strain Loading (B. R. Bass and J. Keeney-Walker)

The effects of negative and positive out-of-plane strain on local crack-tip fields in a model of a 1T-CT specimen are described in this section. Results presented here represent an extension of the studies previously performed on the same specimen and reported in Chap. 7 of Ref. 1. In both cases, analyses were carried out on a 3-D finite-element model of the CT specimen that assumed an incremental elastic-plastic constitutive formulation and generalized plane-strain loading conditions. The present study utilized a finite-element model having substantially greater crack-tip mesh refinement when compared with the model described in Ref. 1. The more refined model was employed to generate improved estimates of the crack-tip stress and strain fields corresponding to cleavage-initiation conditions. A parameter based on the area, A_{CR}, enclosed within a contour of critical maximum principal stress ahead of the crack tip[2] was used to correlate these local crack-tip fields with applied loading at initiation. Results of these correlations from the improved model are presented for a range of imposed out-of-plane strain values.

2.2.2.1 Analysis Methods

A 3-D finite-element model of a geometry having the planform of a 1T-CT specimen was generated with the ORMGEN[3] mesh-generating program. From symmetry conditions, only one-fourth of the specimen is included in the finite-element model (Fig. 2.1). The specimen in Fig. 2.1 has a thickness of 1.016 mm and was analyzed with the ADINA[4] finite-element program using special constraints on the nodal displacements to approximate generalized plane-strain (GPS) conditions. At any planform location in the model, the nodes (through the thickness) are constrained to have the same in-plane displacements. To model the effects of positive or negative out-of-plane strain, the nodes on the outer surface of the specimen are

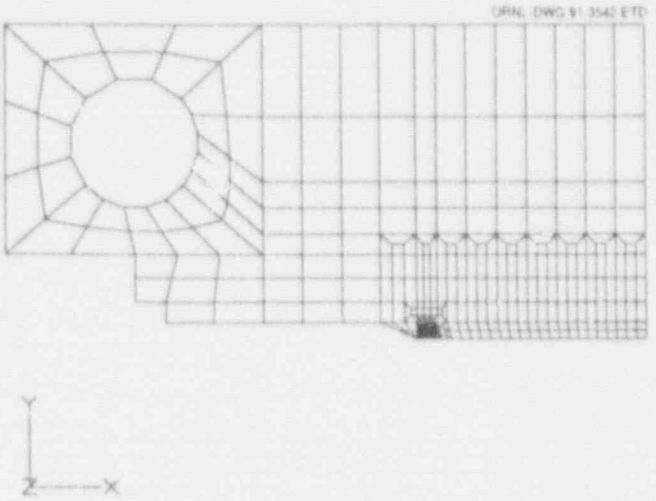

Figure 2.1 Three-dimensional finite-element model of 1T-CT specimen subjected to GPS condition

displaced uniformly in the direction normal to the surface; nodes midway between the midthickness symmetry plane and the outer surface are displaced by half that amount. The model depicted in Fig. 2.1 consists of 5033 nodes and 674 twenty-noded isoparametric elements. Collapsed-prism elements surround the crack tip to allow for blunting and for a 1/r singularity in the strains at the crack front. The radial dimension of the collapsed-prism elements at the crack tip is r = 0.01524 mm ($r/w = 3 \times 10^{-4}$). A detailed plot of the crack-tip region is given in Fig. 2.2. By comparison, the radial dimension of the collapsed-prism element at the crack-tip in the finite-element model of Ref. 1 was r = 0.11 mm (r/w = 0.00215).

The 3-D model of the 1T-CT specimen was analyzed using material properties for A 533 B steel at –75°C (taken from Ref. 5). An incremental elastic-plastic constitutive model (Model 8 in ADINA) was used for these analyses. For all cases, Young's Modulus is E = 206.9 GPa and Poisson's ratio ν = 0.3. The multilinear stress-strain curves for the material are given in Fig. 6.3 of Ref. 1. A material nonlinear only (MNLO) formulation (small-strain theory) was used to model the strain response to deformation. A $2 \times 2 \times 2$ Gauss point rule was employed to compute the global stiffness matrix. Incremental loading was applied to the load-pin hole of the model in the form of a cosine function with a resultant maximum load of 0.035 MN. In tests of 1T-CT specimens at T = –75°C (described in Ref. 5) cleavage initiation was achieved at loads of 0.029

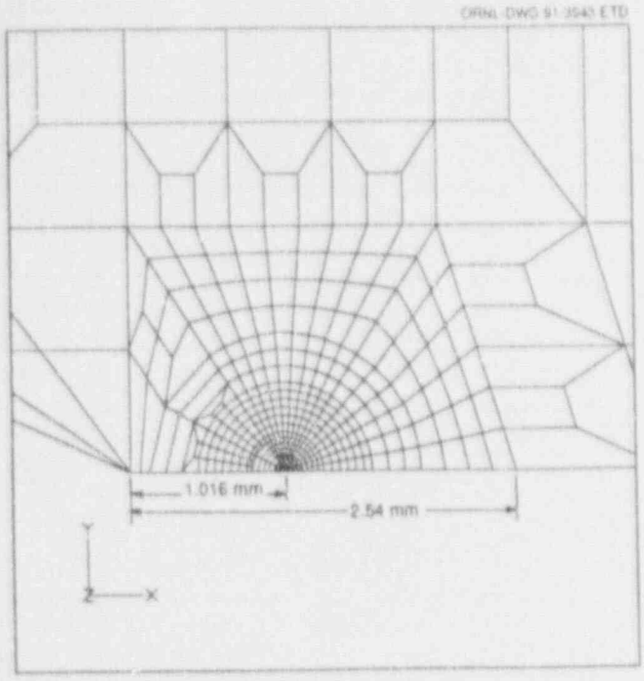

Figure 2.2 Detail of crack-tip region of finite-element model of 1T-CT specimen

and 0.035 MN. Equilibrium iterations were performed in each load step of the ADINA calculations using a convergence tolerance of 1×10^{-4} on an energy norm and 1×10^{-6} on an Euclidian norm of the displacement vector. For each load step of the calculations, energy release rates were determined along the crack front using a virtual crack-extension technique developed by deLorenzi[6] and implemented in the ORVIRT[7] program. (The ORVIRT program functions as a postprocessor on a conventional finite-element solution obtained from the ADINA program.)

2.2.2.2 Analysis Results

The 3-D model of the 1T-CT specimen depicted in Fig. 2.1 was analyzed for the load cases given in Table 2.1. In each load case, the mechanical loading at the load-pin hole and the uniform out-of-plane strains were applied simultaneously and monotonically in 35 equal increments up to the maximum/minimum values indicated in Table 2.1. The out-of-plane strains were imposed via equivalent out-of-plane nodal-point displacement. In Table 2.1, the normalized out-of-plane strain for case 1 ($\varepsilon_z/\varepsilon_0 = -1.05$) was selected to yield a computed J_I value equal to the experimentally determined J_I value ($J_I = 0.0263$ MJ/m^2) reported in Ref. 5 for the initiation load of 0.035 MN.

Table 2.1 Out-of-plane strain conditions imposed on generalized plane-strain model of 1T-CT specimen

Load case	Normalized out-of-plane strain[a] ($\varepsilon_z/\varepsilon_0$)
1	–1.05
2	–0.5
3	0
4	+0.5

[a]Maximum/minimum imposed uniform strain; maximum load of 0.035 MN applied to load pinhole.

The relationship between the area, A_{CR}, within the critical maximum principal stress contour and the applied J_I value for the GPS model of the 1T-CT specimen is shown in Fig. 2.3. The values of area in Fig. 2.3 were determined from the relation $A = V/B$, where V is the volume for which $\sigma_{pl} > 1400$ MPa is satisfied, and B is the thickness of the CT specimen. If a critical value of J_I is measured at crack initiation under plane-strain conditions ($e_{OP} = 0.0$), the critical J value required for initiation under GPS conditions ($e_{OP} \neq 0.0$) can be estimated from Fig. 2.3. Generally, this approach provides an estimate of the elevation or reduction of critical load required for achieving a critical area for initiation, A_{CR}, based on the magnitude and sign of the out-of-plane strain.

Comparison of the refined-mesh results in Fig. 2.3 with the corresponding results in Fig. 7.5 of Ref. 1 indicates that mesh refinement did not substantially alter the J vs A_{CR} relation expressed as a function of out-of-plane strain. Both sets of analyses imply that positive out-of-plane strains lead to a reduction in fracture toughness on the order of a few percent from the reference plane-strain value. Additional results from these calculations will be presented in a topical report on HSST circumferential flaw studies to be issued in FY 1992.

2.2.3 Modified-Boundary-Layer Model of Near-Crack-Tip Region (D. K. M. Shum)

The primary focus of this subtask is on the development of a finite-element-based description of the near-crack-tip region and will provide a more detailed and realistic description of the near-crack-tip fields than was available in

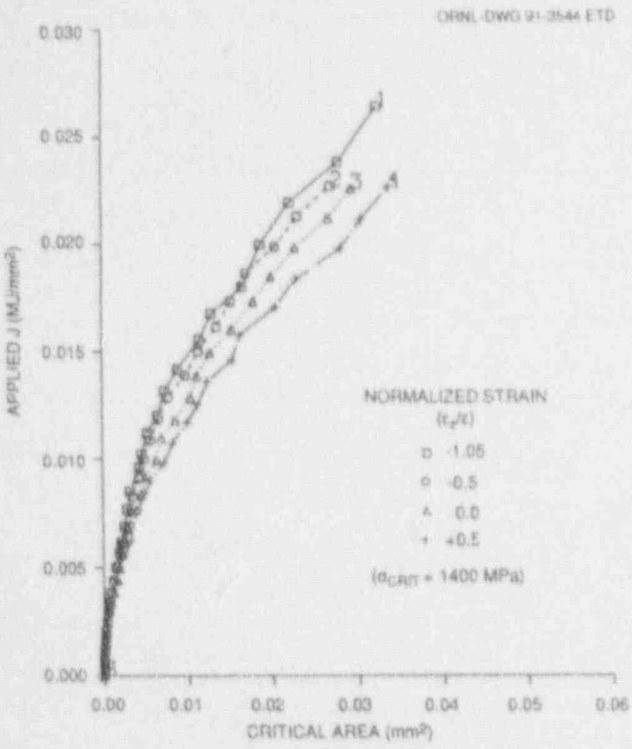

Figure 2.3 Applied J vs area A within maximum principal stress contour of σ_{pl} = 1400 MPa for 1T-CT specimen subjected to five load cases

FY 1990. Results from these near-tip analyses will provide improved inputs to the various fracture-toughness-prediction models developed in the first phase of this work, thereby providing the framework for evaluating and modifying the various fracture models.

A modified-boundary-layer formulation has been adopted in the finite-element description of the near-crack-tip region. In a modified-boundary-layer formulation, the in-plane geometry and loading conditions pertinent to a circumferential flaw are naturally incorporated into the analysis as remote boundary conditions, such as the imposition of remote K- or J-fields. Such an approach permits the evaluation of near-crack-tip stress and strain fields with a degree of accuracy not economically achievable with conventional application of the finite-element method to fracture problems.

In addition to its relevance to the transverse straining issue, it is emphasized that the finite-element-based near-tip model development from this subtask, in the form of a modified-boundary-layer model, is also expected to address various issues related to the transferability of small- and large-specimen toughness data to RPV applications. Specifically, these issues include the problem of estimating the elevation of toughness that occurs due to transverse contraction in a small surveillance specimen tested in the transition region, providing an explanation for the apparent toughness enhancement obtained in the ORNL wide-plate tests, and the interpretation of shallow-flaw toughness values to be obtained within the HSST Program. The unifying feature in all these issues appears to be the role of the second parameter in the associated fracture problem. A brief description of the essential features of such an approach was given in the previous semiannual report.

Benchmarking of the finite-element predictions from the commercial finite-element code ADINA and the ORNL finite-element code ADINA-VPF against known solutions was undertaken. The benchmarking was to verify the accuracy of these codes and ascertain the suitability of using these codes to generate detailed near-crack-tip fields and to study T-stress effects. Also, work has begun to acquire the commercial finite-element code ABAQUS to perform these calculations.

2.2.4 Constraint Effects for Circumferential Flaws (C. W. Schwartz, University of Maryland*)

The Mode I crack-tip stress and strain conditions for a circumferential flaw in a pressure vessel differ from those in conventional laboratory fracture test specimens in one potentially significant aspect: the strains parallel to the crack front are tensile, as opposed to zero (plane strain) or compressive (plane stress). It is reasonable to hypothesize that this condition may influence the constraint at the crack tip and, as a consequence, the resistance of the material to crack initiation.

The variation of cleavage fracture toughness with constraint within the range between plane-stress and plane-strain conditions is well known.[8–10] Conceptually, constraint is a secondary characteristic of the crack-tip stress and strain fields (the primary characteristic being the singularity in the fields) that promotes fracture mechanisms

*Work sponsored by the HSST Program Subcontract No. 19X-07778C between Martin Marietta Energy System, Inc., and the University of Maryland.

within the fracture process zone (e.g., increases crack-opening stresses) and inhibits energy-absorbing plastic flow within the region surrounding the fracture process zone. Constraint is usually associated with high triaxiality of the crack-tip stress fields. Under ideal plane-strain conditions, this triaxiality develops because the contraction parallel to the crack front is prevented, producing tensile stresses parallel to the crack front, in addition to the tensile in-plane stresses. In a circumferentially flawed pressure vessel, the tensile hoop stresses also act parallel to the crack front, further increasing the triaxiality of the near-tip stress state.

In the present study, the nature of the crack-tip constraint for a circumferential flaw in a pressure vessel has been investigated through high-resolution, nonlinear finite-element analyses. This study is focused on the comparison of constraint in the circumferential flaw configuration with that in a corresponding plane-strain reference condition. The flaw geometry considered here is the limiting case of a continuous inner circumferential flaw in a cylindrical pressure vessel. However, the insight gained from the study of this idealized configuration has some relevance for the more realistic case of a finite-length circumferential surface flaw. More complete details of this study are given in Ref. 11.

2.2.4.1 Analysis Model

A circumferentially flawed pressure vessel was simulated using two-dimensional (2-D), nonlinear finite-element analyses. The vessel was treated as a cylinder having an internal radius r_i of 2171.7 mm (85.5 in.) and a wall thickness W of 215.9 mm (8.5 in.); these dimensions are typical for RPVs. The circumferential flaw was assumed continuous around the inner beltline of the vessel with a crack length a equal to 53.98 mm in the radial direction (a/w = 0.25). No crack extension was considered in the analyses.

Three different loading configurations were analyzed: (1) a reference plane-strain condition under axial loading only; (2) axisymmetric conditions under axial loading only; and (3) axisymmetric conditions under combined internal pressure, crack-face pressure, and axial loading. All loads were applied incrementally from values corresponding to essentially linear, very small-scale yielding conditions to levels just beyond general yielding of the vessel wall.

The finite-element model of the assumed geometry incorporated sufficiently fine discretization to permit adequate resolution of the stress and strain fields within distances on the order of ten CTODs from the crack tip; the radial dimension of the elements at the crack tip is ~0.02 mm (r/w = 0.000124). All finite-element calculations were performed using the ABAQUS analysis code.[12]

The material stress-strain behavior was modeled using the Ramberg-Osgood power law-deformation plasticity constitutive model:

$$\varepsilon / \varepsilon_o = \sigma/\sigma_o + \alpha(\sigma / \sigma_o)^n \quad , \qquad (2.1)$$

with the following values for material constants: elastic modulus $E = \sigma_o/e_o = 300$, Poisson's ratio $\nu = 0.3$, $\sigma_o = 1$, $\alpha = 1$, and $n = 10$. These properties were selected, in part, to permit comparisons with previously published results. A small strain formulation was employed in all analyses.

J-integral values were computed using the virtual crack-extension algorithm as implemented in ABAQUS.[12,13] Ten contours were evaluated to establish path independence for the J-integral values.

2.2.4.2 Analysis Results

O'Dowd and Shih[14] have formulated a two-parameter expansion of the near-tip elastic-plastic stress fields in a Ramberg-Osgood power-law hardening material:

$$\sigma_{ij}/\sigma_o = \left[J/(\alpha\varepsilon_o\sigma_o I_n r)\right]^{1/(n+1)} \tilde{\sigma}_{ij}(\theta) + Q\left[(r)/(J/\sigma_o)\right]^q \hat{\sigma}_{ij}(\theta) + \text{higher order terms} \, . \qquad (2.2)$$

The first term represents the usual HRR singularity[8,9] with amplitude equal to J. The second-order term has the dimensionless parameter Q as its amplitude. The functions $\tilde{\sigma}_{ij}(\theta)$ and $\hat{\sigma}_{ij}(\theta)$ capture the angular variation of the stress fields and are expected also to depend on the material hardening; the $\hat{\sigma}_{ij}(\theta)$ functions are normalized such that $\hat{\sigma}_{\theta\theta}$ equals 1 at $\theta = 0$. Note that the second-order expansion in Eq. (2.2) assumes a small-strain formulation because it is based on the HRR solution.

The second-order stress field for a crack in an infinite region can be extracted by subtracting the HRR solution from a two-parameter boundary layer numerical solution at the same J value. The parameters Q, q, and $\hat{\sigma}_{ij}(\theta)$ can then be evaluated. Based on their numerical results, O'Dowd and Shih make the following arguments: (1) the variation of the second-order stress fields with radial distance is very weak, hence $|q| \ll 1$; (2) the $\hat{\sigma}_{ij}(\theta)$ functions vary weakly with θ over $\theta \le \pi/2$; (3) the $\hat{\sigma}_{r\theta}(\theta)$ terms are very small, and thus the $\hat{\sigma}_{rr}(\theta)$ and $\hat{\sigma}_{\theta\theta}(\theta)$ terms correspond to the principal stresses of the second-order stress field; and (4) $\hat{\sigma}_{rr}(\theta) / \hat{\sigma}_{\theta\theta}(\theta) \cong 1$ for $\theta \le \pi/4$, that is, the second-order fields closely approximate a state of hydrostatic stress in this sector. As a consequence of the above arguments, Eq. (2.2) can be reasonably approximated within the sector $\theta \le \pi/4$ as follows:

$$\sigma_{ij}/\sigma_0 \cong J/(\alpha\varepsilon_0\sigma_0 I_n r)^{1/(n+1)}\hat{\sigma}_{ij}(\theta) + Q\delta_{ij}\hat{\sigma}_{ij}(\theta) . \qquad (2.3)$$

In essence, the constant Q is a triaxiality parameter, except for the *second-order* fields.

Following O'Dowd and Shih's approach, the second-order crack-tip fields along the crack plane $\theta = 0$ have been extracted from the computed stresses for the three loading configurations analyzed in the present study. The in-plane tangential and radial stresses are given in Figs. 2.4 and 2.5 for the axisymmetric/combined load configuration; the results for the axisymmetric/axial load and reference plane-strain configuration are qualitatively similar and can be found in Ref. 11. Figures 2.4(*a*) and 2.5(*a*) summarize the total computed stresses and Figs. 2.4(*b*) and 2.5(*b*) give the second-order component only. All load levels in Figs. 2.4 and 2.5 correspond to contained yield conditions. The results shown in these figures are very similar to those found by O'Dowd and Shih. There is a slight variation of the second-order stresses with radial distance—perhaps somewhat more than observed by O'Dowd and Shih, but still quite small. Q is always negative for the three loading configurations considered here and becomes more negative with increasing load level and consequent yielding.

The three loading configurations considered in this study can be compared by considering the second-order tangential stress field along the crack plane:

$$Q^* = Q[r/(J/\sigma_0)]^q ; \qquad (2.4)$$

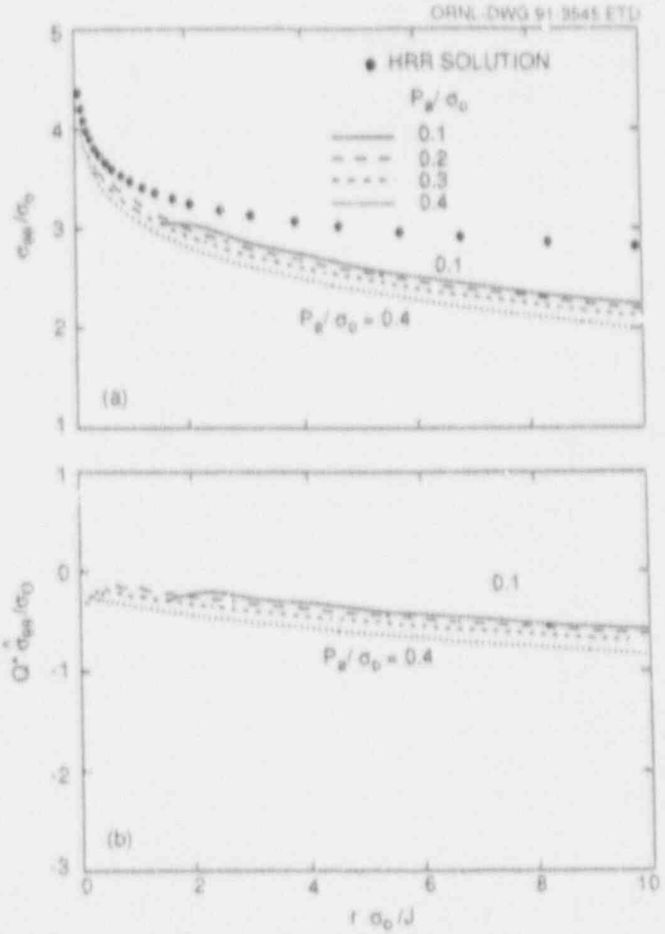

Figure 2.4 Total and second-order tangential normal stresses along crack plane $\theta = 0$ for axisymmetric/combined load configuration. Contours correspond to load levels $p_g/\sigma^0 = 0.1$, 0.2, 0.3, and 0.4. Contained yield conditions obtain at all load levels shown

thus, $Q^* = Q^* = Q$ at $[r/(J/\sigma_0)]^q = 1$. The results of this procedure are summarized in Fig. 2.6 for all three loading configurations. The Q values for all configurations and load values are always negative, with smaller (i.e., more negative) values indicating lower constraint. The constraint in the axisymmetric/axial load configuration is slightly less than that for the plane strain reference case at all load levels. The constraint in the axisymmetric/combined load case, however, is substantially less than in both of the other two configurations.

The low constraint for the axisymmetric/combined load configuration is quite the opposite of what is intuitively

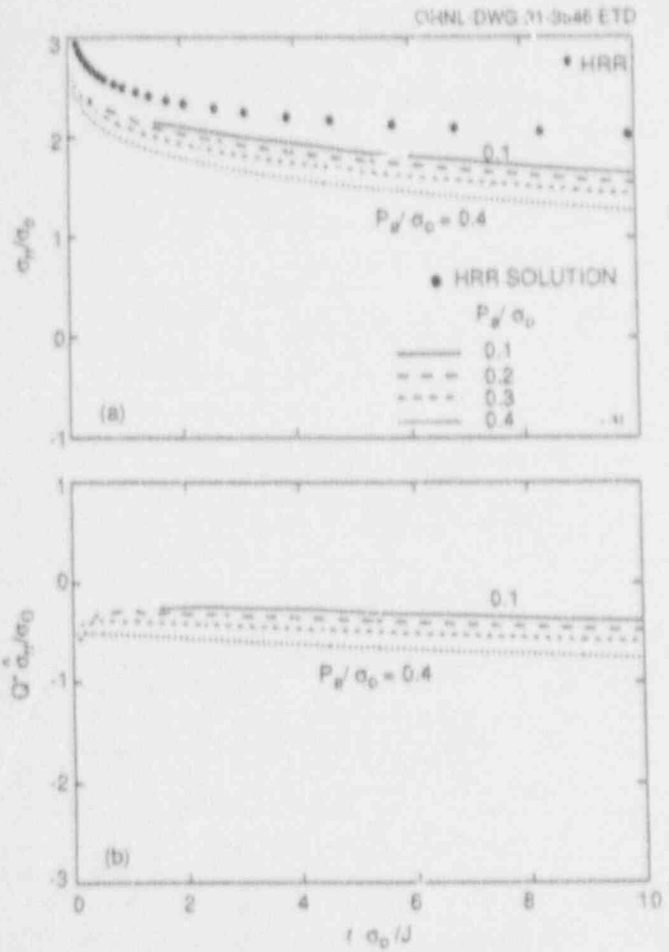

Figure 2.5 Total and second-order radial normal stresses along crack plane $\theta = 0$ for axisymmetric/combined load configuration. Contours correspond to load levels $p_B/\sigma^0 = 0.1$, 0.2, 0.3, and 0.4. Contained yield conditions obtain at all load levels shown

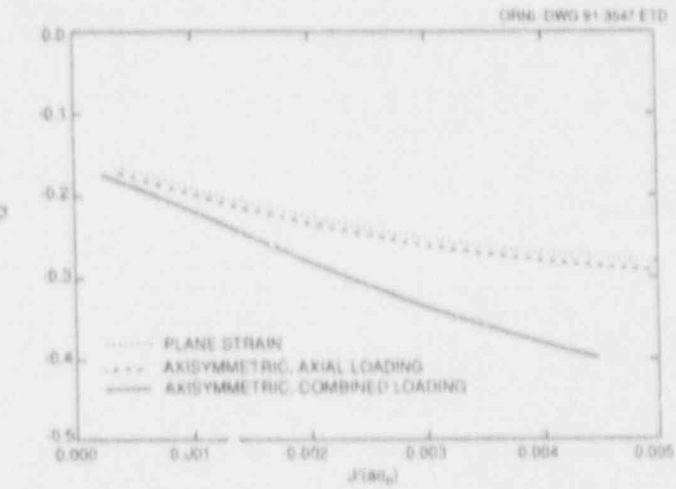

Figure 2.6 Variation of Q with load level for all three loading configurations under contained yield conditions

expected. However, other evidence supports this lower constraint. In the axisymmetric/combined loading case, there are also radial compressive stresses acting parallel to the crack plane that are not present in either the plane strain or axisymmetric/axial load configurations; these stresses are due to the internal pressure loading of the vessel.

Compressive radial stresses correspond to a more negative in-plane stress biaxiality, which in turn is associated with lower constraint. The magnitude of this in-plane stress effect can be quantified in terms of a dimensionless biaxiality parameter B (Ref. 15):

$$B = T(\pi a)^{1/2}/K_I \qquad (2.5)$$

in which T is the magnitude of the second-order term of the remote linear elastic stress fields.[16–19] For the plane-strain configuration, the computed value for B is –0.33. The computed B value for the axisymmetric/axial load case is –1% smaller (more negative) than that for the reference plane-strain configuration; this is consistent with the slightly lower constraint indicated in Fig. 2.6. The computed B value for the axisymmetric/combined load configuration is –0.43, or 30% smaller than that for the reference plane-strain case; this is consistent with the significantly lower constraint indicated for this configuration in Fig. 2.6.

2.2.4.3 Conclusions

The Q-stress approach is a rigorous quantitative measure of crack-tip constraint that appropriately focuses on the details of the near-tip stress fields. By this measure, the constraint at the tip of a shallow circumferential flaw in a pressurized vessel is always less than that in an equivalent plane-strain condition under axial loading only; by implication, the apparent fracture toughness is correspondingly elevated for the circumferential flaw configuration. This difference in constraint is due more to in-plane than out-of-plane effects, however. Specifically, it is due to the more negative in-plane stress biaxiality resulting from the radial pressure applied to the inner surface of the vessel. This stress biaxiality effect will be greatest for shallow flaws, whose tips are nearest the inner surface where the radial

compressive stresses are the largest. Thus, shallow flaws in pressure vessels, which already exhibit higher toughness simply because they are shallow, will exhibit an additional toughness elevation because of stress biaxiality.

Additional factors not yet considered will also affect the constraint magnitudes for circumferentially flawed pressure vessels. Constraint can be expected to change with a/w ratio (e.g., because of the different T-stresses), hardening and other material properties, and the ratio of vessel internal radius-to-wall thickness (which changes the hoop stress and strain magnitudes). Finite-width surface flaws must also be considered, particularly under PTS loading conditions and thermal streaming. These factors will be subjects of future analyses.

2.3 Analyses in Support of the Shallow-Flaw Testing Program (D. K. M. Shum)

Elastic-plastic, plane-strain, finite-element analyses were performed in support of the shallow-crack testing program under Task 6. These analyses were performed in response to the need to extend the length of the 3PB specimens in future tests. The main objectives of these analyses are to determine the size and location of plastic zones in a specimen with a 86.4-cm (34-in.) span as compared to a specimen with a 40.6-cm (16-in.) span. Preliminary analyses were carried out for two specimen geometries: 5.1 × 10.2 × 40.6 cm (2 × 4 × 16 in.) and 10.2 × 10.2 × 91.4 cm (4 × 4 × 36 in.) with a 86.4-cm (34-in.) span, and for two flaw depths, a/w = 0.1 and 0.5. Effects of variability in analytical boundary conditions were compared with experimental results so that proper analytical/experimental correlations could be achieved.

In addition, finite-element analyses were undertaken to determine the validity limits of the Rice-Paris-Merkle (RPM) single-specimen J-integral estimation formula. The RPM formula was developed to determine the applied J-integral value from a single experimental load vs load-line-displacement (LLD) record for deeply cracked, bend-type geometry. The finite-element analyses were undertaken to examine the appropriateness of using the RPM formula for determining the applied J-integral value for shallow-crack geometries.

Results from the finite-element analyses indicate use of the RPM formula based on a deep-crack formulation would result in grossly overestimated J-integral values for the shallow-crack geometry a/w = 0.1. The primary implication of these analyses to the shallow-crack testing program is that correction factors would need to be developed for the shallow-crack geometries. Numerically generated correction factors (η factors) based on the area under the load vs LLD curve have been obtained for the geometries examined to date. Use of these η factors will allow appropriate J-integral values to be determined in shallow-crack specimens using the basic RPM formulation.

2.4 Cleavage Crack-Arrest Toughness and Constraint (G. R. Irwin, University of Maryland*)

The objective of this subtask is the development of an improved fracture model relating cleavage crack-arrest toughness of RPV steels to levels of specimen constraint. The approach focuses on interpretations of events implied by fracture surfaces generated in tests of small- and large-scale specimens from the HSST Program. If the K value is large enough to support a substantial spreading of cleavage, following localized cleavage initiation, it might be reasonable to assume that the cleavage initiation K value is at least as large as the K_{1a} value for cleavage arrest in the same material. A more cautious conclusion, allowing for variability of K_{1a}, would restrict the "lower bound" natural crack-arrest toughness to the smallest possible values of K_{1a}. Actually, from available data, the average of multiple K_{1a} determinations seems to provide a lower bound for multiple K (initiations) tests with small specimens. Possibly much of the observed scatter in the American Society for Testing and Materials (ASTM) E1221 tests of K_{1a} is in the conduct and analysis of the tests rather than in the material. A continued effort toward improved K_{1a} testing is clearly desirable.

An additional feature of interest pertaining to cleavage crack-arrest toughness is the apparent insensitivity of the arrest K values to specimen thickness and constraint. The cleavage arrest K values provided by ORNL thermal-shock experiments pertained to long crack fronts. Due to thermal stress loading, the tension near and parallel to the crack

*Work sponsored by the HSST Program Subcontract No. 19X-07778C between Martin Marietta Energy Systems, Inc., and the University of Maryland.

front was larger than that pertaining to simple plane strain. The cleavage arrest K values provided by these ORNL experiments covered a temperature region of "T minus RT-NDT," which overlaps the temperature region of K_{Ia} values (determined using essentially ASTM method E1221) and the temperature region of crack-arrest K values furnished by dynamic analysis of wide-plate tests at the National Institute of Standards and Technology (NIST). If some upward scatter of K-arrest values in the wide-plate tests is considered, all of these results agree closely with a single-trend curve as a function of $T - RT_{NDT}$, despite very large differences in degree of constraint. The ORNL thermal-shock-experiments (TSE) used A 508 steel, while the wide-plate tests and the small-specimen (E1221) tests used A 533 B steel. Possibly, the temperature shift ($T - RT_{NDT}$) does not completely compensate for steel material differences. However, small specimens of the ORNL A 508 material were tested at Battelle Columbus Division and furnished K arrest values that agreed with results from the TSEs, despite the use of a thickness (25 mm) moderately less than specified in method E1221. In addition to these experimental results, there are mechanistic reasons, related to cleavage behaviors, which indicate that an insensitivity of cleavage crack-arrest toughness to the degree of constraint is quite plausible.

Realistically, in a spreading cleavage fracture, the crack front region is composed of an irregular array of incompletely connected cleavage facets. During cleavage extension, numerous reinitiations produce new facets, filling lagging regions of the average crack front and producing new forward bursts of separation. The connections between facets, often undercut, deform, and break, mainly with ductile fractures, during progressive opening of the general separation. The average forward speed of the cleavage process is regulated mainly by the pause times at reinitiations. The array of cleavage facets composing the crack front somewhat resemble a flattened cloud. Also a contributing factor to the flattening toward an average crack plane is that stresses high enough to produce reinitiation tend to occur close to an arrested edge of a previous facet. In addition, the favored facet orientations are those that deviate only moderately from being normal to the direction of largest tension.

Regarding the influence of constraint upon K values for crack arrest, the effect of constraint upon the crack front facet array must be considered. Note that the cleavage fractures produced by the ORNL TSEs show fracture surface out-of-plane irregularities, along lines parallel to the average crack front, that are much larger than those observed in small-specimen K_{Ia} tests or in the NIST wide-plate tests. This is expected because the increase of tension parallel to the crack front augments the tendency of cleavage facets to form separations on planes that deviate largely from the average plane of the complete separation. In effect, an increase of constraint tends to thicken the crack front facet "cloud" and increase the size of the "fracture process zone." From the experimental results noted previously, the elevation of tensile plastic flow stress by constraint, as would be expected to assist cleavage, is compensated for because constraint has no significant effect upon crack-arrest K values.

Some consideration of the crack-front plastic zone is merited because the forward spreading of cleavage must penetrate that region. During a period when "strain aging" was an active research topic, tests were made, using low-strength steels, of the shift of the Charpy V-notch (CVN) energy curve as a function of temperature in the brittle-ductile transition range after various amounts of cold work. Significant influences of prior plastic deformation of 10% or less were never observed. In the NIST wide-plate tests, the thickness reduction strain near the crack plane was <4%. Thus, the plastic strain before cleavage in the crack-front plastic zone should have no appreciable effect upon the cleavage behavior.

2.5 Elastic-Plastic Fracture in Inhomogeneous Materials and Structures Program (B. R. Bass,* G. Yagawa, University of Tokyo†)

The principal purpose of the EPI program is to investigate the elastic-plastic crack-growth phenomena in inhomogeneous materials and structures, with the goal of developing estimation schemes for fracture resistance through the cooperative work between United States and Japanese research consortia.

The Japanese consortium in charge of the EPI program has been organized under the Century Research Center Corporation since July 1988 as one of the subcommittees of the Nuclear Engineering Research Committee of the Japan

*Computing and Telecommunications Division, Martin Marietta Energy Systems, Inc., Oak Ridge, Tenn.

†Work sponsored under subcontract 19X-50561V, University of Tokyo, Tokyo, Japan.

Welding Engineering Society (JWES). The EPI subcommittee members are from 9 universities, 3 research institutes, and 21 companies. Three working groups (WGs) have been set up under the following subcommittees: Theoretical, Experimental, and Estimation Scheme.

The experimental WG conducts tests and generates experimental data of crack-growth behavior in inhomogeneous specimens. These data are used for numerical analyses to examine the applicability of various elastic-plastic fracture-mechanics parameters to the inhomogeneous material regime. This WG also examines the effects of various factors on fracture behavior, including crack-tip location and crack orientation with respect to fusion line (FL), specimen thickness, and residual stress.

The theoretical WG analyzes the experimental results using various numerical as well as analytical methods not only to understand the crack-growth phenomena in inhomogeneous materials but also to provide the fundamental data for the development of the estimation schemes of crack-growth resistance.

The estimation scheme WG, which was established in the fall of 1989, analyzes the experimental results using conventional estimation schemes to examine the applicability of these methods to the inhomogeneous material regime. The estimation scheme WG also works on the investigation and development of alternative estimation schemes based on experimental as well as numerical results.

2.5.1 Literature Survey

In the last fiscal year, the EPI Program selected the following two categories of estimation schemes of elastic-plastic fracture resistance. (1) J-integral formula used in 2-D fracture-toughness and -resistance tests and (2) J-integral formula for the integrity assessment of 3-D structures with through-wall and surface cracks.

The first category involves the Merkle-Corten's formula J_{M-C} for CT specimens and Rice's formula J_R for 3PB specimens in stationary crack problems, and the J-deformation J_D and the J-modified J_M in growing crack problems. Through experimental studies, various arguments have been made on the validity and applicability of J_D and J_M. On the other hand, incremental fracture-mechanics parameters such as the $\hat{J}$ and T^* integrals have been studied in the theoretical as well as numerical works.
The latter category includes the General Electric/Electric Power Research Institute (GE/EPRI) approach, the R6 approach, and the LBB.NRC approach. This year, the EPI Program also began assessing the applicability of those parameters and approaches to the evaluation of crack-growth resistance in the inhomogeneous material regime through round-robin analyses.

2.5.2 Material and Welding Procedure

The specimens tested this year were machined from the same plates used the previous year. The A 533 grade B class 1 steel was prepared, and the following plates were produced: one base plate and seven welded plates with an FL of 1000 mm in length and ~30 mm in thickness. The configurations of all the plates are identical, that is, 1000 mm long, 500 mm wide, and 50 mm thick. The welding technique used is the submerged-arc welding (SAW) and the k type of bevel is adopted to obtain a phase boundary parallel to the thickness direction. The six welded plates and one base plate were heat-treated at 600°C for 2 h for of stress relief. Among them, one welded plate is used to obtain fundamental material properties, and the other six stress-relieved plates are used to measure crack-growth behavior under the residual-stress condition. The as-welded plate will be used to examine residual stress effects.

2.5.3 Residual-Stress Measurement

One Japanese group performed nondestructive measurements of residual stresses in a heat-treated plate with a weldment using an acoustoelastic technique. The distribution of residual stress along the plane, that is, mean values in the thickness direction, was measured by this method. One U.S. group also measured the distribution of residual stress in the thickness direction of an identical plate using a strain-gage method. The mean values of residual stress in the thickness direction measured by a strain-gage method were much smaller than those of the acoustoelastic method. On the other hand, the component of residual stress in the direction parallel to the FL, measured by another Japanese group using the X-ray method, agreed well with that of the acoustoelastic method. More careful comparisons of the results and procedures are still necessary to examine the accuracy of these methods in measuring residual stresses.

[illegible] been estimated from these measurements that [illegible] esses found in the heat-treated plates are very small compared with the yield stress of the present material. The EPI Program plans to conduct fracture analyses with residual stresses to confirm their effects precisely. CT specimens taken from the as-weld plate will be also tested and analyzed for comparison.

2.5.4 Fracture Experiments on 2-D Specimens

2.5.4.1 Specimens

Some homogeneous and welded CT and 3PB specimens were tested in addition to the experiments conducted last year. Side grooves were machined in all the additional specimens, and initial crack tips were prepared in three locations: heat-affected zone (HAZ), FL, and weld metal (WM). While fabricating the specimens with a crack tip in the HAZ, the initial crack tip was located ~1.5 mm from the FL, with allowance made for some error.

Most additional specimens are the CT type, where the plane dimensions are the same as those of the standard 1T-CT specimen, but the thicknesses chosen were 6, 10, or 19 mm. Initial cracks were set to be normal or perpendicular to the FL.

A few 3PB 19-mm-thick specimens were also prepared to examine the effects of specimen configuration. To avoid any confusion because of different testing procedures, these additional experiments were performed in only two research groups.

A multiple specimen method and an unloading compliance method were utilized to measure the precise crack-growth amount.

2.5.4.2 Effects of Specimen Thickness on Initiation Toughness

The experimental results obtained last year from specimens without side grooves showed some variations of initiation toughness due to thickness effects. However, because of the introduction of side grooves, such variations in initiation toughness could not be observed for the welded specimens whose thickness ranges from 6 to 19 mm.

2.5.4.3 Effects of Crack Orientation on Initiation Toughness

The initiation toughness of two kinds of CT specimens, that is, crack orientation parallel to the FL and normal to the FL, were compared with each other. Two kinds of homogeneous CT specimens, in which initial cracks were machined either parallel or normal to the rolling direction, were tested for comparison.

Significant effects of crack orientation on initiation toughness were observed, but it was confirmed that they might be caused by the anisotropic nature of rolled materials.

In the crack-growth experiments on the CT specimens in which an initial crack was set to be along the FL, it was also observed that a crack starting from the FL turns gradually on the HAZ part, which was harder but less tough than the base metal (BM) and WM parts. It should be noted here that mixed-mode effects have to be taken into account in the above crack-growth phenomena.

2.5.4.4 Effects of Crack-Tip Location on Crack-Growth Resistance

To examine the effects of crack-tip location, the following three kinds of welded specimens were tested: (1) specimens in which the crack tip is placed in the BM; (2) specimens in which the crack tip is placed in front of the FL, that is ,in the HAZ part; and (3) specimens in which the crack is placed across the FL. Initial cracks were normal to the FL in all cases.

The J-integrals evaluated here are the J-deformation J_D and the J-modified J_M. The results can be summarized as follows:

1. The initiation toughness of specimen 1 is greater than that of specimen 2, and then its increasing rate of crack-growth resistance dJ/da decreases in the HAZ part and again increases in the WM part.
2. The initiation toughness of specimen 2 is smallest among the three, but after a crack passes the FL, its crack-growth resistance increases more steeply than before.

It may be expected from these experiments that the local variation of material toughness along the crack-growth path is detectable by monitoring crack-growth resistance by means of the conventional J-integrals.

2.5.4.5 Effects of Specimen Configuration

To examine the effects of specimen configuration, similar experiments were performed on welded 3PB specimens in which initial cracks were placed normal to the FL, and crack-tip locations were varied in the HAZ, FL, and WM.

Similar correlations between crack-growth resistance and crack-tip location were observed in both 3PB and CT specimens. In addition, toughness values obtained from both 3PB and CT specimens agreed well with each other. It was conclued from these results that a specimen configuration such as the CT or 3PB type does not influence crack-growth behavior even in the inhomogeneous material regime. The experimental results obtained thus far are to be utilized for the generation-phase, crack-growth analyses.

2.5.4.6 Direct Measurement of Crack-Tip Behavior

To establish measurement techniques of near crack-tip behavior in an elastic-plastic regime, we examined a grid method and a moire interferometry method, both of which were assisted by computer image processing techniques. This year both methods were applied to measure crack-tip fields of welded specimens made of A 533 B class 1 steel. Last year, the grid method was also applied to measure crack-tip fields in type 304 stainless steel. The results obtained by the grid method can be summarized as follows:

1. The crack-tip displacement field can be roughly divided into three regions in closest order to a crack-tip: the nonlinear region where the slope is steeper than $1/(n+1)$, the HRR region where the slope is $1/(n+1)$, and the linear region where the slope is 0.5. Here n is a hardening exponent of power-law hardening materials. The sizes of these fields strongly depend on hardening exponent and crack growth.
2. In the case of A 533 B class 1 steel, the HRR displacement field is surrounded by the linear region at an initial loading stage. As a crack grows, the HRR field shrinks gradually and disappears due to the extension of the nonlinear region. The above feature agrees well with those of some aluminum alloys ($n \approx 4.12$) measured with a moire interferometry method by A. S. Kobayashi.
3. In the case of type 304 stainless steel, the results for a sufficiently small amount of crack extension are consistent with those of A 533 B class 1 steel. On the other hand, the HRR displacement field is replaced by the linear elastic field for a large amount of crack growth. Such difference of crack-tip singular fields between the two steels for large-scale crack growth may be caused by the different capability of developing crack blunting before stable crack growth.
4. It should also be emphasized here that no significant difference was observed in either displacement or strain distributions measured for homogeneous and welded CT specimens made of A 533 B class 1 steel.

The characteristics of the moire interferometry method in the application to ductile materials such as A 533 B class 1 steel were also clarified this year through preliminary experiments. It was found that a relatively less sensitive moire grid might be useful in the measurement of ductile materials, and also that this method might have the capability of measuring caustic images without polishing the specimen surface.

These two methods will be used to examine experimentally the validity of incremental fracture-mechanics parameters such as the $\hat{J}$ and T^* integrals.

2.5.5 Fracture Experiments on Surface-Cracked Specimens

A series of 3PB specimens containing semelliptical surface cracks were tested this year. For each specimen, a surface crack was machined perpendicular to the FL. That is, half of the crack was placed in the BM and the other half in the WM, with the FL located on the minor axis of the crack. The aspect ratio of the crack is controlled by using a special starter for a fatigue precrack. The crack-mouth-opening displacement (CMOD) was measured using an optical method. After loading, the CTOD was measured using a silicon rubber casting method; the amount of crack growth (Δa) was measured directly using scanning electron microscopy (SEM). The crack-tip-opening angle (CTOA) was evaluated using both CTOD and Δa values.

Both homogeneous and welded specimens containing a semielliptical surface crack were tested to examine the effects of inhomogeneity on crack-growth behavior by varying the aspect ratio and crack depth. The results can be summarized as follows:

1. No significant difference due to inhomogeneity can be observed in the distributions of crack growth and CTOD along the front of a surface crack in welded specimens; that is, those distributions were symmetrical with respect to the centerline of the surface crack, irrespective of weldment.
2. The CTOA values of welded specimens were much smaller than those of homogeneous specimens.

More experiments on various crack orientations will be performed next year. The experimental results will be compared with 3-D elastic-plastic, finite-element analyses.

2.5.6 Fracture-Mechanics Analyses Based on Elastic-Plastic, Finite-Element Methods

Fracture phenomena of inhomogeneous materials are influenced by several factors such as the inhomogeneity of material properties, residual stresses, and location of the crack tip. It is difficult to quantify the effect of each factor on fracture behavior solely through fracture experiments. It seems that numerical analyses are very suitable for such studies.

This year, round-robin, finite-element analyses of stable crack growth were performed on homogeneous and welded CT specimens in which initial cracks were oriented normal to the FL. Material properties were obtained from uniaxial tensile tests performed last year. Generation-phase, crack-growth simulations were performed using a measured relationship between crack (Δa), load-line displacement (δ), and applied load (P). One homogeneous and three welded CT specimens with different crack-tip locations were analyzed. Twenty percent side grooves were machined in all the specimens. The specimens are identified as follows:

1. specimen M5G, a homogeneous CT specimen of BM material;
2. specimen H5G, in which the crack tip is located in front of the phase boundary, that is, in the HAZ;
3. specimen F5G, in which the crack tip is located on the phase boundary; and
4. specimen D5G, in which the crack is located across the phase boundary.

Young's moduli of material Nos. 1 and 2 are taken to be 106 and 175 GPa, respectively, and yield stresses are 550 and 630 MPa, respectively. Nine participants performed the round-robin analyses. All the participants used eight-noded isoparametric elements and a nodal force release technique to simulate stable crack growth. The following fracture mechanics parameter were plotted against Δa:

- J-integral calculated along integration paths, J_{path},
- J-integral evaluated by the Merkle-Corten's formula, J_{M-C},
- J-modified, J_M,
- J-deformation, J_D,
- $\hat{J}$-integral, and
- T^*-integral.

It is well known that the conventional J-integral calculated along integration paths loses physical meaning and path independence when large-scale crack growth occurs. Nevertheless, J_{path} values were calculated along various integration paths because one of the objectives of the analysis was to study the correlation of J_{path} with J_{M-C}, J_M, and J_D during crack growth in inhomogeneous materials. The results can be summarized as follows:

1. Calculated and measured J_D values agree with each other within 10%.
2. All J values increase monotonically in accordance with crack growth, while the T^* value levels off after a certain amount of crack growth. The J-integral showed a trend similar to that of the T^*-integral.
3. The order of magnitudes of the J values is $J_M > J_{M-C} > J_D$. Note that the J_{path} values have shown strong path dependence.
4. Crack-growth resistance of specimen M5G is greater than that of H5G for all of the J-integrals.
5. The slope of the J-R curve for specimen H5G is steeper than that for specimen M5G.

6. The T^*-integral always levels off after a certain amount of crack growth, and the magnitude of T^* for specimen M5G is greater than that for specimen H5G. In specimen H5G, T^* increases gradually after the crack grows across the phase boundary.
7. The behavior of specimen D5G is similar to that of specimen M5G, while the behavior of specimen F5G is similar to that of specimen H5G.

In interpreting these results, note that the HAZ has lower initiation toughness than both WM and BM.

These analyses concluded that crack-growth phenomena in inhomogeneous materials are predictable using the conventional J-integral concepts, although the conventional J-integrals behave differently than the near crack-tip parameters, such as the T^*-integral and the $\hat{J}$-integral.

This year, crack-growth simulations were performed only for CT specimens in which a crack grew perpendicular to the phase boundary. Similar round-robin analyses will be performed next year on crack-generated data obtained from welded 3PB specimens.

2.5.7 Fracture Experiment Under Anisothermal Conditions

One of the fundamental problems related to the EPI Program was fracture under anisothermal conditions. A fracture experiment under anisothermal conditions was performed using the single-edge notched (SEN) specimens taken from the heat-treated base plate of A 533 B class 1 steel. The purpose of the present experiment is to examine the effects of gradual change of material toughness on fracture behavior. Pressure vessel materials may be subjected to such situations on the occasion of PTS events. The ligament length of the specimen was 113 mm, and the crack tip was cooled to –10°C using liquid nitrogen, while the temperature at the end of the specimen was set at 10°C. The temperature gradient at the crack tip was ~0.250°C/mm. For comparison, fracture-toughness tests were performed using CT specimens at temperatures varying from –50 to 10°C. The stress-intensity factor was evaluated by neglecting thermal stress effects. Only one experimental data point was obtained this year. No significant effects of anisothermal conditions on fracture behavior were observed; this may be due to the relatively small temperature gradient. An increased temperature gradient will be tried next year.

2.5.8 Elastic-Plastic, Finite-Element Analyses of 3-D Crack

Three dimensional, elastic-plastic, finite-element analyses were performed on the following specimens:

1. CT specimen,
2. center-cracked tension (CCT) specimen,
3. specimen with a semielliptical surface crack subjected to bending moment or tension, and
4. pipe with a semielliptical inner-surface cra k subjected to four-point bending load.

These analyses were performed mainly to focus on crack-tip singular fields around 3-D cracks and to study the theoretical basis of the J-integral in 3-D cases. The J-integral was evaluated using a line-integration technique. The results obtained are summarized as follows:

1. For the 1T-CT specimen, the HRR stress and displacement fields exist in the vicinity of the crack in the midplane of the specimens. For the 0.32-cm-thick (0.125-in.) CT specimen, the HRR stress field cannot be observed even at the center of specimen, but the HRR displacement field exists at the center of the specimen.
2. For CCT specimens, the HRR stress and displacement fields do not exist. This tendency agrees with results obtained from 2-D analyses.
3. For a plate with a surface crack, the HRR fields exist for a deep crack, irrespective of crack-aspect ratio and loading type, that is, tension or bending moment. On the other hand, the crack-tip fields of shallower surface cracks are not the HRR fields.
4. For a pipe with an inner-surface crack, the crack-tip fields are not the HRR fields.

It has been clearly demonstrated that the HRR fields can be observed only in the vicinity of cracks of limited types of specimens. This tendency seems to be correlated with stress distributions along uncracked ligament; that is, if stress is distributed from tension at a crack tip to

compression at the end of the specimen (just like a CT specimen), the HRR fields could be observed. On the other hand, if tensile stress is dominant along the uncracked ligament (just like a CCT specimen, a plate with a shallow-surface crack and a pipe with an inner-surface crack), the HRR fields could not be observed.

This year, analyses were performed on stationary crack problems. It is expected that material inhomogeneity and crack growth would cause a disturbance of the crack-tip fields, and further analyses will be performed next year.

2.5.9 Estimation Scheme Development

As a first step in the development of simple estimation schemes for inhomogeneous materials, two crack-growth experiments (M5G and D5G), analyzed with elastic-plastic, finite-element methods, were also analyzed using conventional estimation schemes.

The method used this year is the GE/EPRI method. In the inhomogeneous regime, we have several choices of material properties (α and n of the Ramberg-Osgood type relation) for use in the analyses, that is, base metal, weld metal, or some average of the two materials. We performed both the generation-phase analyses, in which a history of the J-integral is evaluated using the measured LLD vs crack-growth curve, and the application phase analyses, in which the maximum load is evaluated using the measured J-R curve.

When this method is applied to the analysis of the M5G specimen (a homogeneous CT specimen of BM), the maximum load was estimated with an error of 10%. When applied to the analysis of the D5G specimen (in which a crack is placed across the FL), the method using material properties of the BM overestimated the experimental results, while the method using material properties of the WM underestimated the experimental results. The simple average of the material properties of BM and WM gave the closest results to the experimental values.

In the experiments and in the round-robin analyses by elastic-plastic, finite-element methods, it is clearly shown that the slope of the J-integral changes during crack growth from HAZ through WM. This behavior is different from the crack-growth behavior in M5G and D5G specimens, in which a crack grows in homogeneous fields. To simulate behavior of crack growth in the H5G and F5G specimens, the use of material properties of a single material may no longer be reasonable; more analyses will be performed next year.

References

1. D. K. M. Shum et al., Martin Marietta Energy Systems, Inc., Oak Ridge Natl. Lab., "Analytical Studies of Transverse Strain Effects on Fracture Toughness for Circumferentially Oriented Cracks," USNRC Report NUREG/CR-5592 (ORNL/TM-11581), May 1991.*

2. J. Keeny-Walker, "A Numerical Study of Local Crack-Tip Fields for Modeling Cleavage Fracture Initiation," Master's Thesis, The University of Tennessee, Knoxville, May 1990.

3. B. R. Bass and J. W. Bryson, Union Carbide Corp. Nuclear Div., Oak Ridge Natl. Lab., "Applications of Energy Release Rate Techniques to Part-Through Cracks in Plates and Cylinders, Volume 1, ORMGEN-3D: A Finite Element Mesh Generator for 3-Dimensional Crack Geometries," USNRC Report NUREG/CR-2997/V1 (ORNL/TM-8277), December 1982.*

4. K. J. Bathe, "ADINA – A Finite Element Program for Automatic Dynamic Incremental Nonlinear Analysis," Massachusetts Institute of Technology Report 82448-1, revised 1978.†

5. D. J. Naus et al., Martin Marietta Energy Systems, Inc., Oak Ridge Natl. Lab., "Crack-Arrest Behavior in SEN Wide-Plates of Quenched and Tempered A 533 B Steel Tested Under Nonisothermal Conditions," USNRC Report NUREG/CR-4930 (ORNL/TM-6338), August 1987.*

6. H. G. DeLorenzi, General Electric Company, "On the Energy Release Rate and the J-Integral for 3-D Crack Configurations," TIS Report 80CRD113, 1980.*

7. B. R. Bass and J. W. Bryson, Martin Marietta Energy Systems, Inc., Oak Ridge Natl. Lab., "Applications of Energy Release Rate Techniques to Part-Through

Cracks in Plates and Cylinders, Volume 2, ORVIRT: A Finite Element Program for Energy Release Rate Calculations for 2-D and 3-D Crack Models," USNRC Report NUREG/CR-2997/V2 (ORNL/TM-8277), February 1983.*

8. D. Broek, *Elementary Engineering Fracture Mechanics*, 3rd ed., Martinus Nijhoff Publishers, The Hague, The Netherlands, 1982.†

9. M. F. Kanninen and C. H. Popelar, *Advanced Fracture Mechanics*, Oxford University Press, New York, 1985.†

10. J. M. Barsom and S. T. Rolfe, *Fracture and Fatigue Control in Structures*, 2nd ed., Prentice-Hall, Englewood, N.J., 1987.†

11. C. W. Schwartz, "Influence of Out-of-Plane Loading on Crack-Tip Constraint," in *Proc. of the ASTM Symposium on Constraint Effects in Fracture*, Indianapolis, May 1991.

12. *ABAQUS User Manual–Version 4.8.5*, Hibbit, Karlsson, and Sorenson, Inc., Providence, R.I., 1989.†

13. D. M. Parks, "The Virtual Crack Extension Method for Nonlinear Material Behavior," *Computer Methods in Applied Mechanics and Engineering* 12, 353–364 (1977).†

14. N. P. O'Dowd and C. F. Shih, "Family of Crack-Tip Fields Characterized by a Triaxiality Parameter: Part I— Structure of Fields," *Journal of the Mechanics and Physics of Solids* 9, 983–1015 (1991).†

15. P. S. Leevers and J. C. Radon, "Inherent Stress Biaxiality in Various Fracture Specimen Geometries," *International Journal of Fracture* 19, 311–325 (1982).†

16. J. R. Rice, "Limitations to the Small-Scale Yielding Approximation for Crack-Tip Plasticity," *Journal of the Mechanics and Physics of Solids* 22, 17–26 (1974).†

17. S. G. Larsson, and A. J. Carlsson, "Influence of Nonsingular Stress Terms and Specimen Geometry on Small-Scale Yielding at Crack Tips in Elastic-Plastic Material," *Journal of the Mechanics and Physics of Solids* 21, 263–277 (1973).†

18. B. A. Bilby et al., "A Finite Element Investigation of the Effect of Specimen Geometry on the Fields of Stress and Strain at the Tips of Stationary Cracks," pp. 37–46 in *Size Effects in Fracture*, Mechanical Engineering Publications Ltd., London, 1986.†

19. C. Betegon and J. W. Hancock, "Two-Parameter Characterization of Elastic-Plastic Crack-Tip Fields," *Journal of Applied Mechanics* 58, 104–110 (1991).†

---

*Available for purchase from National Technical Information Service, Springfield, VA 22161.

†Available in public technical libraries.

3 Material Characterization and Properties

R. K. Nanstad

Primarily for internal management and budgetary control, the HSST Program created a separate task (Task H.3) for the work on material characterization and properties determinations. However, for the reader's convenience, some contributions to this report are placed within other chapters according to the larger tasks that correspond to the particular material studied.

3.1 Characterization of HSST Plate 013B in the L-S Orientation

(S. K. Iskander)

The characterization of HSST Plate 013B in the L-S orientation for the Shallow-Flaws Task is under way. In the first phase, tests will be performed to obtain full CVN curves in the L-S orientation, RT_{NDT}, and the tensile properties in the L orientation as a function of temperature, for both surface and midthickness material. In the second phase, depending on whether the results exhibit a difference between the surface and midthickness properties, crack-initiation-toughness tests (K_{Ic}, K_{Jc}, or J-R) will be performed over the temperature range of interest using 25-mm CT specimens in the L-S orientation from either or both thickness positions.

HSST Plate 013 was manufactured by Lukens Steel in accordance with ASTM Standard Specification for Pressure Vessel Plates, Alloy Steel, Quenched and Tempered, Manganese-Molybdenum and Manganese-Molybdenum-Nickel (A 533), grade B class 1. A characterization block, designated as 13BA-5, was flame-cut from the 187-mm-thick HSST Plate 013B, as shown in Fig. 3.1. The characterization block, together with other flame-cut material to be machined into the shallow-flaw beam specimens, was given a postweld heat treatment (PWHT) of 621°C (1150°F) for 40 h to simulate the PWHT given to RPVs. The characterization will be performed in the same L-S orientation as the 3PB beam tests. HSST Plate 013A (the other half of HSST Plate 013) has been quite extensively characterized previously, but not in the L-S orientation, and apparently no PWHT was given.

The complement of specimens to be machined is given in Table 3.1. The ~187 × 710 × 835 mm (7 3/8 × 28 × 33 in.) characterization block 13BA-5 from HSST Plate 013B will be machined into specimens for the first-phase characterization, as shown schematically in Fig. 3.2. In this first phase of testing, we intend to obtain full CVN curves in the L-S orientation; determine RT_{NDT}; and determine the

Table 3.1 Specimen complement for characterizing HSST Plate 013B in L-S orientation for the shallow-flaws task

	Machined from characterization block 13B–A5 and postweld heat treated at 621°C (1150°F) for 40 h					
	CVN	CVN	P-3 DWT[a]	Tensile[b]	25-mm CT 1TC(T)	SEB[c]
Orientation	L-S	T-L[d]	e	L	L-S	L-S
Surface material	20	20	10	10	30[f]	
Midthickness material	20	20	10	10	30	4

[a]Both drop-weight NDT and RT_{NDT} were −23°C for HSST Plate 013A.
[b]Specimen gages were 6.35 mm in diameter.
[c]Single-edge 3PB specimens were 25 mm thick and 50 mm deep. Test results are required to determine whether geometry and restraint have an effect on crack-initiation toughness.
[d]Required for RT_{NDT} determination.
[e]Not applicable.
[f]Crack tip for 1TC(T) is 25 mm below the surface.

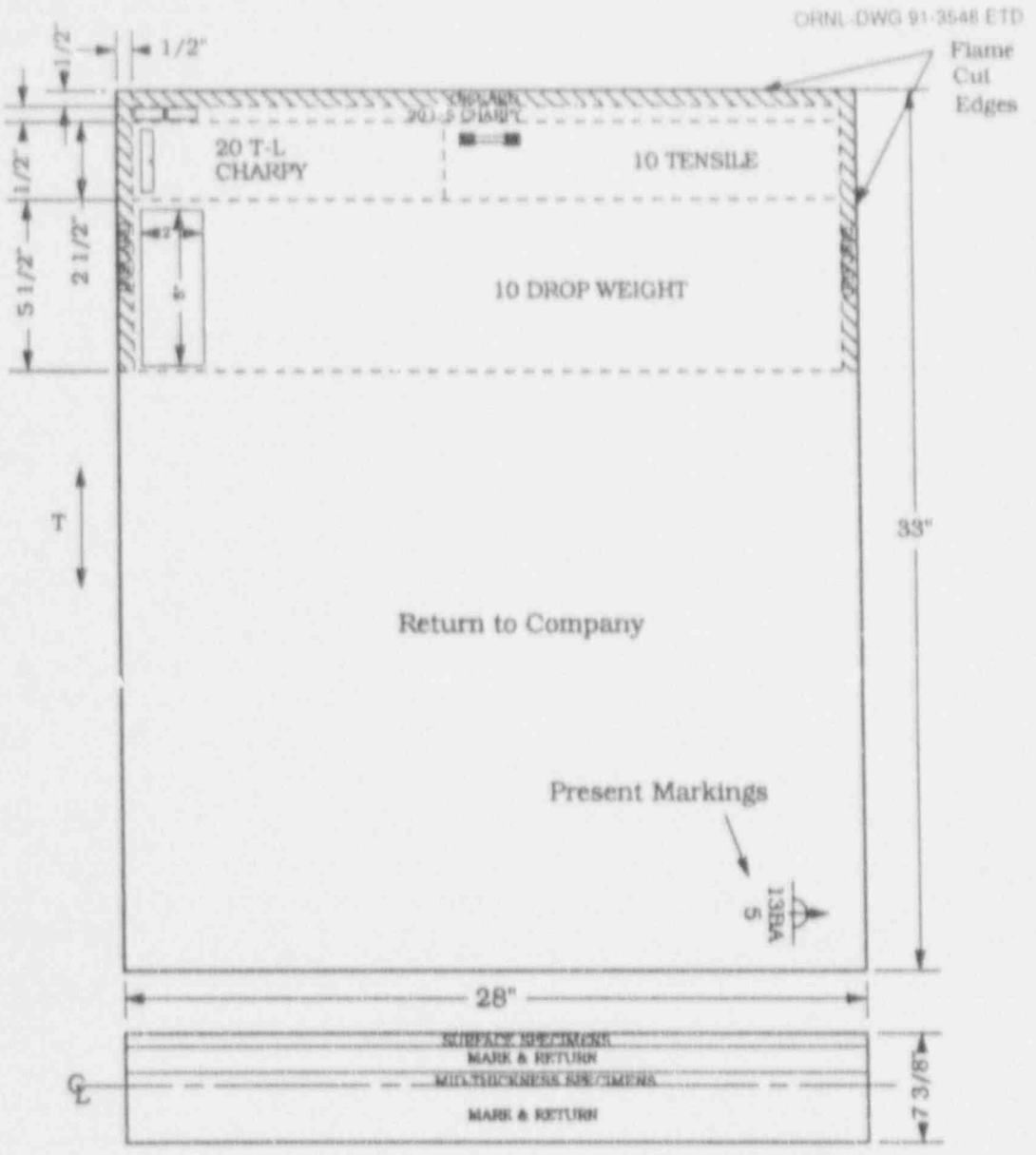

Figure 3.1 Location of ~187 × 710 × 835 mm characterization block 13BA-5 in HSST Plate 013B in relation to other slabs destined to be machined into beams for shallow-flaw program

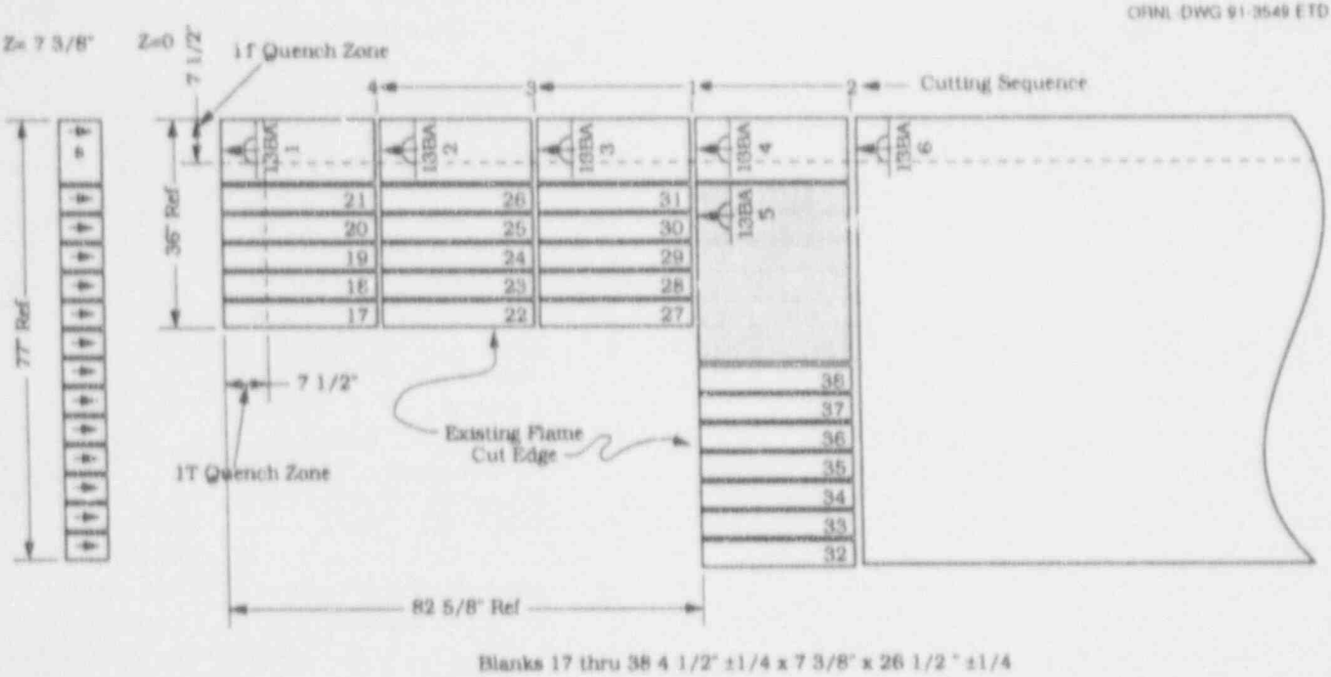

Figure 3.2 Schematic showing cut-up of characterization block 13BA-5 into specimens for first phase of tests

tensile properties in the L orientation, as a function of temperature, for both surface and midthickness material.

In the second phase, depending on whether the results exhibit a difference between the surface and midthickness properties, 25-mm-thick, standard compact [1TC(T)] specimens will be machined and tested from either or both thickness positions. Crack-initiation-toughness tests (K_{Ic}, K_{Jc}, or J-R) over the temperature range of interest in the L-S orientation will be performed.

A hardness traverse across the plate thickness will also be performed as a confirmation of significant (or lack of) variations in the properties in the thickness direction. Previous tests on HSST Plate 013A in other orientations did not show a significant variation in properties through the thickness.

In the final phase, a small number of 25-mm-thick, 50-mm-deep, 3PB specimens will be tested to compare the crack-initiation toughness with that from 25-mm-thick CT specimens.

3.2 Thermal Aging of Stainless Steel Cladding (F. M. Haggag and R. K. Nanstad)

Thermal aging at relatively low temperatures (343°C) has been shown to significantly degrade the Charpy impact toughness of type 308 stainless steel welds. The stainless steel cladding applied to the inner surface of RPVs is very similar to that material. Hence, an experimental program was initiated to evaluate the effects of thermal aging on stainless steel cladding relative to its contribution to toughness degradation during irradiation experiments as well as long-term effects.

Since the irradiation of the three-wire series-arc cladding to the highest fluence of 5×10^{19} neutrons/cm^2 (>1 MeV) was conducted at 288°C for 1605 h, tensile, CVN, precracked CVN (PCVN), and compact fracture-toughness specimens were thermally aged at 288°C for 1605, 20,000, and 50,000 h. Test results from the 1605-h specimens are summarized below. Thermal aging of stainless steel cladding at 288°C, and the ferritic steel on which it is overlaid, to accumulated times of 20,000 h (expected to be completed by November 1992) and 50,000 h is in progress.

Also, other cladding specimens are being aged at 343°C together with type 308 stainless steel weld materials from another NRC program.

Thermal aging of the three-wire stainless steel weld overlay cladding at 288°C for 1605 h resulted in an appreciable decrease (16%) in the CVN upper-shelf energy (USE), but the effect on the 41-J transition temperature shift was very small (3°C). The combined effect following neutron irradiation at 288°C to a fluence of 5×10^{19} neutrons/cm^2 (>1 MeV) was a 22% reduction in the CVN USE and a 29°C shift at the 41-J level. The effect of thermal aging on the tensile properties was very small or negligible. However, the combined effect after neutron irradiation was an increase (6 to 34% at test temperatures from 288 to −125°C) in the yield strength and no apparent change in ultimate strength and total elongation.

The preliminary analysis of the 0.5TC(T) fracture-toughness specimens indicates that thermal aging reduced the initiation fracture toughness (J_{Ic}) at room temperature and at 120°C; however, there was no apparent effect at 288°C. The effect of thermal aging on the tearing modulus was insignificant for all test temperatures (room temperature, 120, and 288°C). The effect of thermal aging at 288°C on the J_{Ic} at a test temperature of 288°C will be further clarified from J_{Ic} tests following the 20,000-h aging. Furthermore, the effect of thermal aging on the dynamic fracture toughness (K_{Id}) will be reported shortly, following the testing of PCVN specimens that were thermally aged with the other specimens.

3.3 ASTM Fracture-Toughness Testing Standards Development

(D. E. McCabe, D. J. Alexander, and R. K. Nanstad)

D. J. Alexander, D. E. McCabe, and R. K. Nanstad have participated in two ASTM working groups for fracture-toughness standards. The first is a Common Method that will combine K_{Ic}, J_{Ic}, J-R, and CTOD test methods into a single method. The second will combine the existing J_{Ic} and J-R test standards. McCabe has also participated in preparing a draft standard for testing in the transition region.

The Common Method has been written and presented to the ASTM membership. As part of the development, several sets of data have been gathered and distributed for analysis. This paper round robin is intended to reveal possible problems with the method and to point out areas of ambiguity in the draft document. ORNL is participating in this round robin. We have received the data sets and converted them into a compatible format for our existing analysis programs. These data will be analyzed for comparison with the Common Method. In addition, we are augmenting our analysis routine to include new developments from the Common Method.

The second working group is combining the J_{Ic} (E813) and J-R (E1152) standards. This group has also produced a draft document that combines the two earlier standards, and they are presently working on new additions to the draft to address some of the problems not covered by the present standards. The two major areas of this effort include (1) a data-shifting procedure for J-R data that is offset from the origin and (2) testing in the ductile-to-brittle transition regime.

The data-shifting procedure will attempt to bring data to the origin so a better estimate of J_{Ic} can be made. Work from ORNL was presented that used a polynomial expression to determine the offset. In addition, a procedure with a power-law expression proposed initially was determined to be unsuitable. However, the working group decided to use a linear fit to data, rather than the proposed polynomial expression, primarily because the linear procedure was simpler and easier to implement.

Testing in the transition regime is a great departure for the J standards, which have heretofore not allowed analysis of tests that fail by cleavage fracture. The present draft standard would allow J_{Ic} to be determined if there are enough satisfactory data points before the cleavage fracture event. The working group is also considering including a cleavage-toughness parameter under specified limits.

3.4 Analysis of Transition Region Fracture-Toughness Results

(D. E. McCabe)

A first draft of an ASTM standard, Test Practice for Fracture Toughness in the Transition Range, was written for the use of ASTM Task Group E24.08.08 on Ductile-Brittle Transition. The draft was based on published information, and many important issues were supported by experimental data developed within the HSST Program. The document was prepared to stimulate debate and promote technical input by the task group. The practice contains features that are unique to transition range testing, such as closer control of specimen precracking loads, specimen design to maximize valid K_{Jc} capacity, and recommended procedures for dealing with the K_{Jc} data scatter characteristics in the midtransition range. A primary objective of this standard will be to recommend the number of replicate tests necessary to locate the median of the material K_{Jc} toughness distribution.

Lower-bound K_{Jc} characterization will not be attempted now but can be considered a long-term objective.

3.5 Study of Low-Toughness Zones

(D. E. McCabe)

The work in this subtask is a joint project involving ORNL, Battelle-Columbus Division, and the University of Maryland (UM). The objectives are to develop data and to study issues relative to a user request to modify Appendix G of the *Code of Federal Regulations* (10 CFR 50). The request was to use the K_{Ic} curve instead of the K_{Ia} curve for establishing LTOP pressure/temperature limits.

A review article, "Investigation of the Bases for the Use of the K_{Ic} Curve," was prepared and presented at the American Society of Mechanical Engineers (ASME) Pressure Vessels and Piping Conference in San Diego. Issues addressed were those relevant to the aforementioned user request. Subjects reviewed were specimen size effects, determination of the shape of the lower-bound K_{Ic} curve for irradiated materials, evaluation of the significance of crack pop-ins, the difference between naturally formed cracks (such as arrested cracks) vs fatigue precracks on the observed K_{Ic} toughness, and the lower-bound K_{Ia} transition toughness after irradiation damage. Evidence gathered for the review article has suggested that fracture toughness of irradiated material can fall below the CVN 41-J ΔRT_{NDT} transposed K_{Ic} curve. On the other hand, the similarly transposed K_{Ia} curve was ~28°C conservative compared to K_{Ia} data but showed good correspondence between the 41-J shift and the K_{Ia} shift.

The task at UM was to evaluate the previously discussed issue of whether materials show a different K_{Ic} toughness when the starting crack tip is arrested (natural crack) vs a fatigue precrack. ORNL provided UM with bend bar specimens of A 508 at a strength level comparable to that used in thermal shock experiments TSE-5 and -5A. Tests were made at three temperatures with duplicate specimens of each crack type. The results are summarized in Fig. 3.3. In several cases the first event was a crack pop-in and occurred most frequently with the "natural cracks." If one favors final instabilities as the critical event, then this experiment suggests that there is no difference in toughness due to the two initial crack conditions.

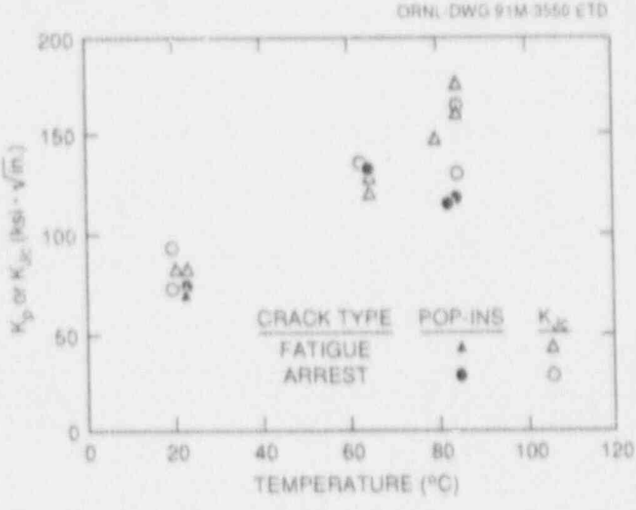

Figure 3.3 Results from University of Maryland 3PB tests of hardened A 508 steel. Tests were conducted with specimens precracked in fatigue and with cleavage-arrested cracks

3.6 Effects of Cyclic Straining on Irradiation-Hardened Steel

(D. E. McCabe and R. K. Nanstad)

This study was undertaken to evaluate the effect of cyclic strain, which might develop at the tip of a crack in a reactor

vessel from normal operating cycles, on the fracture-toughness behavior of the material. The working theory was that prior crack-tip cyclic strains might lead to local cyclic softening of irradiation-hardened material, resulting in better fracture toughness than that indicated by the usual material characterization studies. Typical applied K levels were used for a 25.4-mm-deep (1-in.) semielliptical surface crack on the inside diameter of a reactor vessel wall during an operating cycle.

Tests were conducted with 1T-C(T) specimens of A 508 steel heat-treated to a high-strength, low-toughness condition (yield strength of 620 to 689 MPa). Five specimens were fatigue precracked at room temperature, and the K_{max} at finish was kept below 20 MPa$\sqrt{m}$. For baseline K_{Ic}, two specimens were tested at −100°C. Specimen 3 was cycled at 1 cycle per minute between 9 and 32 MPa$\sqrt{m}$ for 100 cycles at 160°C. Subsequent testing at −100°C gave a K_{Ic} of 47 MPa$\sqrt{m}$. Specimen 4 was cycled at 160°C between 9 and 61 MPa$\sqrt{m}$ for 100 cycles and tested at −100°C. The final test at −100°C gave a K_{Ic} of 69.5 MPa$\sqrt{m}$. Specimen 5 was similarly prepared and tested, except it was given only one prior cycle, and the test at −100°C gave 67.2 MPa$\sqrt{m}$. A summary of results is presented in Table 3.2. Therefore, it was concluded from these results that (1) prior loading at upper-shelf temperatures improves resistance to cleavage fracture, and (2) the mechanism of improved fracture resistance is warm prestress as opposed to that of cyclic softening.

Table 3.2 Results of cyclic strain tests of hardened A 508 steel

Specimen	Test condition	Temperature (°C)/ number of cycles	K_{Ic} at −100°C (MPa$\sqrt{m}$)
1	Baseline (as received)	None	44.9
2	Baseline (as received)	None	42.3
3	Cycle 9 to 32 MPa$\sqrt{m}$	160/100	47.0
4	Cycle 9 to 61 MPa$\sqrt{m}$	160/100	69.5
5	Cycle 9 to 61 MPa$\sqrt{m}$	160/100	67.2

4 Special Technical Assistance

J. G. Merkle

4.1 ORNL/NRC Review of Reactor Pressure Vessel Evaluation Report for Yankee Nuclear Power Station

(R. D. Cheverton, T. L. Dickson, J. G. Merkle, R. K. Nanstad, and D. L. Selby)

In early August 1990, NRC requested[1] that ORNL coordinate and participate in a review of a report entitled *Reactor Pressure Vessel Evaluation Report for Yankee Nuclear Power Plant*.[2] The review was to cover primarily the PTS analysis described in Sect. 6 and the USE analysis described in Sect. 3. The request also indicated that Idaho National Engineering Laboratory (INEL) would provide thermal/hydraulic input, and Pacific Northwest Laboratory (PNL) would provide input with regard to the VISA code, which was used by the Yankee utility for the probabilistic fracture-mechanics analysis.

The NRC request also specified that work would be completed and a letter report delivered on September 17, 1990, as well as a planning meeting to be held on August 9, 1990. This meeting was held as scheduled, but because of prior commitments and delays in establishing a subcontract and in obtaining necessary information from the utility, the completion date was changed to November 5, 1990.

The following technical tasks were identified as necessary parts of the review:

1. check input to the fracture-mechanics analyses;
2. investigate the validity of and compare results from the probabilistic fracture-mechanics codes OCA-P[3] and VISA-II;[4]
3. evaluate appropriateness of flaw density, flaw-size distribution function, flaw-aspect ratios, vessel region division, and stress-intensity factor influence coefficients used in the Yankee Rowe VISA-II calculation;
4. calculate the conditional probability and frequency of failure for the Yankee Rowe vessel using OCA-P;
5. evaluate the methodology used for estimating upper-shelf fracture toughness;
6. evaluate fracture-toughness curves for unirradiated material, calculation of RT_{NDT}, and surveillance program;
7. review definition of postulated PTS transients and estimate their frequencies;
8. evaluate the methodology for estimating mean values of the calculated frequency of failure;
9. evaluate completeness of list of postulated PTS transients and review estimated frequencies;
10. evaluate the thermal/hydraulic mixing analyses for transients involving stagnation in one or more loops;
11. evaluate the appropriateness of the RETRAN program for the PTS-transient thermal/hydraulic analyses;
12. compare Yankee Rowe's version of VISA-II with PNL's version;
13. evaluate input to the fracture-mechanics analyses;
14. evaluate vessel inspection program;
15. evaluate adequacy of modeling used for RETRAN analyses; and
16. compare RETRAN with version of RELAP-5 used for NRC/ORNL IPTS studies of H. B. Robinson plant.[5]

The following team members contributed directly to the ORNL coordinated effort:

- ORNL: R. D. Cheverton, T. L. Dickson, J. G. Merkle, R. K. Nanstad, and D. L. Selby
- SAIC: D. A. Bozarth, J. W. Minarick, and K. A. Williams
- PNL: F. A. Simonen and L. W. Ward

Science Applications International Corporation (SAIC) personnel were included in this effort because of their earlier involvement in the development of the integrated-pressurized-thermal-shock (IPTS) methodology.[5]

To a large extent the adequacy and accuracy of the Yankee evaluation were judged on the basis of the methodology developed as a part of the NRC/ORNL IPTS study;[5] the NRC PTS rule (10 CFR 50.61); and the NRC Regulatory

Guide 1.154, which identifies acceptable IPTS methodologies and a maximum permissible value of the calculated frequency of vessel failure (through-wall-cracking).

Primary sources of information pertaining to the review were the Yankee report (YAEC No. 1735); Regulatory Guide 1.99, Rev. 2 (radiation-damage correlations); Regulatory Guide 1.154; 10 CFR 50.61; radiation-damage evaluations performed by G. R. Odette (University of California) and A. L. Hiser, Jr. (NRC), who were not specified as members of the above team; the Yankee Rowe emergency operating procedures (EPOs); and Refs. 3–5.

4.1.1 Scope of Review

A general view of the Yankee Rowe reactor vessel is shown in Fig. 4.1. The scope of the review includes a review of "all" aspects of the PTS evaluation, USE considerations, LTOP, and vessel inspection. The PTS evaluation includes (1) postulation of PTS transients and estimation of their frequencies of occurrence; (2) thermal/hydraulic analyses to obtain the downcomer coolant temperature, primary-system pressure and vessel inner-surface fluid-film heat transfer coefficient, each as a function of time in the transient; (3) radiation-induced increase in the reference nil-ductility transition temperature (RT_{NDT}) for the vessel plate and weld material [this requires knowledge of the vessel fast-neutron fluences, operating temperatures, and chemistry (copper and nickel)]; (4) a probabilistic fracture-mechanics analysis to determine the conditional probability of vessel failure, $P_i(F|E)$ for each transient believed to be a significant contributor to the frequency of failure; (5) a summation of the frequencies of failure for each transient to obtain the overall frequency of failure; and (6) an uncertainty analysis, or equivalent, to obtain a "mean" value of the frequency for comparison with the maximum permissible values given in Regulatory Guide 1.154. Each of these items was considered in the review.

4.1.2 PTS Transients and Their Frequencies

There are two questions of particular concern regarding PTS transients and their frequencies. (1) Have the actual dominant transients been postulated? (2) Are the estimated frequencies of occurrence of the transients that are suspected of being dominant realistic or at least conservative?

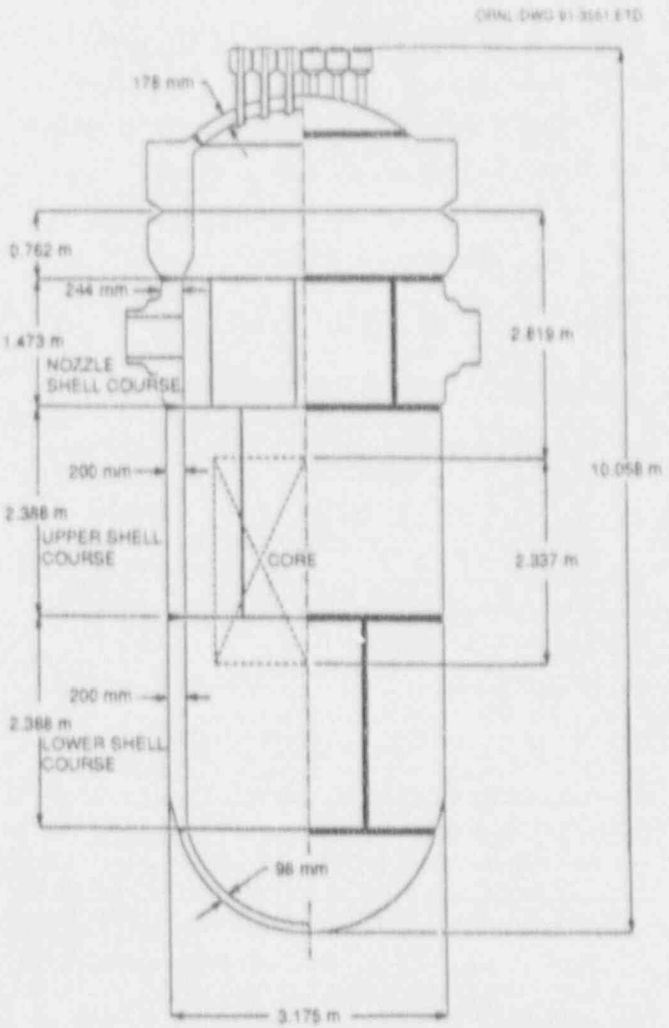

Figure 4.1 RPV weld and plate locations

The consensus of the reviewers is that insufficient information was available to make an accurate judgement with regard to the selection of transients. Even so, if consideration of a single transient or category of transients indicates an excessively high frequency of failure, then consideration of other transients may not be necessary. The reviewers followed this line of thinking in addition to making numerous comments, suggestions, and estimates regarding definition of transients and their frequencies.

The Yankee report identifies a small-break loss-of-coolant accident (LOCA) (SBLOCA-7) as the dominant transient and assigns a frequency of occurrence to this transient of $\sim 5 \times 10^{-4}$/year. However, the reviewers suggest a more

realistic value of 2×10^{-3}, which is considered to be a mean value. If other LOCAs are included to account for their contribution in a conservative manner, assuming that SBLOCA-7 represents the most severe of the LOCAs, the effective frequency is increased to 4×10^{-3}.

4.1.3 PTS Transient Thermal/Hydraulics

The question of particular concern regarding the Yankee thermal/hydraulic analysis is whether the PTS transient described by the calculated primary-system pressure, downcomer coolant temperature, and vessel inner-surface heat-transfer coefficient is likely to be more severe than indicated. The reviewers believe that the coolant temperature is more likely to be lower than higher, and the pressure is more likely to be higher than lower. Thus, with regard to these two parameters, the severity of the transient is more likely to be greater than less. The heat-transfer coefficient, on the other hand, is more likely to be less, and this would tend to reduce the severity. However, based on sensitivity studies in Ref. 5, it is believed that the reduction would not be significant. Therefore, the reviewers concluded that the calculated transient was less severe than a best estimate.

4.1.4 Radiation Effects

4.1.4.1 Increase in RT_{NDT}

There are two values of RT_{NDT} of particular interest with regard to 10 CFR 50.61 and Regulatory Guide 1.154. For 10 CFR 50.61, a $+2\sigma$ value is needed for comparison with the PTS screening criteria. For Regulatory Guide 1.154, a mean value and a distribution are needed for use in a probabilistic fracture-mechanics analysis.

ORNL and Yankee estimates for 10 CFR 50.61 $+2\sigma$ values, minus the 2σ, are given in Table 4.1 for 1990. Assuming 2σ is ~33°C, it is apparent that all values exceed the screening criteria, which are 132°C for axial flaws and 167°C for circumferential flaws. As required by Regulatory Guide 1.99, Rev. 2, the copper concentration in the welds was assumed to be 0.35 wt % because measurements are not available. Based on the BR-3 weld chemical-composition data, the concentration of nickel was assumed to be 0.7 wt %.

"Best estimate" values of RT_{NDT} for the upper axial weld were obtained using Regulatory Guide 1.99, Rev. 2, with an addition of 24°C in the ORNL analyses to account for the lower irradiation temperature (263°C compared to 288°C). An irradiation-temperature correction factor of 1°C/1°C is believed to be appropriate for the materials, fluences, and temperatures of interest.

In the absence of specific data for the Yankee welds, the best estimate of the copper concentration in the welds is 0.29 wt %, with $1\sigma = 0.07$ wt %. Based on the BR-3 data, the best estimate of the nickel concentration is 0.7 wt %. The best estimate of fast-neutron fluence for the inner surface of the upper axial weld is 1.24×10^{19} neutrons/cm^2. This fluence, with an appropriate attenuation formula, and the above chemistry were used to calculate RDT_{NDT} as a function of crack depth in the ORNL probabilistic fracture-mechanics analysis of Yankee Rowe.

4.1.4.2 Decrease in USE

There are two specific concerns regarding USE. One is whether the vessel satisfies the LUS analysis for levels A, B, and C loading conditions in accordance with criteria recommended by the ASME Sect. XI Working Group on Flaw Evaluation. The other pertains to the selection of upper-shelf fracture-toughness values for the probabilistic fracture-mechanics analysis.

Time did not permit a review of the calculated K_I values corresponding to load levels A, B, and C. However, the J R curves used for comparison with the K_I values were reviewed. ORNL believes there is adequate margin for each of the loading levels, assuming, of course, that the K_I values are correct.

ORNL estimated an appropriate upper-shelf fracture-toughness value for use in the probabilistic fracture-mechanics analysis to be ~154 MPa$\cdot\sqrt{m}$ for the upper axial weld. The Yankee report used a value of 220 MPa$\cdot\sqrt{m}$, which was also used for the ORNL IPTS studies.[5] ORNL sensitivity studies associated with this review indicate that the effect on P(FIE) of the difference between 140 and 200$\cdot\sqrt{m}$ is insignificant.

Table 4.1 Licensee and staff estimates of reference temperature RT_{NDT}, without $+2\sigma$ margin, for YNPS beltline materials in 1990 (Based on September 1990, revised fluences)

YNPS beltline material	1990 revised peak fluences ($\times 10^{19}$ neutrons/cm^2)	Unirradiated reference temperature (°C)		Increase in reference temperature resulting from irradiation (°C)		Reference temperature RT_{NDT} in 1990 (°C)	
		ORNL estimate	Licensee estimate	ORNL estimate	Licensee estimate	ORNL estimate	Licensee estimate
Upper plate	2.6	–13	–1	143	142	130	141
Lower plate	2.31	–1	–1	181	180	180	179
Upper axial weld[a]	1.24	–13	–13	162	162	149	149
Lower axial weld[a]	1.2	–13	–13	161	161	148	148
Circumferential weld	2.31	–13	–13	183	183	170–192	170

[a]Based on Cu = 0.35%, Ni = 0.7%.

4.1.5 PTS Fracture Mechanics

4.1.5.1 Comparison of the PNL and Yankee Versions of VISA-II

Four categories of differences can be considered for composing PNL and Yankee versions of VISA: methodology, details, input, and errors. Formal documentation of the Yankee Rowe version of the code was not available for review, and this prevented a comprehensive comparison of basic methodology. A phone conversation, however, revealed no differences in basic methodology, although the Yankee version included three differences in detail: (1) residual stresses in the welds; (2) a more accurate representation of Regulatory Guide 1.99, Rev. 2; and (3) a somewhat different set of K_I values corresponding to pressure loading. Inclusion of the residual stress increases P(FIE) for the welds by a factor of ~2 for the specific case examined.

With regard to K_I calculations, it is not clear whether the K_I influence coefficients in the Yankee version correspond to R/w = 7 (appropriate for Yankee) or R/w = 10 (built into the PNL version of VISA-II). A comparison indicates that this difference would not affect initiation and arrest of shallow flaws (a/w < 0.5) but could be significant for a/w > 0.5.

The input parameters for the Yankee calculations were reviewed item by item for consistency with Regulatory Guide 1.154 and PNL's recommendations for application of VISA-II.[4] While several details of the Yankee inputs differed from those used in previous NRC studies, sensitivity calculations indicate that these differences should not have a major impact on calculated failure probabilities. Inputs for pressures, temperatures, and radiation-induced embrittlement do have very significant impacts; these are discussed later.

The ORNL review of the PNL version of VISA-II revealed three errors, and it is assumed that these errors also existed in the Yankee version of VISA-II. These errors are discussed further in Sect. 4.1.6.2.

4.1.5.2 Comparison of OCA-P and the PNL Versions of VISA-II

Before this review, the VISA-II and OCA-P codes had not been reviewed in detail since 1984. Because both are being used by utilities and others for evaluating vessel integrity, and especially because VISA-II is being used in connection with the Yankee relicensing application, it is prudent at this time to carefully review and compare both codes for further validation.

Reviews of both codes were performed by flow-charting, to a fine level of detail, the probabilistic methodologies and comparing calculations for wall temperatures, stresses, and K_I values. The temperature and stress comparisons, which involved comparison with independent validated commercial codes, indicated that the VISA II and OCA-P subroutines are valid.

OCA-P and VISA-II both use influence-coefficient and superposition techniques for calculating K_I values, but the details are different. The OCA-P procedure is more accurate, but the differences normally are not significant, and, for the Yankee analysis performed thus far, the differences also are believed to be insignificant.

The detailed comparison of the two codes by means of flow-charting revealed three errors in VISA-II, two of which were almost trivial, but one results in an excessive number of stable arrests and thus an underestimate of P(F|E). These errors have been corrected in the PNL version but presumably were not corrected in the Yankee version. One comparison calculation indicates that correcting the errors increases P(F|E) by a factor of ~10, but for the specific Yankee analysis, the difference is believed to be less.

After the corrections discussed above were made to VISA-II, OCA-P and VISA-II were compared by using both to calculate the "Rancho Seco" transient with R/w = 10. All input was the same, and only one region of the vessel containing a single flaw was considered. The temperature and stress distributions agreed very well, and the K_I values agreed reasonably well, particularly for a/w < 0.5. The number of initial initiations agreed within 12%, and the values of P(F|E) were within 3%. The number of arrests for OCA-P was three times greater than for VISA-II but was a factor of ~10 less than the number of initiations, in which case the difference in arrests has very little effect on P(F|E). Thus, the tentative conclusion is that OCA-P and the corrected PNL version of VISA-II agree well, and both appear valid for their intended purpose. It is important to remember, however, that there are choices to be made in important input/modeling parameters that can result in significantly different values of P(F|E). Flaw density and its uncertainty are two of the more important choices.

4.1.5.3 ORNL OCA-P Analysis of P(F|E) for Yankee Rowe

The ORNL OCA-P analysis of Yankee Rowe used the neutron fluences, which correspond to 1990 and region definitions and volumes given by YAEC.* P(F|E) was calculated for the upper axial weld only, and the copper and nickel concentrations for this region (Cu = 0.29, 1σ = 0.07; Ni = 0.7) were best-estimate values taken from a Babcock and Wilcox Owners' Group report†. The number of flaws corresponding to a mean value of P(F|E) was essentially the same as that used in the Yankee analysis (one flaw in the region). A uniform stress of 41 MPa was included to simulate a residual stress, and the transient calculated was the SBLOCA-7 transient described in Ref. 2. Based on these conditions, $P(F|E) = 4 \times 10^{-2}$. Adding the contribution of all regions, assuming uniform flaw density and accounting for double counting, increases P(F|E) to $>8 \times 10^{-2}$. If repressurization to 10.69 MPa occurs and the time of occurrence is 20 min, P(F|E) increases to $>1 \times 10^{-1}$. These values are less than the corresponding mean values, even though the mean flaw density was used, because the calculated primary-system pressure and downcomer coolant temperature are believed to be less severe than those corresponding to mean values.

4.1.6 ORNL Estimates of Frequency of Failure for Yankee Rowe

The frequency of vessel failure is calculated as follows:

$$\varphi(F) = \sum_i^i \varphi_i(E)\, P_i(F|E)\,,$$

where

$\varphi(F)$ = total frequency of failure (failures/reactor year),

$\varphi_i(E)$ = frequency of the ith PTS transient (events/reactor year),

$P_i(F|E)$ = probability of failure for the ith event (failures/event).

*Written communication from Yankee Atomic Electric Company to William Russell of the US NRC, September 28, 1990.

†K. E. Moore and A. S. Heller, "B&W 177-FA Reactor Vessel Beltline Weld Chemistry Study," BAW-1799, B&W Owner's Group Materials Committee (July 1983).

For the SBLOCA-7 transient, $\varphi(E) = 2 \times 10^{-3}$/year or 4×10^{-3} if the transient conservatively bounds all other similar LOCAs. Both values are considered to be reasonable mean values.

Using the lower of the two,

$$\varphi(F)\ (SBLOCA\text{-}7) > 2 \times 10^{-3} \times 8 \times 10^{-2}$$

$$= 2 \times 10^{-4}/\text{year}\ .$$

With repressurization as described above,

$$\varphi(F)(SBLOCA\text{-}7R) > 2 \times 10^{-3} \times 1 \times 10^{-1}$$

$$= 2 \times 10^{-4}/\text{year}\ .$$

These values are less than the mean because of the transient system pressure and coolant temperatures used, as mentioned previously. However, it is apparent that they are substantially greater than the value of 5×10^{-6} failures/year given in Regulatory Guide 1.154 as a maximum permissible value of the mean frequency of vessel failure for PTS loading conditions.

4.1.7 Tentative Conclusions

1. Values of RT_{NDT} calculated for Yankee Rowe in accordance with the rules in 10 CFR 50.61 for comparison with the PTS-Rule Screening criteria are substantially greater than the screening criteria values.
2. The PNL version of VISA-II and the OCA-P probabilistic fracture-mechanics codes, which are referenced in Regulatory Guide 1.154, are in good agreement and valid for their intended purpose. (During this review, an error was found in VISA-II and has subsequently been corrected. The above statement pertains to the corrected version.)
3. The 1990 mean frequency of failure calculated by ORNL for the Yankee Rowe vessel is $>2 \times 10^{-4}$/year and thus exceeds the value corresponding to the "primary acceptance criterion" in Regulatory Guide 1.154 (5×10^{-6}/reactor year). As stated in the Regulatory Guide, however, this does not necessarily mean that the vessel is unsafe to operate.
4. There are many unanswered questions regarding details of the Yankee IPTS-type[5] evaluation of vessel integrity. It seems unlikely, however, that answers will substantially alter the above estimated values of $\varphi(F)$.

4.2 LUS Criteria Development

(J. G. Merkle)

The ASME Sect. XI Working Group on Flaw Evaluation (WGFE) has recently completed the development of safety criteria for nuclear pressure vessels containing LUS materials. The HSST Program and NRC staffs have participated actively in this process. Example calculations have shown that the required USE is sensitive to several factors, which therefore must be considered carefully. These factors include vessel wall thickness, pressure in the crack, thermal stress, plastic zone size effects, the assumption of plane strain vs plane stress (plane strain is more accurate), flaw orientation, the reference pressure for the safety factor calculation, and the statistical significance of the toughness values (mean or lower bound). Since calculated instability pressures are going to be above the safety valve settings and therefore of low probability, it seems reasonable to consider reducing the required safety factors on pressure as the probability of exceeding the required toughness value increases.

Some vessels may have only circumferential LUS welds. For those vessels, an axially oriented quarter-thickness deep surface crack in the beltline region is highly improbable. For this case, a more reasonable set of flaw configurations would be an axially oriented through-crack across the LUS weld with a total length equal to the maximum width of the weld (and therefore with the crack fronts in base metal) and a circumferentially oriented internal quarter-thickness part-through surface crack in the LUS weld. This suggestion was originally made to the ASME by a utility, with no qualifications concerning fracture mode, and the NRC objected. The idea seems sound for the upper-shelf temperature range, but less so for lower temperatures. This is because the postulated flaw configuration is not likely to be produced by stable tearing originating in the weld, if the base metal has good upper-shelf toughness, but could more easily be produced by unstable cleavage. This proposal was reconsidered by the ASME WGFE for the upper-shelf temperature range only. Such consideration implicitly couples the redefined reference flaw geometries to the results of the mandatory reinspection of an LUS vessel to guard against prior pop-ins as well as fabrication defects.

Considering the merits and limitations of preliminary proposals, guidelines were formulated for the development of firm criteria. It was recognized that criteria are needed both to limit the amount of ductile crack extension and to prevent tearing instability. It was also recognized that J-R curves exhibit scatter and size effects only partially understood, making extrapolations for instability calculations subject to error. Therefore, it was decided to formulate criteria in terms of conservative measures of toughness for levels A, B, and C and to replace the instability calculations necessary to determine full safety margins with calculations demonstrating flaw stability for specified load margins. The latter calculations will require less J-R curve extrapolation. Compensating adjustments have been made to the specified load margins, based on the expected ratio of lower-bound toughness to mean toughness, so that results in terms of safety will remain roughly the same as those obtained by using previously proposed criteria based on mean toughness.

In developing the criteria for levels C and D, it was deemed desirable to specify different safety criteria for the two load categories because of the differences in the associated event probabilities and structural performance requirements. It was also deemed undesirable for the code to deal explicitly with PTS loadings, or to specify system analysis procedures or definitions, because this might interfere with the regulatory process for individual plants. Because the criteria being developed apply only to upper-shelf conditions, meeting these criteria cannot be a substitute for meeting the PTS criteria described in USNRC Regulatory Guide 1.154.

For levels A and B, the reference flaw is the Appendix G flaw, oriented along the weld of concern or having whatever orientation in LUS base metal is most conservative. A conservative measure of toughness is also employed. A reference pressure, called the accumulated pressure, P_{acc}, is used for safety-margin verification. The accumulated pressure is the highest pressure that can occur in the system, as estimated by a calculation that includes the effects of pressure-relief valve settings and fluid discharge rates through those valves. The accumulated pressure is limited to 10% above component design pressure, so for a vessel design pressure of 17 MPa (2500 psi) the accumulated pressure cannot exceed 19 MPa (2750 psi). The limited crack-growth criterion requires that at a pressure of 1.15 P_{acc} and specified thermal loading, stable crack growth must not exceed 2.5 mm (0.10 in). The stability criterion requires that at a pressure of 1.25 P_{acc} and the same thermal load, ductile flaw growth must remain stable.

For levels C and D, the reference flaw-depth range is from zero to one-tenth of the base metal wall thickness, plus the cladding thickness, but is not to exceed 25.4 mm (1.0 in.). Flaw shapes and orientations are the same as for levels A and B. The reference toughness for level C is conservative, while for level D it is the mean toughness. Loads are as determined by plant specific analyses for the specified load categories, with no additional safety factors. For level C, stable crack growth must not exceed 2.5 mm (0.10 in.), and the flaw must remain stable. For level D, the flaw must either remain completely stable or it must not extend beyond an a/t of 0.75, and the remaining ligament must be safe against tensile instability.

References

1. Letter from L. C. Shao, NRC, to W. D. Adams, ORO, "FY 1990 Nuclear Regulatory Research Order No. 60-90-476 for Oak Ridge National Laboratory," August 2, 1990.*

2. Yankee Atomic Electric Co., "Reactor Pressure Vessel Evaluation Report for Yankee Nuclear Power Plant," YAEC No. 1735, July 1990.*

3. R. D. Cheverton and D. G. Ball, Union Carbide Corp., Nuclear Div., Oak Ridge Natl. Lab., "OCA-P, A Deterministic and Probabilistic Fracture Mechanics Code for Application to Pressure Vessels," USNRC Report NUREG/ CR-3618 (ORNL-5991), May 1984.†

4. F. A. Simonen et al., Pacific Northwest Lab., Richland, Wash., "VISA II – A Computer Code for Predicting the Probability of Reactor Pressure Vessel Failure," NUREG/CR-4486 (PNL-5775), March 1986.†

5. D. L. Selby et al., Martin Marietta Energy Systems, Inc., Oak Ridge Natl. Lab., "Pressurized Thermal Shock Evaluation of the H. B. Robinson Nuclear Power Plant," U.S. NRC Report NUREG/CR-4183 (ORNL/TM-9567), September 1985.†

*Available in NRC Public Document Room for inspection and copying for a fee.

†Available for purchase from National Technical Information Service, Springfield, VA 22161.

5 Fracture-Mechanics Computer Programs

T. L. Dickson

5.1 Background Information

This is the first report period since Task 5 was changed from Crack-Arrest Technology to Fracture-Mechanics Computer Programs.

During this period, OCA-P,[1] a fracture-mechanics simulation code previously developed at ORNL, was used in the review of the probabilistic fracture mechanics portion of the Yankee Rowe Pressure Vessel Evaluation Report. OCA-P is based on Linear Elastic Fracture Mechanics (LEFM) principles and is capable of performing both deterministic and probabilistic fracture analyses of RPVs subjected to PTS loading conditions.

A work plan for enhancing OCA-P to meet NRC specifications required to perform the PTS Sensitivity Analyses for Yankee Rowe was completed.

5.2 Yankee Rowe Review

The probabilistic fracture mechanics portion of the Yankee Rowe Pressure Vessel Evaluation was performed with VISA-II,[2] a fracture-mechanics code developed by NRC and Pacific Northwest Laboratories. The initial scope of the Yankee Rowe review was to perform a rigorous comparison of the methodologies and results of VISA-II and OCA-P. When this effort uncovered some differences in the probabilistic methodologies and results of OCA-P and VISA-II, the workscope was enlarged to include using OCA-P to independently analyze the Yankee Rowe vessel.

5.2.1 Deterministic Validation of OCA-P

Although the deterministic methodologies used by VISA-II and OCA-P are quite different, the deterministic solutions (thermal response, stress analysis, and stress-intensity factor solutions) were found to be in good agreement. OCA-P thermal response and stress analysis solutions were also found to be in excellent agreement with solutions obtained using the general-purpose, finite-element solution codes, ADINA-T[3] and ADINA,[4] providing further validation of OCA-P.

5.2.2 Probabilistic Validation of OCA-P

Significant differences were found between the probabilistic solutions of VISA-II and OCA-P. OCA-P predicted a conditional probability of failure higher than VISA-II by an approximate factor of 8. OCA-P was enhanced to print out a more detailed summary of the probabilistic analysis results (e.g., number of initiations, reinitiations, crack arrests, and terminating stable crack arrests) to facilitate a more rigorous comparison of the probabilistic solutions.

An examination of the probabilistic methodologies of VISA-II and OCA-P was performed. The methodologies of both codes were flow-charted down to a fine level of detail. The examination revealed three differences between the probabilistic methodologies of VISA-II and OCA-P. Two of the differences were relatively minor, but one was of a fundamental nature.

VISA-II was predicting considerably more stable crack arrests than OCA-P. These differences were discussed in detail with the VISA-II code developers at Pacific Northwest Laboratories. They were in agreement with the ORNL suggested modifications to the VISA-II code. After the modifications were made to the VISA-II code, the probabilistic solutions of VISA-II and OCA-P were in reasonably good agreement.

5.2.3 Independent OCA-P Analysis of Yankee Rowe

In order to apply OCA-P to the Yankee Rowe vessel, the methodology specified in Regulatory Guide 1.99, Revision 2 (Ref. 5), for calculating the amount of radiation-induced embrittlement was incorporated into the code.

5.3 Yankee Rowe Sensitivity Analyses

During this period, a work plan for enhancing OCA-P to perform PTS sensitivity analyses for Yankee Rowe to meet NRC specifications was completed. The primary enhancements are to include in OCA-P the capability to model subsurface flaws (subclad and embedded) and variational fluence fields. The ASME Sect. XI (Ref. 6) methodologies for calculating stress-intensity factors for

surface and subsurface flaws will be incorporated into the OCA-P code.

5.4 Conclusions

During the Yankee Rowe Review, the deterministic solutions of OCA-P were validated against VISA-II, ADINA-T, and ADINA. The probabilistic methodology was closely scrutinized, and it appears that the probabilistic methodology of OCA-P is compatible with the revised version of VISA-II. These are important steps toward developing a new N-QA probabilistic fracture-mechanics code, a task scheduled for next fiscal year.

A continuing effort is under way to develop a well-structured, validated, well-documented, and "user friendly" probabilistic fracture-mechanics code. This will enable incorporation of future fracture technology advances (such as thermal streaming induced stresses, ductile tearing analyses, shallow-flaw, fracture-initiation enhancement, etc.) to proceed in an orderly and systematic manner.

References

1. R. D. Cheverton and D. G. Ball, Union Carbide Corp. Nuclear Div., Oak Ridge Nat. Lab., "OCA-P, A Deterministic and Probabilistic Fracture Mechanics Code for Application to Pressure Vessels," USNRC Report NUREG/CR-3618 (ORNL-5991), May 1984.*

2. F. A. Simonen et al., Pacific Northwest Lab., Richland, Washington, "VISA II—A Computer Code for Predicting the Probability of Reactor Pressure Vessel Failure," USNRC Report NUREG/CR-4486 (PNL-5775), March 1986.*

3. K. J. Bathé, Massachusetts Institute of Technology, Cambridge, Mass., "ADINAT—A Finite Element Program for Automatic Dynamic Incremental Nonlinear Analysis of Temperatures," December 1978.†

4. K. J. Bathé, Massachusetts Institute of Technology, Cambridge, Mass., "ADINA—A Finite Element Program for Automatic Dynamic Incremental Nonlinear Analysis," December 1978.†

5. *U. S. Nuclear Regulatory Commission, Regulatory Guide 1.99*, Rev. 2, "Radiation Embrittlement of Reactor Vessel Materials," U. S. Nuclear Regulatory Commisison, Washington, D.C., May 1988.‡

6. The American Society of Mechanical Engineers Boiler and Pressure Vessel Code, Section XI, *Rules for Inservice Inspection of Nuclear Power Plant Components*, 1986.†

*Available for purchase from National Technical Information Service, Springfield, VA 22161.
†Available in public technical libraries.
‡Available in NRC public document room.

6 Cleavage-Crack Initiation

T. J. Theiss

6.1 Introduction

This task emphasizes cleavage-initiation toughness and the specimens that are used to evaluate cleavage-fracture toughness. The task was begun in FY 1990 and is currently divided into three subtasks: (6.1) Shallow-Crack Fracture-Toughness Testing, (6.2) Lower-Bound Initiation Toughness, and (6.3) Gradient Effects on Fracture Toughness. The testing portion of subtask 6.1, Shallow-Crack Fracture-Toughness Testing, is reported as a part of Task 10, Fracture Evaluation Tests. In conjunction with the shallow-crack fracture-toughness testing program, HSST continued support for the joint Edison Welding Institute (EWI) and The Welding Institute (TWI) project to develop shallow-crack fracture-mechanics tests.

6.2 Shallow-Crack Fracture-Toughness Testing (T. J. Theiss and S. T. Rolfe)

The current testing portion of the shallow-crack program is divided into two phases: a development phase and a production phase. During the development phase the experimental techniques necessary for shallow-crack testing are to be verified. A limited data base of shallow-crack fracture-toughness values appropriate for application to RPV analyses will be generated as a part of the production phase. During this reporting period, the development phase of the experimental Shallow-Crack Program was completed. Previous shallow-crack work has been detailed in prior semiannual reports and in open literature.[1–3] Details of the testing are reported in Chap. 10, Fracture Evaluation Tests.

6.2.1 Test Matrix

Two crack depths (one shallow and one deep) were tested during the development phase of the project. The nominal crack depth chosen was a ≈ 9 mm (a ≈ 0.4 in.), which is prototypic of the flaw depths that resulted in initiation in the IPTS studies.[4–6] One specimen was tested with a flaw depth of 14 mm (0.55 in.) for comparison. Presently, the relative influence of absolute crack depth a or normalized crack depth a/w is not fully understood. For the specimen sizes being considered in this project, it is believed that absolute crack depth rather than a/w will be the primary variable of interest. However, this assumption will be verified by testing additional crack depths during the production phase of the project.

To properly transfer shallow-crack fracture-toughness data to the RPV, the effect of out-of-plane constraint on the toughness must be well understood. To investigate the effects of out-of-plane constraint in the beams, the beam thickness was varied to examine the effect on toughness. Three thicknesses were used: B = 50, 100, and 150 mm (2, 4, and 6 in.). At least one deep-crack specimen and two shallow-crack specimens were tested using beams of each thickness. The span for the 50-mm-thick beam is 4W or 406 mm (16 in.). The spans for the 100- and 150-mm beams was increased to 864 mm (34 in.) to assure failure without exceeding the load capacity of the beam fixture.

The temperature for all developmental testing work is within the lower transition region for A 533 B steel. RT_{NDT} for this material is –35°C (–30°F).[6] The testing temperature for all the tests except one was T = –60°C (–76°F). T – RT_{NDT} was therefore –25°C (–46°F). One test was run at RT_{NDT}. During the production phase of the project, testing will be performed at multiple temperatures in the lower transition region to fully quantify the temperature range in which the toughness elevation takes place.

6.2.2 Test Results

Load vs CMOD curves were generated and examined for each beam tested. To normalize the load between beams of different spans, thicknesses and slightly different beam depths, the applied stress (rather than applied load) that would exist in an uncracked beam was plotted vs CMOD. The applied stresses for the test and analyses results were calculated from the applied loads and the beam geometries according to elastic strength of materials equations. The stress vs CMOD test data are consistent and agree well with the analytical data, providing additional confidence in the test data. The analytical stress vs CMOD curves were generated using a plane-strain, elastic-plastic, finite-element ADINA[7] model. The test data represent beams of three different thicknesses. The consistency of the test data and the agreement with the plane-strain analytical data indicate little loss of out-of-plane constraint due to insufficient specimen thickness in the test data.

The toughness data expressed in terms of CTOD vs temperature are presented in Table 6.1 and shown in Fig 6.1 along with the material characterization curve.[8] Data from three crack depths ($a/w = 0.50, 0.15$, and 0.10) and three thicknesses (B = 50, 100, 150 mm) are presented. The deep-crack toughness values are slightly higher than the material characterization curve and are consistent with previous CT specimen data[9] from the same heat of material tested before this program. The trend of the results in Fig. 6.1 indicates a significant increase in the measured fracture toughness for shallow-crack specimens in the lower transition region. The a/w = 0.15 datum also appears to exhibit a shallow-crack toughness elevation. The ratio of the mean shallow-crack toughness to deep-crack toughness is 4.4 for the beams tested at –60°C (–76°F). The ratio of the shallow-to-deep lower-bound toughness is 2.9, which is consistent with the shallow crack elevated toughness for A 36 and A 517 steel determined at the University of Kansas.[10,11] As indicated in Refs. 10 and 11, the shallow- and deep-crack toughness for A 533 B is expected to converge on the lower shelf.

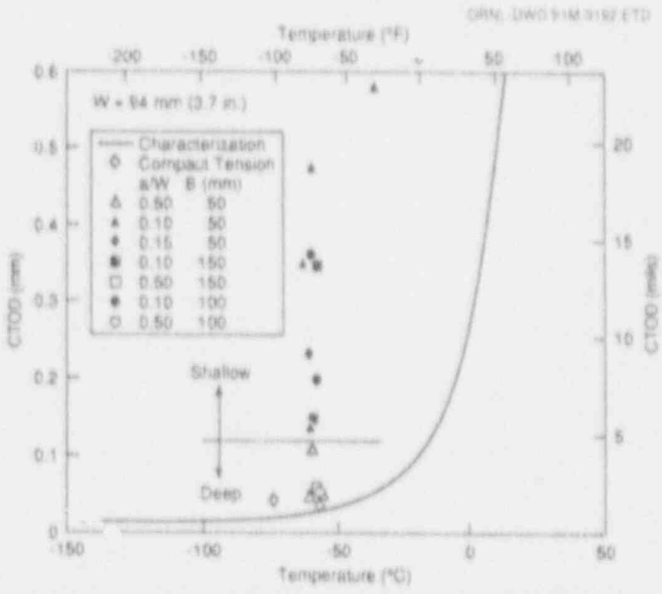

Figure 6.1 HSST test data with material characterization curve and previous CT data

Table 6.1 HSST test data[a]

HSST beam	Temperature (°C,	S (mm)	B (mm)	W (mm)	a (mm)	a/w	Rotation factor	Measured elastic compliance (mm/kN)	Failure load (kN)	Measured failure CMOD (mm)	Toughness CTOD (mm)
3	–35.6	406	50.6	99.7	10.0	0.102	0.47	3.09×10^{-4}	600	0.808	0.587
4	–60.6	406	50.7	99.5	51.8	0.520	0.30[b]	3.38×10^{-3}	128	0.461	0.0469
5	–55.3	406	50.6	99.1	51.2	0.517	0.30[b]	3.14×10^{-3}	140	0.442	0.0488
6	–59.2	406	50.6	99.5	51.9	0.522	0.30[b]	3.52×10^{-3}	185	0.758	0.109
7	–59.4	406	50.7	94.2	10.2	0.108	0.48[b]	3.27×10^{-4}	483	0.250	0.138
8	–59.5	406	50.8	94.2	9.63	0.102	0.50	3.12×10^{-4}	657	0.652	0.478
9	–62.3	406	50.9	94.0	9.52	0.101	0.47	3.09×10^{-4}	552	0.508	0.352
10	–60.2	406	50.9	94.3	14.0	0.149	0.45[b]	4.77×10^{-4}	489	0.434	0.232
11	–56.7	864	102	93.9	8.36	0.0890	0.48	3.08×10^{-4}	472	0.312	0.198
12	–56.7	864	102	94.7	49.8	0.526	0.26	4.44×10^{-3}	117	0.574	0.0560
13	–59.6	864	102	94.0	8.81	0.0938	0.48[b]	3.29×10^{-4}	502	0.514	0.360
14	–57.4	864	152	92.5	8.69	0.0939	0.48	2.25×10^{-4}	723	0.504	0.349
15	–58.5	864	153	94.5	8.66	0.0917	0.47	2.14×10^{-4}	684	0.257	0.147
16	–57.8	864	153	94.0	50.0	0.532	0.33	2.81×10^{-3}	170	0.530	0.0576

[a]Yield stress = 468 MPa at T = –60°C and 440 MPa at T = –35°C. The yield stress was estimated from room-temperature values and adjusted for the lower temperatures.

[b]Rotation factor not explicitly determined for these specimens. Rotation factor used is average of similar tests.

CTOD and the plane-strain stress-intensity factor K_{Ic} are related according[12] to

$$CTOD = K_{Ic}^2(1-\nu^2)/(2\sigma_y E) \quad . \qquad (6.1)$$

The ratio of shallow-to-deep toughness in terms of K_{Ic} is equal to the square root of the ratio in terms of CTOD. The lower-bound shallow-crack toughness is ≈70% greater than the lower-bound deep-crack toughness at –60°C. The spread of the data is also reduced, expressing the toughness in terms of K_{Ic}.

If it is assumed that the shallow-crack toughness curve has the same shape as the deep-crack toughness curve, the shallow-crack toughness increase can be expressed as a temperature shift. Previous A 36 data supports this assumption.[10] The lower-bound shallow-crack datum at T = –60°C (–76°F) and the single datum at T = 35°C (–30°F) are shifted 46 to 48°C (83 to 87°F) from the characterization curve, respectively. The lower-bound deep-crack datum is shifted about 16°C (28°F) from the characterization, indicating a temperature shift for the shallow-crack specimens of 30°C (55°F).

Beams 50, 100, and 150 mm thick (2, 4, and 6 in.) were tested to investigate the influence of differing out-of-plane-constraint levels on the toughness of shallow and deep-crack specimens. Toughness data are plotted as a function of beam thickness for all of the tests conducted at T = –60°C (–76°F) in Fig. 6.2. As shown in Figs. 6.1 and 6.2, the toughness values for the shallow- and deep-crack specimens from the 100- and 150-mm-thick (4- and 6-in.) beams are generally consistent with the 50-mm-thick (2-in.) data. However, there appears to be slightly more data scatter associated with the 50-mm-thick (2-in.) beams than with the 100- and 150-mm-thick (4- and 6-in.) beams. It is interesting to note that the lowest shallow- and deep-crack toughness values were both from beams with the least thickness (B = 50 mm). Beams of three thicknesses were tested to select the appropriate beam size for the production phase testing. The testing temperature is expected to be greater for many of the beams tested in the production phase of the program. As the temperature increases, additional loss of out-of-plane constraint is anticipated. Therefore, even though the 50-mm beam thickness might be sufficient at lower temperatures, the 100-mm beam thickness was chosen for future testing because the greater thickness might be required at the higher temperatures.

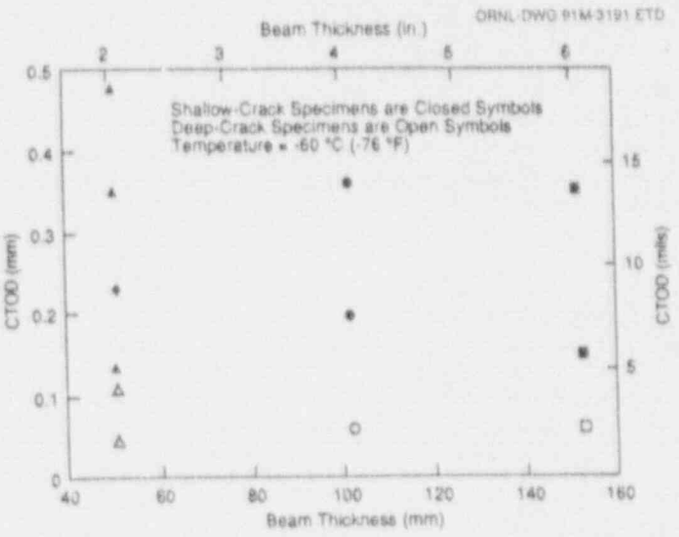

Figure 6.2 HSST test data at three thicknesses tested at –60°C

6.2.3 Modified Irwin Correction

The toughness data were converted to K_c, critical stress-intensity factor values according to the following equation:[13]

$$K_{c(} = \{m\sigma_y E^* CTOD\}^{1/2} \quad . \qquad (6.2)$$

It was decided to set the constraint factor m to 2 for deep- and shallow-flaw specimens until additional information was available on the variation of the constraint parameter for shallow flaws. Examination of the K data and ASTM E399 revealed that only the 150-mm (6-in.) deep-crack test result would meet the validity requirement for sufficient beam thickness, and none of the data would meet the validity requirement for crack depth. Therefore, the plane stress form of Eq. (6.2) was used because the data did not satisfy the ASTM E399 validity requirements. The goal of the shallow-crack program is to investigate the toughness as a function of crack depth and apply the results to an RPV, which is a highly constrained application. The deep-crack test results, therefore, should maintain plane-strain constraint or be adjusted to estimate the plane-strain toughness. Because specimens required to maintain plane-strain constraint are prohibitively large, the data taken from the deep-crack specimens have been adjusted for loss of out-of-plane constraint via Irwin's β_c correction.[14] Application of the Irwin β_c correction reduces the average deep-crack critical

toughness from 109 MPa$\sqrt{m}$ (99.2 ksi$\sqrt{in.}$) to a corrected plane-strain value of 90.5 MPa$\sqrt{m}$ (82.4 ksi$\sqrt{in.}$) as shown in Table 6.2. The magnitude of the reduction is relatively minor.[14] The small magnitude of the correction and the consistency between the data of different thicknesses indicate that little loss of out-of-plane constraint is present in the deep-crack data in spite of the fact that the validity requirements have not been met.

Relaxation of crack-tip constraint in either direction (in-plane or out-of-plane) has the effect of elevating the critical toughness. The Irwin β_c correction successfully accounts for loss of out-of-plane constraint, and, therefore, a modification (of the β_c correction) proposed by Merkle[15] to account for the loss of in-plane constraint associated with shallow flaws was applied. This modification is based on the assumption that the critical dimension in the constraint of a beam is the distance from the point of greatest constraint to the nearest free surface, not including the crack surface. In deep-crack beams, this distance is half the beam thickness; in shallow-crack specimens, the critical dimension is the crack depth. By using the appropriate critical dimension, the Irwin β_c correction can be modified to account for both loss of out-of-plane constraint (insufficient thickness) and loss of in-plane constraint (shallow-crack effect).[15] As shown in Table 6.2 and Fig. 6.3, the modified Irwin correction applied to the HSST data adjusts both deep- and shallow-crack toughness data to the same value.

Since the shallow- and deep-crack toughness data can be adjusted to the same value, the modified correction could potentially be used to "predict" the shallow-crack fracture-toughness from deep-crack toughness data. Although the shallow-crack toughness data were available, the modified Irwin correction was applied to the data to determine if "predictions" could be made of the shallow-crack toughness using only deep-crack data. The "predicted" shallow-crack toughness was determined from the adjusted plane-strain, deep-crack toughness according to:[15]

$$K_c = K_{Ic} * (1 + 1.4\ \beta_{Ic}^2)^{1/2} \quad , \qquad (6.3)$$

Table 6.2 Actual and "predicted" toughness values using modified Irwin β_c correction[a,b]

HSST beam	a (mm)	B (mm)	K_c actual (MPa$\cdot\sqrt{m}$)	K_{Ic} (MPa$\cdot\sqrt{m}$)	K_c predicted (MPa$\cdot\sqrt{m}$)
4	51.8	50.7	95.2	79.1	120
5	51.2	50.6	97.3	80.1	120
6	51.9	50.6	145	99.7	120
12	49.8	102	104	94.2	98.7
16	50.0	153	105	99.6	94.2
Average deep flaw			109	90.5	111
7	10.2	50.7	163	81.0	216
8	9.63	50.8	304	101	227
9	9.52	50.9	261	95.0	229
10	14.0	50.9	212	99.0	169
11	8.36	102	196	81.9	256
13	8.81	102	264	93.0	245
14	8.69	152	260	92.0	247
15	8.66	153	168	78.1	248
Average shallow flaw			229	90.1	230

[a] Average of deep-crack adjusted values was used to "predict" toughness for shallow-flaw specimens.
[b] Only tests conducted at T = –60°C are included.

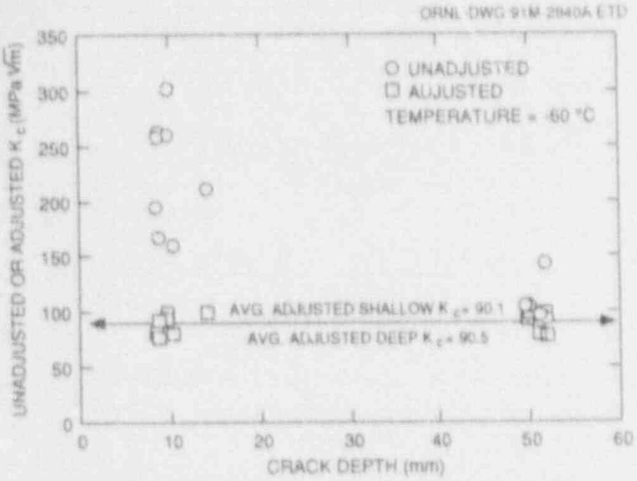

Figure 6.3 Application of modified Irwin β_c correction to shallow- and deep-crack-toughness data

where

K_{Ic} = 90.5 MPa-$\sqrt{m}$ (82.4 ksi-$\sqrt{in.}$),

$\beta_{Ic} = (K_{Ic}/\sigma_y)^2/2a$.

The agreement between the "predicted" shallow-crack toughness estimated using the modified Irwin correction and the actual toughness from the shallow-crack specimens is good. The average "predicted" shallow-crack toughness using the deep-crack data with the modified Irwin β_c correction is 230 MPa-$\sqrt{m}$ (209 ksi-$\sqrt{in.}$); the average actual shallow-crack toughness is 229 MPa-$\sqrt{m}$ (208 ksi-$\sqrt{in.}$). Examination (Table 6.2) of the actual vs "predicted" toughness for each shallow-crack test shows good agreement between the individual "predicted" and actual shallow-crack toughness values. It should be noted that the modified Irwin correction "predicted" the shallow-crack toughness for crack depths ranging between a = 8.36 to 14.0 mm (0.329 to 0.553 in.). The "predicted" shallow-crack toughness shows little scatter because the individual values only vary with the crack depth. The ability of the modified Irwin β_c correction to predict the elevated shallow-crack toughness from deep-crack data depends on similar out-of-plane constraint being present in the data of different thicknesses.

6.2.4 Future Work

The application of the shallow-crack, fracture-toughness data to reactor vessel analyses remains the final goal of the program. To reach that goal, more specimens should be tested with multiple crack depths and at several temperatures within the transition region. These tests are planned as a part of the production phase of the experimental testing program. The results generated to date are encouraging but not conclusive as to the manner in which to apply the data to an RPV. Prior experimental work within the HSST Program has included tests on thick-walled vessels that have contained relatively shallow flaws.[16] These tests offer a means to validate the technology of applying shallow-flaw toughness data to an RPV.

In addition, numerical analyses of the test specimen and the application (i.e., an axially oriented flaw in an RPV) need to be performed and interpreted. These analyses will provide a means for checking transferability of the test results to an RPV. The conditions under which the modified Irwin correction can be used in reactor vessel analyses need to be established.

6.3 Lower-Bound Initiation Toughness

(W. L. Fourney, G. R. Irwin, J. W. Dally, X. J. Zhang, and R. Bonenberger, University of Maryland)

A new experimental method has been developed by the research group at UM to measure the lower-bound initiation toughness in reactor-grade steel. The method uses two relatively small specimens (Notched Round-Bar and Modified Charpy) subjected to dynamic loading as the fracture specimens.[17–19] Lower-bound initiation toughness is achieved through enhanced constraint in the specimens and dynamic loading. The notched round-bar specimen provides enhanced constraint compared with similarly sized plate specimens. The modified-Charpy specimen is side-grooved, which enhances the constraint.

6.3.1 Notched Round-Bar Testing

Current research at UM has developed a systematic procedure for precompressing the notch to produce first a pseudo crack and then a natural crack. The amount of precompression on a specimen to be tested at a specific temperature is empirically determined. However, methods for interpreting SEM photomicrographs and strain-gage traces after the test permit verification of the adequacy of precompression.

In the precompression study of notched round bars it was observed that specimens tested during the last series of tests

were more difficult to break (successfully) than specimens tested during the previous round-bar program. A successful break means that the primary failure mode is by cleavage, with little or no prior ductile tearing. This difficulty was apparent at both test temperatures (20 and 42°C) but more pronounced at the higher temperature. It was confirmed that the A 533 B material employed in the last series of tests was different from the material tested during the previous round-bar program. In particular, the RT_{NDT} for the new material was –23°C, while the RT_{NDT} for the material used earlier was –2°C. This difference in RT_{NDT} effectively means that the new material will exhibit more ductility than the prior material at the same testing temperatures. This difference in material explains the difficulties encountered in successfully breaking the recent round-bar specimens.

While the experimental results from the round-bar specimens of A 533 B suffer to some degree because of the differences described above, the results are usable. It is possible to plot K_{Id} as a function of $T - RT_{NDT}$ and to obtain lower-bound crack-initiation toughness for $T - RT_{NDT}$ up to 50°C.

6.3.2 Modified-Charpy Specimens

The final draft of a paper, *Lower-Bound Initiation Toughness with a Modified-Charpy Specimen*, was submitted to ASTM and will be presented at the ASTM meeting held in Indianapolis, Indiana, in April 1991.

References

1. T. J. Theiss, Martin Marietta Energy Systems, Inc., Oak Ridge Natl. Lab., "Recommendations for the Shallow-Crack Fracture Toughness Testing Task Within the HSST Program," USNRC Report NUREG/CR-5554 (ORNL/TM-11509), August 1990.*

2. T. L. Dickson and T. J. Theiss, "Potential Impact of Enhanced Fracture-Toughness Data on Pressurized-Thermal Analysis," in *Proc. of the U.S. Nuclear Regulatory Commission Eighteenth Water Reactor Safety Meeting*, Rockville, Md., October 22–24, 1990, USNRC Conference Proceedings Report NUREG/CP-0014, Vol. 3, March 1991.*

3. T. J. Theiss, G. C. Robinson, and S. T. Rolfe, "Preliminary Test Results from the Heavy-Section Steel Technology Shallow-Crack Toughness Program," *Proc. of the ASME Pressure Vessel and Piping Conference: Pressure Vessel Integrity Session*, Vol. 213, San Diego, Calif., June 23–27, 1991.†

4. R. D. Cheverton and D. G. Ball, Martin Marietta Energy Systems, Inc., Oak Ridge Natl. Lab., "Pressurized-Thermal-Shock Evaluation of the H. B. Robinson Nuclear Power Plant," USNRC Report NUREG/CR-4183 (ORNL/TM-9567/V1), pp. 263–306, September 1985.*

5. R. D. Cheverton and D. G. Ball, Martin Marietta Energy Systems, Inc., Oak Ridge Natl. Lab., "Pressurized-Thermal-Shock Evaluation of the Calvert Cliffs Nuclear Power Plant," USNRC Report NUREG/CR-4022 (ORNL/TM-9408), pp. 201–44, September 1985.*

6. R. D. Cheverton and D. G. Ball, Martin Marietta Energy Systems, Inc., Oak Ridge Natl. Lab., "Preliminary Development of an Integrated Approach to the Evaluation of Pressurized Thermal Shock as Applied to the Oconee 1 Nuclear Power Plant," USNRC Report NUREG/CR-3770 (ORNL/TM-9176), pp. 5.1–5.51, May 1986.*

7. K. J. Bathé, Massachusetts Institute of Technology, Cambridge, Mass., "ADINA-87, A Finite Element Program for Automatic Dynamic Incremental Nonlinear Analysis," MIT Report 82448-1, 1975.

8. D. J. Naus, Martin Marietta Energy Systems, Inc., Oak Ridge Natl. Lab., "SEN Wide-Plate Crack-Arrest Tests Using A 533 Grade B Class 1 Material: WP-CE Series," USNRC Report NUREG/CR-5408 (ORNL/TM-11269), November 1989.*

9. D. J. Ayres et al., Electric Power Research Institute, "Tests and Analyses of Crack Arrest in Reactor Vessel Materials," Appendix G, Material Characterization, EPRI NP-5121SP, April 1987.

10. W. A. Sorem, R. H. Dodds, Jr., and S. T. Rolfe, "An Analytical Comparison of Short Crack and Deep Crack CTOD Fracture Specimens of an A36 Steel," *WRC Bulletin 351*, Welding Research Council, New York, February 1990.†

11. J. A. Smith and S. T. Rolfe, "The Effect of Crack Depth to Width Ratio on the Elastic-Plastic Fracture Toughness of a High-Strength Low-Strain Hardening Steel," *WRC Bulletin 358*, Welding Research Council, New York, November 1990.†

12. J. M. Barsom and S. T. Rolfe, *Fracture and Fatigue Control in Structures*, Prentice-Hall, Englewood Cliffs, N.J., 1987.†

13. M. G. Dawes, "Elastic-Plastic Fracture Toughness Based on the COD and J-Contour Integral Concepts," *Elastic-Plastic Fracture, ASTM 668*, J. D. Landes, J. A. Begley, and G. A. Clarke, eds., American Society for Testing and Materials, Philadelphia, 1979, pp. 307–333.

14. J. G. Merkle, Martin Marietta Energy Systems, Inc., Oak Ridge Natl. Lab., "An Examination of the Size Effects and Data Scatter Observed in Small-Specimen Cleavage Fracture Toughness Testing," USNRC Report NUREG/CR-3672 (ORNL/TM-9088), April 1984.*

15. J. G. Merkle, "An Approximate Method of Elastic-Plastic Fracture Analysis for Nozzle Corner Cracks," pp. 674–702, *Elastic-Plastic Fracture, ASTM 668*, J. D. Landes, J. A. Begley, and G. A. Clarke, eds., American Society for Testing and Materials, Philadelphia, 1979.†

16. R. D. Cheverton, S. K. Iskander, and D. G. Ball, "Review of Pressurized-Water-Reactor-Related Thermal Shock Studies," pp. 752–766 in *Fracture Mechanics: Nineteenth Symposium, ASTM STP 969*, T. A. Cruse, ed., American Society for Testing and Materials, Philadelphia, 1988.†

17. W. L. Fourney et al., University of Maryland, "HSST Program Semiann. Prog. Rep. October 1989–March 1990," USNRC Report NUREG/CR-4219, Vol. 7, No. 1 (ORNL/TM-9593/V7&N1), pp. 24–26, March 1991.*

18. W. L. Fourney et al., University of Maryland, "HSST Program Semiann. Prog. Rep. April–September 1989," USNRC Report NUREG/CR-4219, Vol. 6, No. 2 (ORNL/TM-9593/V6&N2), pp. 21–22, October 1990.*

19. R. J. Bonenberger, "Lower-Bound Initiation Toughness with a Modified-Charpy Specimen," Master's thesis, University of Maryland, 1990.

---

*Available for purchase from National Technical Information Service, Springfield, VA 22161.

†Available in public technical libraries.

7 Cladding Evaluations

J. Keeney-Walker*

7.1 Objective

The objective of this task is to achieve a more comprehensive representation of the effects of cladding in the probabilistic analysis of vessel fracture. In addition to the scheduled subtasks, a high-priority, unbudgeted subtask was requested by the NRC HSST Program monitor. Analyses were performed in this task to evaluate a vendor's proposal for including clad-base material differential expansion stresses in a proposed alternate procedure for performing the analysis required to demonstrate compliance with the Sect. XI LTOP requirements.

7.2 Introduction

Analyses of LTOP in an RPV were performed under the HSST Program at ORNL at the request of the NRC. The objective of these analyses was to compare the ORNL analysis results with values previously calculated by the Combustion Engineering Owners Group † (CEOG). CEOG's results remain proprietary and cannot be disclosed.

The ORNL analyses employed 3-D finite-element techniques and a thermoelastic constitutive formulation to model a clad RPV containing two different surface flaws. The K_I values for these surface flaws were determined for conditions at selected times in two LTOP transients previously defined by CEOG.† Contributions to the K_I values were calculated separately for loadings that were a result of internal pressure, crack-face pressure, cladding/base metal differential thermal expansion, and weld residual stresses. These components of crack loading were compared with CEOG results† obtained from LEFM using superposition and influence coefficients for generating stress-intensity factors.

In the following sections, the ORNL analysis methodology is described, including finite-element models, material properties, and loading conditions. The ORNL and CEOG analysis results are then compared and discussed.

7.3 Analysis Input

7.3.1 Geometry and Material Properties

Finite-element methods were used to analyze a generic RPV‡ with cladding; the through-wall dimensions are shown in Fig. 7.1. The vessel has an inner radius of 2206.6 mm (86.875 in.), a wall thickness (t_b) of 219.1 mm (8.625 in.), and a cladding thickness (t_c) of 7.9 mm (0.3125 in.) Two semielliptical axial surface flaws were analyzed, with length-to-depth ratios of 6:1 and maximum depths of 18.9 mm (0.744 in.) (t_c + 5% t_b) and 40.8 mm (1.606 in.) (t_c + 15% t_b). The vessel base material is SA 533 grade B class 1 steel, and the cladding is type 304 stainless steel. The vessel material properties reported in Table 7.1 are assumed to be temperature-independent.

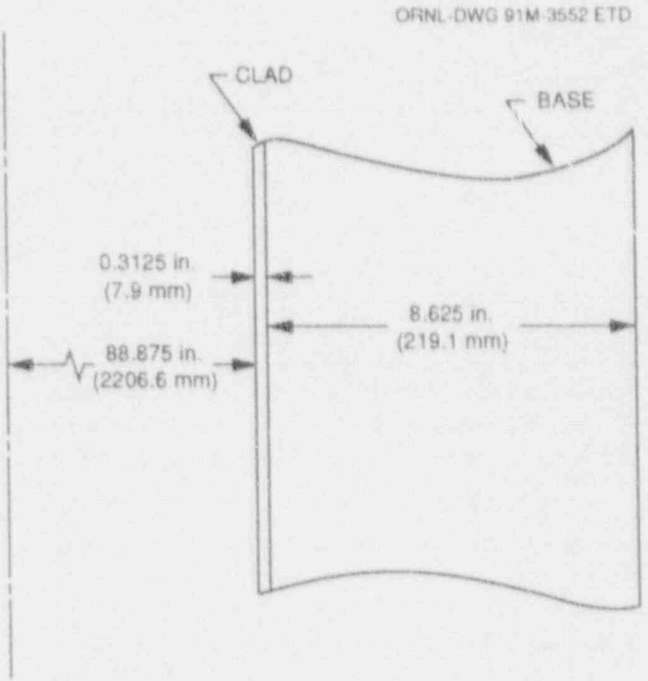

Figure 7.1 Dimensions of generic RPV used by ORNL and CEOG for LTOP analyses

*Computing and Telecommunications Division, Martin Marietta Energy Systems, Inc., Oak Ridge, Tenn.

†Combustion Engineering Owners' Group, "Low-Temperature Overpressurization Transient Pressure-Temperature Limit for Determination of Low Temperature Overpressure Protection Setpoints," Proprietary Report CEN-381-P, December 1988.

‡D. J. Ayres, Combustion Engineering, Inc., personal communication to B. R. Bass, ORNL, December 7, 1990.

Table 7.1 Material properties for cladding and base metals[a]

Material	Elastic modulus (GPa)	Poisson's expansion	Thermal expansion (°C)	Thermal conductivity (W/m-K)	Density (kg/m^2)	Specific heat (J/kg-K)
Base	196.5	0.3	13.5×10^{-6}	42.7	7833.0	502.4
Clad	186.2	0.3	16.4×10^{-6}	17.3	7833.0	502.4

[a]Film coefficient = 567.3 W/m^2K.

The following three models were used in the ORNL analyses: (1) a 3-D finite-element model of a cylinder, (2) a 3-D finite-element model of a cubic element from a cylinder, and (3) an influence coefficient model implemented in the OCA-P[1] probabilistic fracture-mechanics code. Both models 1 and 2 used generalized plane-strain boundary conditions to impose displacement restraints appropriate for conditions in an RPV. This methodology permits the use of increased mesh refinement in the crack-tip region of the model.

The ORNL 3-D finite-element model of the cylinder is shown in Figs. 7.2 and 7.3. The model consists of 6768 nodes, 1234 twenty-noded isoparametric brick elements, and 192 wedge elements at the crack front, with the midside nodes shifted to the quarter-point position for a $1/\sqrt{r}$ singularity in the stress and strain fields. One quarter of the cylinder is modeled due to symmetry, and a generalized plane-strain condition is applied in the axial direction. Mesh convergence studies[2] for RPV cylinders containing shallow flaws demonstrated that meshes on the order of 8700 degrees of freedom produced converged K_I values within 1%. The finite-element model of the cylinder employed in this study has >15,000 degrees of freedom and is estimated to provide comparable accuracy in K_I values.

The ORNL 3-D, finite-element model of the cube shown in Figs. 7.4 and 7.5 has the same through-wall thickness as the cylinder. This model consists of 6763 nodes, 1184 twenty-noded isoparametric brick elements, and 240 wedge elements at the crack front with midside nodes shifted to the quarter-point position. A generalized plane-strain condition is applied on two surfaces to approximate the displacement boundary conditions on a cube of material in the RPV containing a surface crack.

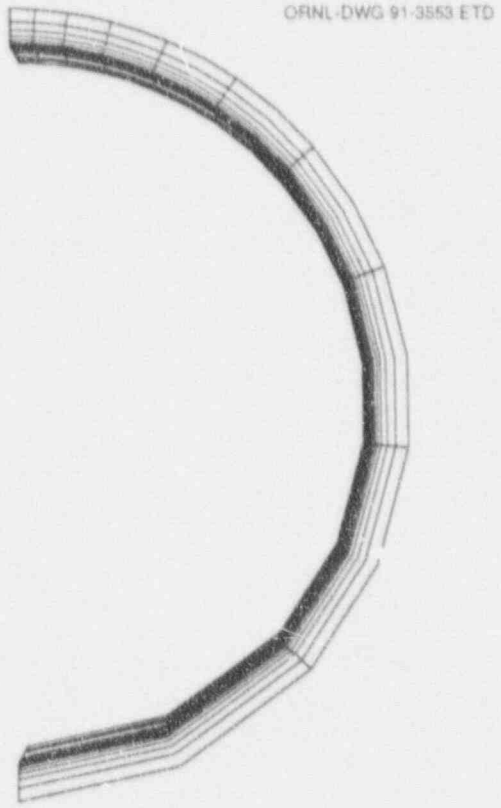

Figure 7.2 Three-dimensional, finite-element model of clad cylinder

The model implemented in OCA-P utilizes influence coefficients for an RPV having a slightly different geometry from that given in Fig. 7.1. The OCA-P vessel has an inner radius of 2047.2 mm (86.0 in.), a total wall thickness of 215.9 mm (8.5 in.), and a cladding thickness of 5.4 mm (0.2125 in.). (Constraint imposed on the scheduled completion of this study precluded the generation of influence coefficients for the geometry of Fig. 7.1.)

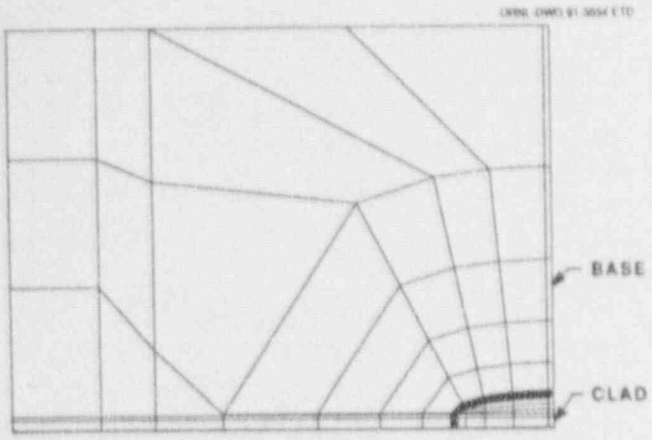

Figure 7.3 Close-up view of crack-tip region of clad cylinder

7.3.2 Loading Conditions

Four different load cases were applied to the 3-D cylinder model: (1) thermal stress due to a temperature gradient and differential thermal-expansion coefficients for the clad and base material, (2) internal pressure, (3) crack-face pressure, and (4) weld residual stresses in the base material. The clad stress-free temperature was taken to be the operating temperature of the vessel.

Cooldown rates of –7°C/h (20°F/h) and 38°C/h (100°F/h) were used to define thermal-loading for the ORNL analyses.[1] Thermal analyses were performed using the ORNL heat-conduction program ONE-R[1] to determine the temperature distribution through the wall as a function of time. These were based on the vessel dimensions in Fig. 7.1 and the material properties and film coefficient in Table 7.1, the results of which compared well with CEOG.*,† Through-wall temperature profiles were used to interpolate temperatures for the 3-D cylinder and cube models at two time points (warm and cold end) of each cooldown transient. The temperature of the inner surface of the vessel for the –7°C/h (20°F/h) cooldown was 148°C (297.6°F) (warm end) and 19°C (84.3°F) (cold end), and 195°C (383.3°F) (warm end) and 103°C (217.0°F) (cold end) for the 38°C (100°F/h) cooldown. The temperature distributions through the wall of the vessel for the two cooldown rates at both warm and cold ends are shown in Figs. 7.6 and 7.7.

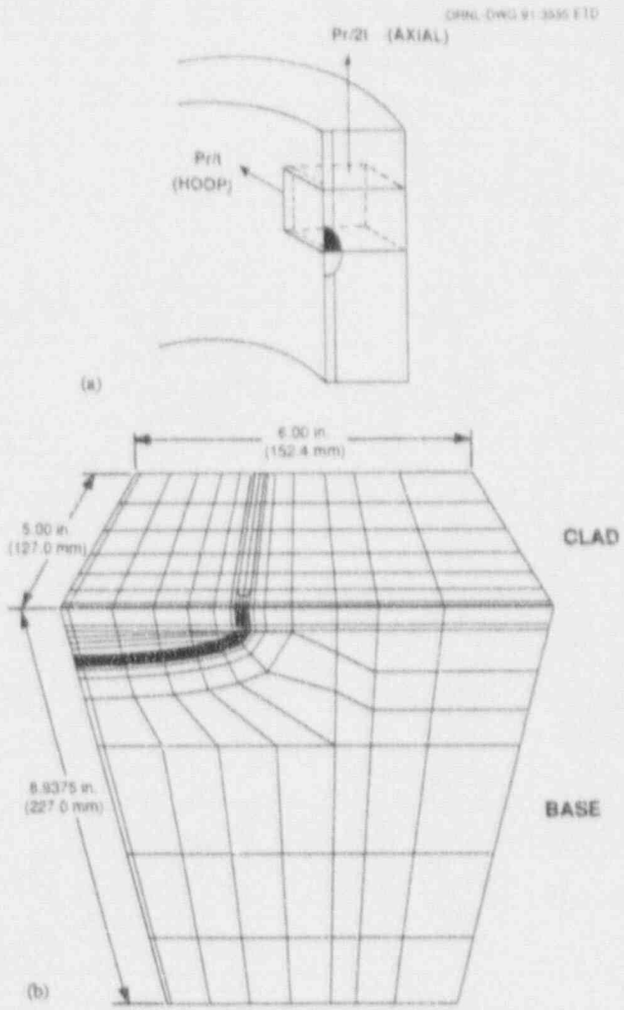

Figure 7.4 Schematic showing portion of RPV with flaw modeled using finite-element techniques. (*a*) RPV containing surface crack and (*b*) 3-D finite-element model of clad cube

The internal pressure and crack-face pressure were applied as unit loads to the 3-D finite-element models in separate cases. For the cylinder, 3-D pressure elements were employed on the inner surface, and a force applied in the axial direction on the generalized-plane-strain boundary provided a statically equivalent endcap loading. The 3-D cube model had generalized-plane-strain boundary conditions imposed on the vertical surfaces of the model to simulate deformation restraint consistent with that found in an RPV shell, that is, plane surfaces remain plane. Loading due to internal pressure was applied on these surfaces in the form of resultant forces derived from a Pr/t stress

*D. J. Ayres, Combustion Engineering, Inc., personal communication to B. R. Bass, ORNL, December 7, 1990.
†D. J. Ayres, Combustion Engineering, Inc., personal communication to B. R. Bass, ORNL, December 20, 1990.

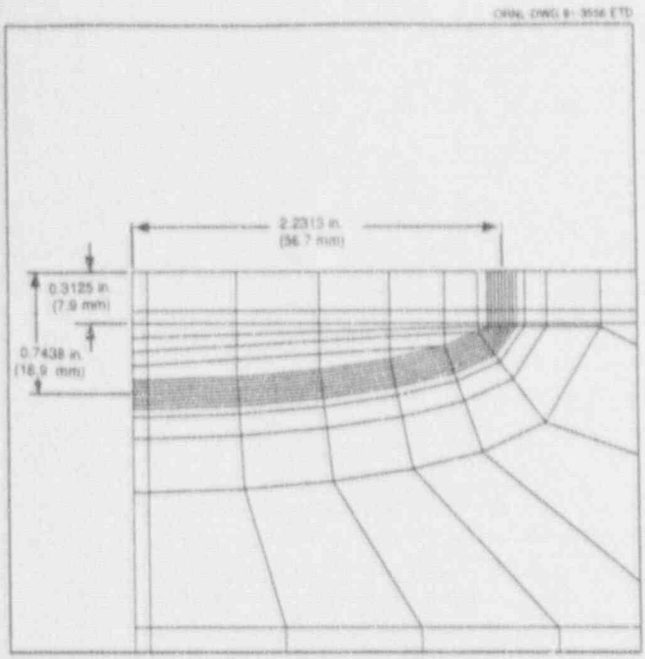

Figure 7.5 Close-up view of crack-tip region of clad cube

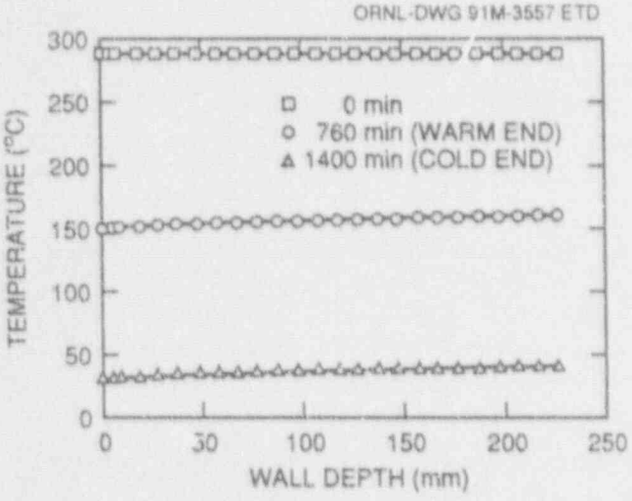

Figure 7.6 Through-wall temperature distribution of –7°C/h cooldown transient at warm and cold ends

distribution in the hoop direction and Pr/2t stress distribution in the axial direction. The crack-face pressure was applied to both models using 3-D pressure elements. The K_I values computed for a unit load were multiplied by

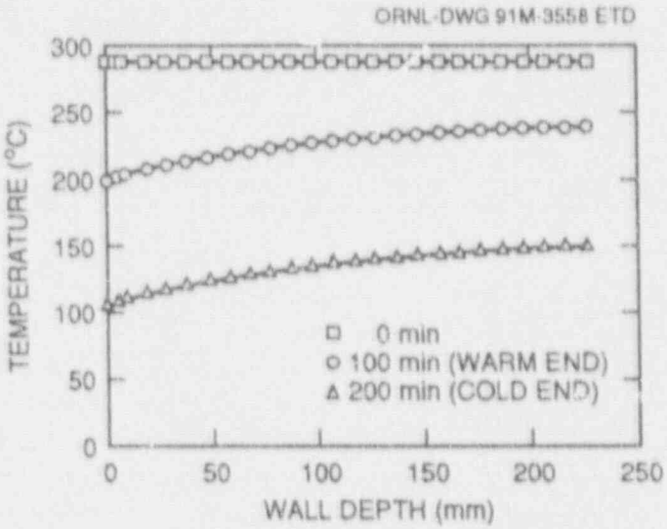

Figure 7.7 Through-wall temperature distribution of 38°C/h cooldown transient at warm and cold ends

the specified pressures*,† to obtain K_I values for comparison with the CEOG analyses.

The residual stresses in the base metal (due to welding when the vessels are fabricated) are generally tensile on the inside and outside surface and compressive in the midwall. These stresses were produced in the 3-D cylinder by applying a fictitious temperature distribution through the vessel wall in the form of a cosine functio. (Fig. 7.8).

7.4 Analysis Results and Discussion

Thermoelastic analyses were performed for the 3-D cylinder and cube models using the ADINA/ORVIRT[3,4] system and the material properties from Table 7.1. The four different load cases were applied to the cylinder, and all but the residual stress case were applied to the cube. The OCA-P analyses consisted of the internal pressure loading and the crack-face, pressure-loading cases.

*D. J. Ayres, Combustion Engineering, Inc., personal communication to B. R. Bass, ORNL, December 20, 1990.

†Combustion Engineering Owners' Group, "Low-Temperature Overpressurization Transient Pressure-Temperature Limit for Determination of Low-Temperature Overpressure Protection Setpoints," proprietary slides from presentation to the U.S. Nuclear Regulatory Commission, June 1990.

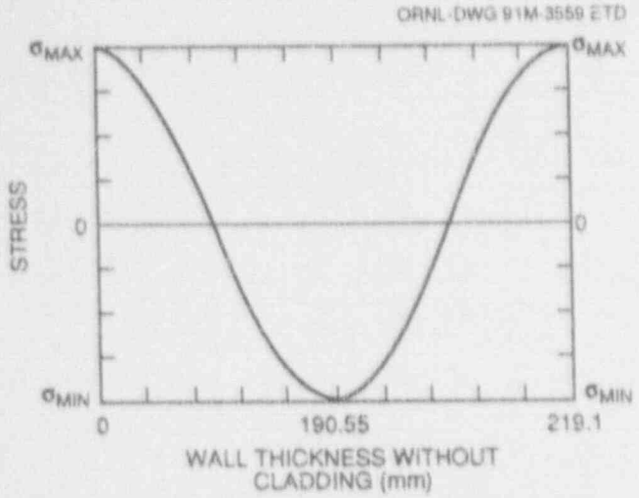

Figure 7.8 Through-wall weld residual stress distribution for RPV

For each case the K_I values (at the deepest point of the flaw) compared well for the three ORNL models. The K_I value for the case of crack-face pressure was ~10% of K_I for the internal pressure case. Also, K_I increases for the deeper flaw in the pressure and residual stress cases and decreases for the thermal stress case. The K_I contributions from each case in the ORNL study are compared with results from CEOG for the two cooldown rates and crack depths. The percent difference between K_I for the CEOG and ORNL 3-D cylinder models ranged from 1 to 14% for pressure loading, 3 to 11% for thermal loading, 24 to 30% for residual stresses, and 1 to 15% for the total contributions.

The percent difference between the ORNL and CEOG analyses for total K_I contributions produced by the component loads increases for the shallower-flaw depth and the faster cooldown rate. The greatest difference between the individual contributions in the analyses were the K_I values generated for the weld residual stress case. This discrepancy cannot be explained without obtaining additional information concerning the CEOG analysis techniques.

7.5 Conclusion

For this set of analyses, the differences between the ORNL and CEOG calculations of K_I values were larger for the relatively shallower (t_c + 5% t_b) flaw: 10% for the –7°C (20°F/h) cooldown and 15% for the 38°C (100°F/h) cooldown. These differences could be greater for shallower flaws (t_c or $2t_c$) analyzed by CEOG.*†

References

1. R. D. Cheverton and D. G. Ball, Martin Marietta Energy Systems, Inc., Oak Ridge Natl. Lab., "OCA-P, A Deterministic and Probabilistic Fracture-Mechanics Code for Application to Pressure Vessels," USNRC Report NUREG/CR-3618 (ORNL-5991), May 1984. ‡

2. D. G. Ball et al., Martin Marietta Energy Systems, Inc., Oak Ridge Natl. Lab., "Stress-Intensity Factor Influence Coefficients for Surface Flaws in Pressure Vessels," USNRC Report NUREG/CR-3723 (ORNL/CSD/TM-216), February 1985.‡

3. K. J. Bathe, "ADINA—A Finite Element Program for Automatic Dynamic Incremental Nonlinear Analysis," Report A-1, Massachusetts Institute of Technology, Cambridge, Mass., 1984. §

4. B. R. Bass and J. W. Bryson, Union Carbide Corp. Nuclear Div., Oak Ridge Natl. Lab., "Applications of Energy Release Rate Technique to Part-Through Cracks in Plates and Cylinders, Volume 2. ORVIRT: A Finite Element Program for Energy Release Rate Calculations for 2-Dimensional and 3-Dimensional Crack Models," USNRC Report NUREG/CR-2997/Vol. 2 (ORNL/TM-8527/V2), February 1983.‡

*Combustion Engineering Owners' Group, "Low-Temperature Overpressurization Transient Pressure-Temperature Limit for Determination of Low-Temperature Overpressure Protection Setpoints," proprietary slides from presentation to the U.S. Nuclear Regulatory Commission, June 1990.

†D. J. Ayres, Combustion Engineering, Inc., personal communication to B. R. Bass, ORNL, December 20, 1990.

‡Available for purchase from National Technical Information Service, Springfield, VA 22161.

§Available in technical public libraries.

8 Pressurized-Thermal-Shock Technology

T. L. Dickson* and D. K. M. Shum

8.1 Background

The OCA-P computer program incorporates an axisymmetric model of the reactor vessel's thermal-hydraulic boundary conditions existing during a PTS transient. The one-dimensional (1-D) transient heat-transfer model incorporated into OCA-P calculates the radial temperature profile in the vessel wall at each time step throughout the PTS transient. The radial temperature profile is then used to calculate equibiaxial thermal stresses that vary in the radial direction only. At the time OCA-P was written, the axisymmetric model was believed to provide conservative results because all beltline welds were subjected to the maximum effect of thermal stresses resulting from the PTS radial temperature profile.

Recently published results from thermal-hydraulic experiments performed in the decommissioned HDR RPV in Germany have raised concerns that thermal streaming may represent a significant source of additional thermal stresses not currently included in the OCA-P analysis.[1–4] Thermal streaming beneath the RPV inlet nozzles can occur when cold safety coolant is injected into a stagnant reactor primary coolant loop. Flow stagnation in the primary coolant loop may occur during a LOCA if the primary system leak size is such that the water level in the steam generators falls below the level of the U-bends, thereby breaking the primary coolant loop siphon.

Thermal streaming in the RPV downcomer annulus flow generates a nonuniform circumferential temperature distribution in the reactor vessel wall. Thermal stresses resulting from the nonuniform circumferential temperature distribution could be important in the PTS analysis of flaws in circumferential welds. Thermal-streaming stresses in the vessel wall are proportional to the stream plume strength. Analysis and testing required to characterize the plume strength are conducted within companion elements of the NRC research program.

*Computing and Telecommunications Division, Martin Marietta Energy Systems, Inc., Oak Ridge, Tenn.

8.2 Task Objective

The primary task objective, within the HSST Program, is the emphasis on development of the OCA-P computer program to permit the effect of thermal-streaming plumes to be incorporated into the PTS analysis of circumferential welds. One aspect of this development is the formulation of a closed-form solution for the stress-intensity factor that considers the effects of a nonuniform circumferential temperature distribution in the RPV wall within the context of LEFM. This closed-form solution will provide the stress-intensity factor as a function of vessel geometry and crack length. The closed-form solution will, in turn, involve closed-form solutions for the elastic stresses within the RPV wall due to nonuniform circumferential cooling and the stress-intensity factor influence coefficients as a function of crack length. This section focuses on the generation of benchmark solutions for the elastic stresses under thermal-streaming conditions using the finite-element method. These benchmark solutions will be used to validate the closed-form elastic stress solutions discussed previously.

8.3 Finite-Element Model

The general-purpose, finite-element code ABAQUS[5] is used to generate the benchmark solutions. The finite-element model is formulated to examine the general thermal-streaming problem in two dimensions with the capability to incorporate (1) a variable-convection, heat-transfer coefficient at fluid-to-solid interfaces with respect to vessel temperature and/or location around the circumference of the vessel, and (2) pressure loading concurrent to the thermal-streaming loads. The finite-element model can be used to examine plane-strain or generalized plane-strain conditions subject to elastic or elastic-plastic material response assumptions.

The H. B. Robinson vessel geometry considered has an outer radius of 2.22 m (87 in.), an outer radius-to-wall thickness ratio of 9.4, and a cladding thickness of 0.56 cm (0.22 in.). The thermal-streaming transient considered is periodic with respect to the circumferential direction of the vessel with a period of 120°. The three-loop vessel was modeled because well-defined data existed from the IPTS studies.[6] Future studies may consider four-loop designs.

The finite-element model, which, from symmetry conditions, models a 120° circumferential section of the vessel, is shown in Fig. 8.1. The finite-element model in Fig. 8.1 is made up of 240 generalized plane-strain elements and 791 nodes. These elements behave as conventional eight-node isoparametric elements, except for an extra degree-of-freedom that allows for uniform straining in a direction perpendicular to the plane of the mesh. In a plane-strain analysis, axial displacement of the vessel is prevented. In a generalized plane-strain analysis uniform axial displacement of the vessel in response to the imposed thermal loading is permitted.

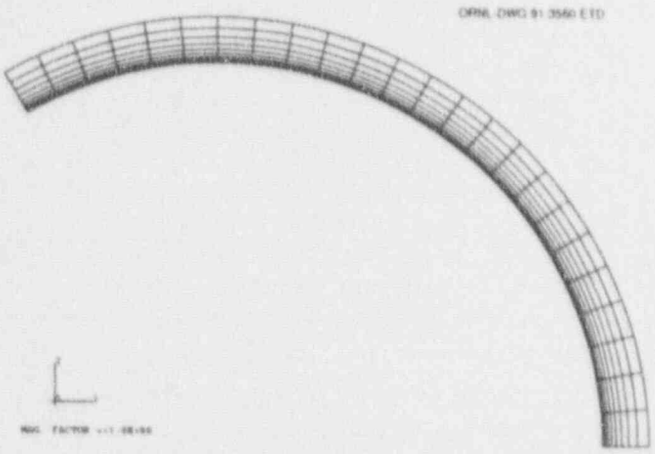

Figure 8.1 Finite-element model of the H. B. Robinson RPV. A 120° circumferential section of vessel is indicated

The severity of a thermal-streaming transient is characterized by (1) the difference between the well-mixed cooling-water temperature and the vessel operating temperature, (2) the difference between the centerline and the well-mixed temperature of the cooling water referred to as the "plume strength" of the thermal-streaming transient, and (3) the variation of cooling-water temperature from the centerline to the well-mixed region. Analysis results have been obtained for the following thermal-streaming transient: (1) the operating temperature of the vessel prior to the imposition of the transient is 288°C (550°F), and (2) the thermal transient, designated as event 9.22B in the IPTS studies[6] and considered to be a dominant transient, is assumed as the well-mixed cooling-water temperature. Event 9.22B is indicated in Fig. 8.2. This thermal transient is modified to include a plume strength of 13.9°C (25°F) according to the equation

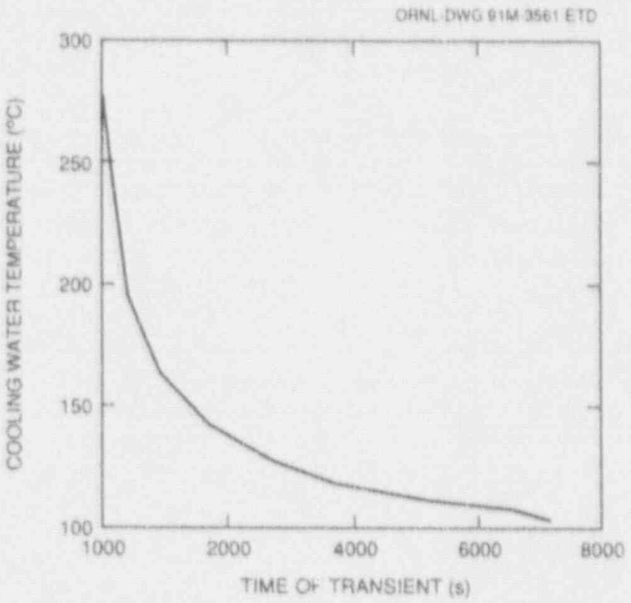

Figure 8.2 Thermal transient designated as event 9.22B in IPTS studies

$$T(y,t) = T_W(t) - [T_{CL}(t) - T_W(t)]\, e^{-0.0042y2} \quad ,$$

where $T_W(t)$ is the well-mixed temperature according to event 9.22B, $[T_{CL}(t) - T_W(t)]$ is by definition the plume strength, and y is the circumferential distance along the inner surface of the vessel as measured from the centerline of the cooling water in units of inches.

The German publications have suggested plume strengths of considerably larger magnitudes; however, Dr. T. G. Theofanous is of the opinion that U. S. Pressurized-Water Reactor (PWR) designs have smaller plume strengths than those in the German publications. The 13.9°C (25°F) plume strength was arbitrarily chosen for the studies but is believed to be consistent with REMIX[7] predictions for U.S. PWR designs. It is anticipated that the methodology for incorporating thermal streaming into OCA-P will use plume strength as a user-specified input parameter.

The convection heat-transfer coefficient is assumed to be constant at a value of 400 Btu/(hr•ft^2•°F). The mechanical and thermal properties of the cladding and the base material are independently specified. Thermal properties are prescribed in terms of thermal conductivity k, mass density ρ, specific heat c, and thermal-expansion coefficient α. Analysis results have been obtained assuming elastic material response in terms of Young's modulus E and Poisson's ratio ν. The material properties

for the cladding are k = 10 Btu/(hr•ft•°F), E = 27,000 ksi, ρ = 489 lb_m/ft^3, ν = 0.3, c = 0.12 Btu/(lb_m•°F), and $\alpha = 1 \times 10^{-6}$/°F. The material properties for the base material are k = 24 Btu/(hr•ft•°F), E = 28,000 ksi, ρ = 489 lb_m/ft^3, ν = 0.3, c = 0.12 Btu/(lb_m•°F), and $\alpha = 8 \times 10^{-5}$/°F.

8.4 Finite-Element Analysis Results

In considering thermal-streaming effects on initiation of circumferential flaws, the axial stress component is of primary interest. Analysis results up to 7200 s into the postulated transient have been obtained. The axial stress component at the centerline and well-mixed locations on the inner surface of the vessel are indicated in Figs. 8.3 and 8.4 for the cases of plane-strain and generalized plane-strain conditions, respectively. Analysis results indicate that both the magnitude and the time of occurrence of the maximum value of the axial stress is very sensitive to the assumption of plane-strain or generalized plane-strain conditions for the present combination of thermal transient and vessel geometry. On the other hand, the axial stress distribution appears to be relatively insensitive to the thermal-streaming aspect of this analysis, as characterized by the plume strength of 13.9°C (25°F). Whether this insensitivity to thermal-streaming effects would continue to hold for more severe transients, as characterized by higher values of the plume strength, has not been investigated.

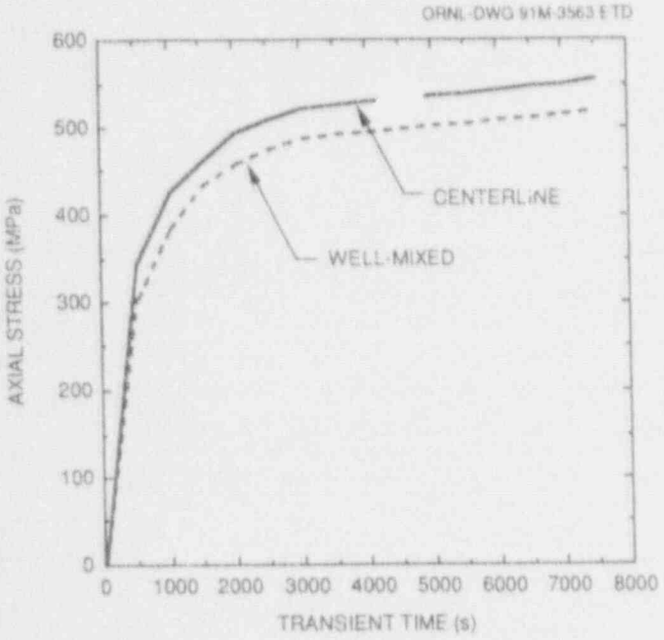

Figure 8.3 Axial stress component at centerline and well-mixed locations on inner surface of vessel for case of plane-strain conditions

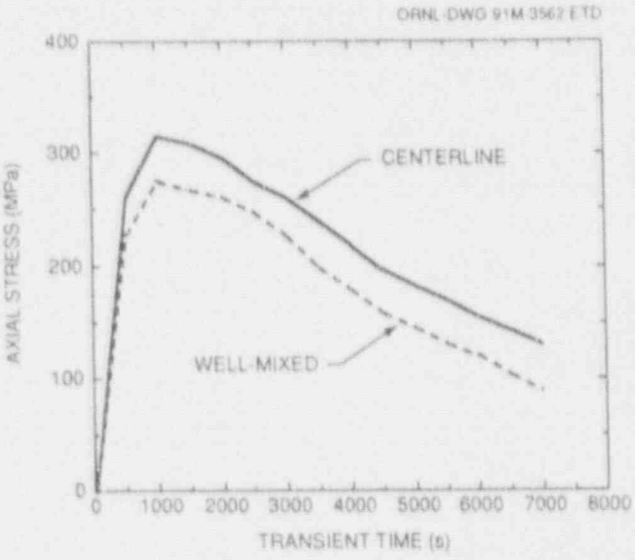

Figure 8.4 Axial stress component at centerline and well-mixed locations on inner surface of vessel for case of generalized plane-strain conditions

8.5 Anticipated Activities

Further multidimensional, finite-element analyses will be performed. The results from these analyses will be used to incorporate a methodology into OCA-P to include the effects of thermal streaming.

References

1. M. Geib, "Verification of OCA-P and VISA II on Behalf of Strains and Stresses Induced During HDR-TEMB Thermal Mixing Tests," Battelle-Institute, Frankfurt, Germany, 1988.*

2. G. E. Neubrech et al., "Crack Initiation and Crack Growth During Thermal-Shock Tests in the Reactor Pressure Vessel of the HDR Under Corrosive Medium Conditions," *Int. J. Press. Ves. and Piping* 24, 1-5 (1988).*

3. L. Wolf et al., "Application of Engineering and Multidimensional Finite-Difference Codes to HDR Thermal Mixing Experiments," *Nucl. Eng. & Des.* 108, 137–165 (1988).*

4. H. Kordish, "Analysis of Initiation and Growth of a Circumferential Crack in the HDR-RPV Cylinder Under Pressurized Thermal Shock," pp. 1–15 in *Trans. of the Tenth Intern. Conf. on Structural Mechanics in Reactor Technology, PostSMiRT Conference, No. 2, Monterey, CA*, August 1989, The American Association for Structural Mechanics in Reactor Technology, 1990.*

5. ABAQUS *Theory Manual*, version 4-8, Hibbitt, Karlsson and Sorensen, Inc., Providence, R.I., 1989.*

6. D. L. Selby et al., Martin Marietta Energy Systems, Inc., Oak Ridge Natl. Lab., "Pressurized-Thermal-Shock Evaluation of the H. B. Robinson Nuclear Power Plant," USNRC Report NUREG/CR-4183 (ORNL/TM-9567), September 1985.†

7. K. Iyer et al., REMIX: A Computer Program for Temperature Transients Due to High Pressure Injection After Interruption of Natural Circulation, School of Nuclear Engineering, Purdue University, May 1986.

---

*Available for purchase from National Technical Information Service, Springfield, VA 22161.

†Available in public technical libraries.

9 Analysis Methods Validation

B. R. Bass*

During this report period, work was performed in support of the Project for Fracture Analysis of Large-Scale International Reference Experiment (Project FALSIRE). Analyses of large-scale experiments performed for the Project FALSIRE Workshop were compared and evaluated. Results from the comparisons are being used in preparation of an interpretive report summarizing results, conclusions, and recommendations of the workshop. Preparation of an invited technical paper to be presented at the 11th International Conference on Structural Mechanics in Reactor Technology (SMiRT), scheduled for August in Tokyo, Japan, was completed.

9.1 Project FALSIRE Workshop

(B. R. Bass,* J. Keeney-Walker,* C. E. Pugh, C. W. Schwartz,† H. Schulz,‡ and J. Sievers‡)

Project FALSIRE was sponsored by the Fracture Assessment Group (FAG) of Principal Working Group No. 3 (PWG/3) of the Organization for Economic Cooperation and Development (OECD)/Nuclear Energy Agency's (NEA's) Committee on the Safety of Nuclear Installations (CSNI). On behalf of the CSNI/FAG, the HSST Program and the Gesellschaft für Reaktorsicherheit (GRS), Köln, Germany, had responsibility for organization arrangements related to Project FALSIRE. The CSNI/FAG was formed to evalute fracture prediction capabilities currently used in safety organizations in Western Europe, Japan, and the United States. H. Schulz from GRS, Köln, Germany, is chairman of the CSNI/FAG.

The CSNI/FAG planned Project FALSIRE to assess various fracture methodologies through interpretive analyses of selected large-scale fracture experiments. The reference experiments eventually selected by CSNI/FAG for detailed analysis and interpretation are given in Table 9.1.

The CSNI/FAG established a common format for comprehensive statements of these experiments, including supporting information and available analysis results. These statements formed the basis for evaluations that were performed by an international group of analysts using a variety of techniques. A three-day workshop was held in Boston during May 1990, where all participating analysts examined these evaluations in detail.

Comparative assessment of the solutions presented at the Project FALSIRE Workshop are being carried out by GRS-Köln, ORNL, and other participants in the workshop. A comprehensive report of the findings, conclusions, and recommendations from the workshop is being prepared on the basis of these assessments as a cooperative effort between GRS-Köln, ORNL, and other members of the CSNI/FAG. From this material, an invited paper was prepared for presentation at the 11th SMiRT Conference in August 1991 in Tokyo, Japan. A letter report on Project FALSIRE will also be issued to the NRC in September 1991 by the HSST Program. At the end of 1991, the comprehensive draft report is scheduled to be completed by the CSNI/FAG and forwarded to the CSNI/PWG-3 for final review.

During March, plans were reinstated to meet with Dr. Schulz and members of his staff at GRS-Köln during late May 1991. The meeting was originally scheduled for March 1991 but was cancelled due to an NRC prohibition on international travel during the Gulf War. The purpose of this meeting is to discuss plans for (1) completion of the draft report on the Project FALSIRE Workshop and (2) a second round of international analyses sponsored by the CSNI/FAG that will focus on upcoming large-scale fracture experiments. During this trip a meeting is also scheduled with the staff at UKAEA-Risley to discuss using recent spinning-cylinder tests in the second phase of the CSNI/FAG project.

9.2 Discussion of Project FALSIRE Results

Although analysis results from the Project FALSIRE Workshop are still being evaluated, several observations can be made concerning predictive capabilites of current fracture assessment methodologies as reflected in the large-scale experiments described in the previous section. Generally, these experiments were designed to verify fracture methodologies under prototypical combinations of geometry, constraint, and loading conditions. However,

*Computing and Telecommunications Division, Martin Marietta Energy Systems, Inc., Oak Ridge, Tenn.
†University of Maryland, College Park, Maryland.
‡GRS, Köln, Federal Republic of Germany.

Table 9.1 Large-scale fracture experiments analyzed in CSNI/FAG Project FALSIRE

Experiment	Testing organization	Country
NKS-3	Material Prüfungsanstalt (MPA) der Universitat Stuttgart	FRG
NKS-4	Material Prüfungsanstalt (MPA) der Universitat Stuttgart	FRG
PTSE-2	Oak Ridge National Laboratory	USA
Spinning Cylinder I (SC-I)	Atomic Energy Authority (AEA) Risley, United Kingdom	UK
Spinning Cylinder II (SC-II)	Atomic Energy Authority (AEA) Risley, United Kingdom	UK
Step B PTS	Japan Power and Engineering Inspection Corp. (JAPEIC)	Japan

because complexities of the experiments do not permit a clear separation of the effects of the many variables involved, it has proved difficult to interpret those transients for which expected results were not achieved. Modeling requirements for the experiments incorporate history-dependent mechanical, thermal, and body force loadings; temperature-dependent material and fracture-toughness properties; residual stress states; and 3-D effects. Interactions of both cleavage and ductile modes of fracture must be modeled for certain transients. For these reasons, it could be anticipated that comparisons of analysis predictions with available structural data from the experiments would yield results that vary significantly. Examples of comparisons that produce substantial difference between measured data and computed values are found in CMOD vs time plots for experiments NKS-4 and PTSE-2. The largest differences occur in the PTSE-2 transient. These analysis results highlight the importance of obtaining high-quality material properties and structural response data (CMOD, strains, etc.) from the experiments to model structural behavior of the specimen prior to performing fracture-mechanics evaluations.

In applications of J_R methodology based on small-specimen data, all analyses correctly distinguished between stable crack growth and ductile instability conditions for each experiment. These included both estimation schemes and detailed finite-element analyses. However, as a technique to predict crack extension, J_R methodology was partially successful in some cases (NKS experiments) but not in others (PTSE-2, spinning-cylinder experiments.) In PTSE-2, differences between pretest characterization data and posttest in situ data for material and fracture-toughness properties gave rise to questions concerning whether J_R curves from CT specimens were representative of the flawed region of the vessel. None of these temperature-dependent J_R curves were consistent with all phases of ductile tearing observed in PTSE-2. It should be pointed out that the PTSE-2A transient included load-history (i.e., warm-prestressing) effects that were not incorporated into the J_R methodology. The substantial differences between fracture-toughness curves generated from the spinning cylinders and from CT specimens focused attention on other factors, including the possibility that crack-tip behavior in the spinning cylinder is not characterized by a single correlation parameter. Alternative criteria under consideration include two-parameter models in which K or J is augmented by the next higher-order term T[1] or Q* in the series expansion of the stresses around the crack tip. Other measures considered in dealing with the transfer of small-specimen data to large structures include the stress-triaxiality parameter q, which is proportional to the ratio of hydrostatic to effective stress.[2] Also, the local approachs have been applied as an alternative to JR methodology for performing fracture-toughness evaluations. For the spinning cylinders, clarification of the initial stress state in

*H. Clausmeyer, K. Kussmaul, and E. Roos, "Der Einfluss des Spannungszustandes auf den Versagensablauf angerissener Bauteile aus Stahl," *Mat.-wiss. u. Werkstofftech* 20, 102–117 (1989).

front of the crack tip (due to cyclic fatiguing) may be an important consideration.

Preliminary evaluation of the analyses presented at the CSNI/FAG Workshop in Boston showed valuable results. Interpretation of discrepancies revealed in comparisons of these analyses is still ongoing. Additional details concerning comparative analyses of the contributed solutions will be included in the forthcoming final report on Project FALSIRE. Recommendations will be made for future development of fracture methodologies to improve these predictive capabilities.

References

1. A. M. Al-Ani and J. M. Hancock, "J-Dominance of Short Cracks in Tension and Bending," *J. of Mechanics and Physics of Solids* 39(1), 23–43 (1991).*

2. N. P. O'Dowd and C. F. Shih, "Family of Crack-Tip Fields Characterized by a Triaxiality Parameter: Part I–Structure of Fields," *J. of Mechanics and Physics of Solids* 9, 983–1015 (1991).*

*Available in public technical libraries.

10 Fracture Evaluation Tests

T. J. Theiss

The purpose of this task is to provide experimental support for all remaining tasks within the HSST Program. Currently, the only testing under way is the shallow-crack fracture-toughness testing program described in Chap. 6, "Cleavage Crack Initiation." The motivation for the shallow-crack program and the test results and interpretation are detailed in Chap. 6. This chapter describes the details of the testing in support of the shallow-crack fracture-toughness program.

The specimen configuration chosen for testing shallow cracks in the shallow-crack project is the single-edge-notch-bend (SENB) specimen with a through-thickness crack (as opposed to surface crack). The bend specimen better simulates the varying stress field in a reactor wall under PTS conditions. In addition, previous shallow-crack work has utilized SENB specimens.[1,2] The straight-through notch simulates an infinitely long, axially oriented crack in an RPV. To better simulate the conditions of a shallow flaw in the wall of a reactor vessel, the specimen depth W and thickness B should be as large as practicable. PWR vessel walls are nominally 200 to 280 mm thick (8 to 11 in.). An ≈100-mm-deep (4-in.) beam has been selected for use in the HSST shallow-crack project. Beams 50, 100, and 150 mm thick (2, 4, and 6 in.) were tested to investigate the influence of differing out-of-plane-constraint levels on the toughness of shallow- and deep-crack specimens. The stress state in beams of this size simulates the stress state in a flawed vessel wall. To maintain consistency with ASTM standards, the beams are being tested in 3PB. All testing is being conducted on reactor material (A 533 grade B, class 1)[2] with the cracks oriented in the L-S orientation to maintain consistency with the conditions of an RPV. Figure 10.1 shows three of the specimens tested in the shallow-flaw program.

Table 10.1 gives a summary of the development phase test matrix, showing the number of tests performed at each condition. Fourteen specimens have been tested to date. Of the 14 beams tested, 5 were deep-cracked and 9 were shallow (a/w = 0.10–0.15). Eight of the beams tested were 50 mm (2 in.) thick, 3 beams were 100 mm (4 in.) thick, and 3 beams were 150 mm (6 in.) thick. All beams except one were tested at –60°C (–76°F). The final beam (B = 2 in., a/w = 0.1) was tested at –35°C (–30°F).

Instrumentation is attached to the specimens to make possible J-integral and CTOD measurement of fracture toughness. The J-integral is determined from the LLD using the reference bar technique. CTOD is being determined from CMOD using clip gages mounted on the crack mouth of the specimen. Currently, toughness data are being expressed in terms of CTOD according to ASTM E1290-89, Crack-Tip Opening Displacement (CTOD) Fracture Toughness Measurement.

Table 10.1 Test matix for HSST development beams[a,b]

Beam thicknesses (mm)	Number of beams at crack depths, a/w, of			
	0.50	0.15	0.10	Total
50	3	1	4	8
100	1		2	3
150	1		2	3
Total	5	1	8	14

[a]All beams were tested at T = –60°C (–76°F) except one of the 50-mm, a/w = 0.10 beams, which was tested at T = –35 °C (–30°F).

[b]Nominal beam depth was 94 mm (3.7 in.).

The plastic component of CTOD is determined experimentally from the plastic component of CMOD and the rotation factor. The plastic displacement of the crack flanks is assumed to vary linearly with distance from the plastic center of rotation. In this way, the plastic CMOD can be related to the plastic CTOD. The plastic center of rotation is located ahead of the crack tip a distance equal to the rotation factor (RF) multiplied by the remaining ligament (W-a).[1] Numerous experimental and analytical techniques have been used to determine the RF (Refs. 3–7), although no single technique seems to be universally accepted. The RF in ASTM E1290 is given to be 0.4 but is a function of specimen geometry and material. In this study two experimental methods were used to determine the RF. The first method was the use of dual clip gages located at different distances from the crack mouth, and the second was to locate the neutral axis of the beam ahead of the crack tip using strain gages, assuming that the plastic center of rotation was located at the neutral axis of the beam. The strain-gage method resulted in much more consistent and acceptable values of the RF than the dual

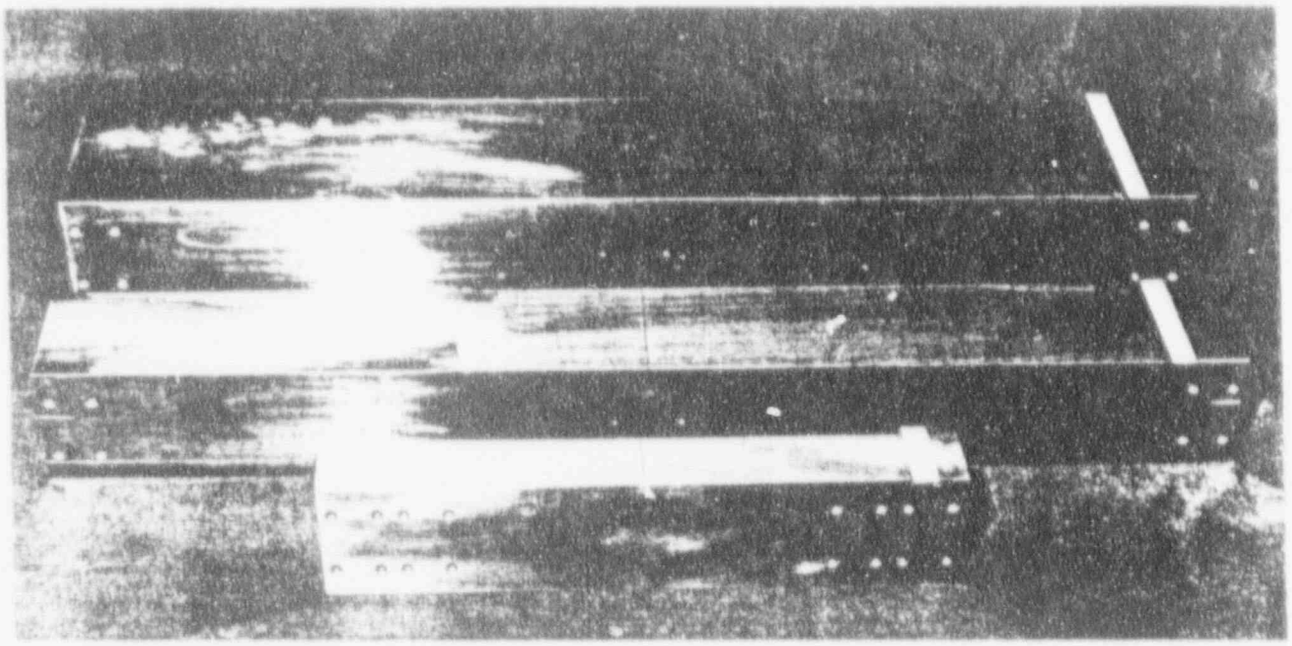

Figure 10.1 Three specimen thicknesses used in shallow-flaw testing program to investigate size effects

clip-gage approach and was used for all CTOD calculations. The RF was found to be insensitive to beam thickness and to vary between about 0.3 for the deep-crack specimens to 0.48 for the shallow-crack specimens. The RF for eight of the beams was determined using the strain-gage method. The RF for the other beams was taken as the average of the values based on crack depth. Table 6.1 gives the RF determined according to the preferred technique and the value used to determine the CTOD.

The two techniques used to attach the clip gages to the specimens were to (1) attach the gage directly to the crack mouth and (2) attach the clip gage to a shim with a beveled edge that was welded to the specimen. Compliance values from each test were compared to expressions included in ASTM E813, J_{Ic}, A Measure of Fracture Toughness. Results of this comparison showed that attaching the clip gages to shims is the better technique. Data from the specimens in which the clip gages were attached directly to the crack mouth of the specimen were slightly in error. The error is due to lack of point contact between the clip gages and the specimen, which introduces displacements other than opening of the crack mouth in the clip-gage measurement. Examination of the data shows, however, that correction of the error would have a negligible effect on the deep-crack data and would increase CTOD fracture toughness about 5 to 7% in the shallow-crack data. Since the exact correction is unknown for the beams in which the clip gages were attached directly to the specimen mouth and the errors are relatively minor, no adjustment of the data has been applied.

Initial notches were inserted into the specimens using electron discharge machining (EDM). The notches were then fatigue precracked to produce sharpened initial flaws. Fatigue precracking was performed according to the guidelines detailed in ASTM E399, Plane-Strain Fracture Toughness of Metallic Materials. Crack growth was monitored by means of the change of crack-mouth-opening compliance, using the clip gage data and the equations for crack length in ASTM E813. The equations in ASTM E813 relating crack length to compliance are invalid for shallow-crack specimens. However, a change in compliance of 10 to 15% generally gave sufficient crack growth. In a few cases the fatigue growth did not exceed 1.3 mm (0.050 in.). Examination of the results from these cases revealed no noticeable bias in the toughness values. After fracture, fatigue crack growth was visually measured according to the 9-point method as outlined in ASTM E813 or E1290. The greatest difference between any two crack-growth measurements for all the tests was 1.8 mm (0.070 in.). The average maximum difference in crack-growth measurements was ~0.9 mm (0.035 in.). Crack growth met

all remaining requirements in ASTM E813 or E1290 for crack profile and orientation.

An auxiliary beam fixture was procured as a backup in the event the primary fixture was unavailable. The fixture was delivered during the current reporting period. The fixture is capable of either 3 or 4-point loading using either a 550-kip Instron machine or a 220-kip MTS machine with a static capacity of 220 kips. The beam fixture is capable of testing beams with a maximum span of 910 mm (36 in.) and up to 127 mm (5 in.) thick.

Several pieces of the Midland Vessel were received during this reporting period. Welds in the Midland vessel are being investigated by the Metals and Ceramics Division of ORNL. Surplus weld material was received and stored for future use. The test pieces are 460 mm (~18 in.) long, 127 mm (5 in.) deep, and 76 mm (3 in.) thick, with the weld in the center of the beam. Cladding is intact on all of the beams. Approximately 12 beams have been stored. These beams are being considered for future use in the shallow-crack program because they are from an actual reactor vessel and are almost identical in size as the smallest beams tested to date in the shallow-flaw fracture-toughness testing program.

References

1. W. A. Sorem, R. H. Dodds, Jr., and S. T. Rolfe, The University of Kansas, "An Analytical Comparison of Short Crack and Deep Crack CTOD Fracture Specimens of an A36 Steel," *WRC Bulletin 351*, Welding Research Council, New York, February 1990.*

2. J. A. Smith, and S. T. Rolfe, "The Effect of Crack Depth to Width Ratio on the Elastic-Plastic Fracture Toughness of a High-Strength Low-Strain Hardening Steel," *WRC Bulletin 358*, Welding Research Council, New York, November 1990.*

3. B. Cottrell et al., "On the Effect of Plastic Constraint on the Ductile Tearing in a Structural Steel," *Eng. Frac. Mech.* 21(2), 239–244 (1985).*

4. Q.-F. Li, "A Study About J_i and δ_i in Three-Point Bend Specimens with Deep and Shallow Notches," *Eng. Frac. Mech.* 22(1), 9–15 (1985).*

5. D.-Z. Zhang and H. Wang, "On the Effect of the Ratio a/W on the Value of δ_i and J_i in a Structural Steel," *Eng. Frac. Mech.* 26(2), 247–250 (1987).*

6. G. Matsoukas, B. Cottrell, and Y.-W. Mai, "On the Plastic Rotation Constant Used in Standard COD Tests," *Int. J. Fract.* 26(2), R49–R53 (1984).*

7. T. L. Anderson, H. I. McHenry, and M. G. Dawes, "Elastic-Plastic Fracture Toughness Tests with Single-Edge Notched Bend Specimens," pp. 210–229 in *Elastic-Plastic Fracture Test Methods: The User's Experience, ASTM STP 856*, E. T. Wessel and F. J. Loss, eds., American Society for Testing and Materials, Philadelphia, 1985.*

*Available in public technical libraries.

CONVERSION FACTORS[a]

SI unit	English unit	Factor
mm	in.	0.0393701
cm	in.	0.393701
m	ft	3.28084
m/s	ft/s	3.28084
kN	lb_f	224.809
kPa	psi	0.145038
MPa	ksi	0.145038
$MPa \cdot \sqrt{m}$	$ksi \cdot \sqrt{in.}$	0.910048
J	ft•lb	0.737562
K	°F or °R	1.8
kJ/m^2	$in.\text{-}lb/in.^2$	5.71015
$W \cdot n^{-3} \cdot K^{-1}$	$Btu/h\text{-}ft^2\text{-}°F$	0.176110
kg	lb	2.20462
kg/m^3	$lb/in.^3$	3.61273×10^{-5}
mm/N	$in./lb_f$	0.175127
T(°F) = 1.8(°C) + 32		

[a]Multiply SI quantity by given factor to obtain English quantity.

NUREG/CR-4219
Vol. 8, No. 1
ORNL/TM-9593/V8&N1
Dist. Category RF

Internal Distribution

1. D. J. Alexander
2. B. R. Bass
3. J. W. Bryson
4. E. W. Carver
5–6. R. D. Cheverton
7. J. M. Corum
8. W. R. Corwin
9. T. L. Dickson
10. F. M. Haggag
11. J. J. Henry
12. W. F. Jackson
13. J. E. Jones Jr.
14. S. K. Iskander
15. J. Keeney-Walker
16. W. J. McAfee
17. D. E. McCabe
18. E. T. Manneschmidt
19. J. G. Merkle
20–21. R. K. Nanstad
22. D. J. Naus
23. C. B. Oland
24–29. W. E. Pennell
30. C. E. Pugh
31. G. C. Robinson
32. D. K. M. Shum
33. R. L. Swain
34. T. J. Theiss
35. E. W. Whitfield
36. ORNL Patent Section
37. Central Research Library
38. Document Reference Section
39–40. Laboratory Records Department
41. Laboratory Records (RC)

External Distribution

42. L. C. Shao, Director, Division of Engineering, U.S. Nuclear Regulatory Commission, Washington, DC 20555
43. C. Z. Serpan, Jr., Division of Engineering, U.S. Nuclear Regulatory Commission, Washington, DC 20555
44–45. M. E. Mayfield, Division of Engineering, U.S. Nuclear Regulatory Commission, Washington, DC 20555
46. A. Taboada, Division of Engineering, U.S. Nuclear Regulatory Commission, Washington, DC 20555
47. W. L. Fourney, Department of Mechanical Engineering, University of Maryland, College Park, MD 20742
48. J. D. Landes, The University of Tennessee, Knoxville, TN 37996-2030
49. S. T. Rolfe, The University of Kansas, Lawrence, KS 66045-2235
50. A. R. Rosenfield, Battelle Columbus Division, Columbus, OH 43201
51. C. W. Schwartz, Department of Civil Engineering, University of Maryland, College Park, MD 20742
52. E. T. Wessel, 312 Wolverine, Haines City, FL 33844
53. Office of Assistant Manager for Energy Research and Development, DOE–OR, Oak Ridge, TN 37831
54–55. Office of Scientific and Technical Information, P. O. Box 62, Oak Ridge, TN 37831
56–305. Given distribution as shown in category RF (NTIS-10)

NRC FORM 335 (2-89) NRCM 1102, 3201, 3202

U.S. NUCLEAR REGULATORY COMMISSION

BIBLIOGRAPHIC DATA SHEET

(See instructions on the reverse)

1. REPORT NUMBER (Assigned by NRC, Add Vol., Supp., Rev., and Addendum Numbers, if any.)

NUREG/CR-4219
ORNL/TM-9593/V8&N1
Vol. 8, No. 1

2. TITLE AND SUBTITLE

Heavy-Section Steel Technology Program

Semiannual Progress Report for October 1990–March 1991

3. DATE REPORT PUBLISHED

MONTH	YEAR
February	1992

4. FIN OR GRANT NUMBER

B0119

5. AUTHOR(S)

W. E. Pennell

6. TYPE OF REPORT

Semiannual

7. PERIOD COVERED (Inclusive Dates)

October 1990 to
March 1991

8. PERFORMING ORGANIZATION – NAME AND ADDRESS (If NRC, provide Division, Office or Region, U.S. Nuclear Regulatory Commission, and mailing address; if contractor, provide name and mailing address.)

Oak Ridge National Laboratory
Oak Ridge, TN 37831-6285

9. SPONSORING ORGANIZATION – NAME AND ADDRESS (If NRC, type "Same as above"; if contractor, provide NRC Division, Office or Region, U.S. Nuclear Regulatory Commission, and mailing address.)

Division of Engineering
Office of Nuclear Regulatory Research
U. S. Nuclear Regulatory Commission
Washington, DC 20555

10. SUPPLEMENTARY NOTES

11. ABSTRACT (200 words or less)

The Heavy-Section Steel Technology (HSST) Program is conducted for the Nuclear Regulatory Commission (NRC) by Oak Ridge National Laboratory (ORNL). The program focus is on the development and validation of technology for the assessment of fracture-prevention margins in commercial nuclear reactor pressure vessels. Reorganization of the original HSST Program into separate programs with emphasis on fracture-mechanics technology (HSST) and materials-irradiation effects (HSSI) was previously completed. The revised HSST Program is organized in 10 tasks: (1) program management, (2) fracture methodology and analysis, (3) material characterization and properties, (4) special technical assistance, (5) crack-arrest technology, (6) cleavage-crack initiation, (7) cladding evaluations, (8) pressurized-thermal-shock technology, (9) analysis methods validation, and (10) fracture evaluation tests. The program tasks have been structured to place emphasis on the resolution fracture issues with near-term licensing significance. Resources to execute the research tasks are drawn from ORNL with subcontract support from universities and other research laboratories. Close contact is maintained with related research programs both in the United States and abroad.

12. KEY WORDS/DESCRIPTORS (List words or phrases that will assist researchers in locating the report.)

Pressure vessels, cleavage-crack initiation, compact specimens, finite-element analysis, fracture correlation parameters, hydrostatic constraint, and shallow-flaw fracture toughness data.

13. AVAILABILITY STATEMENT

Unlimited

14. SECURITY CLASSIFICATION

(This Page)
Unclassified
(This Report)
Unclassified

15. NUMBER OF PAGES

16. PRICE

THIS DOCUMENT WAS PRINTED USING RECYCLED PAPER

NUREG/CR-4219, Vol. 8, No. 1

HEAVY-SECTION STEEL TECHNOLOGY PROGRAM

FEBRUARY 1992